MANIFOLD AND PORT DESIGN FOR BALANCED FLOW AND INCREASED TURBULENCE IN A TWO-STROKE, OPPOSED PISTON ENGINE

by

James Rieser

A Thesis

Submitted to the Faculty of Purdue University

In Partial Fulfillment of the Requirements for the degree of

Master of Science

School of Engineering Technology

West Lafayette, Indiana

December 2021

THE PURDUE UNIVERSITY GRADUATE SCHOOL
STATEMENT OF COMMITTEE APPROVAL

Dr. Jason Ostanek, Chair

Department of Engineering Technology

Dr. Britney Newell

Department of Engineering Technology

Professor William Hutzel

Department of Engineering Technology

Approved by:

Dr. Duane Dunlap

Dedicated to my family for helping me to excel in college.

ACKNOWLEDGMENTS

Thank you to Dr. Ostanek for all the assistance and guidance with the project from teaching how to use ANSYS to pointing out other areas that should be considered in the project.

Thank you to Professor Hutzel for the years of mentoring, suggestions on how to write well, and for the Teaching Assistantship (TA) in the Applied Energy Lab (AEL).

Thank you to Professor Newell for the willingness to devote time out of your schedule to help with my project.

Thank you to Beau Burbrink for advice on the project and for the advice for preparing the proposal for this project.

TABLE OF CONTENTS

LIST OF TABLES

LIST OF FIGURES

LIST OF ABBREVIATIONS

3D – Three Dimensional

CAD – Computer Aided Design

CFD – Computational Fluid Dynamics

TKE – Turbulent Kinetic Energy

GLOSSARY

Air Fuel Ratio – This is the ratio of the mass of air to the mass of fuel within the cylinder.

Compression Ratio – The ratio of the in-cylinder volume at bottom dead center to the volume of the combustion chamber.

Exhaust Manifold Design – This term refers to the geometries of the exhaust manifold and the runners of the exhaust manifold, namely the shape, size, and whether it is tapered.

Exhaust Ports Design – This term refers to the shape, size, and angle of the ports on the exhaust side of the cylinder.

Flame Speed – The rate at which the flame expands within the cylinder.

In-Cylinder Air Flow – This refers to the way that the air flows within the cylinder like swirl and tumble.

Intake Manifold Design – This term refers to the geometries of the intake manifold and the runners of the intake manifold, namely the shape, size, and whether it is tapered.

Intake Ports Design – This term refers to the shape, size, and angle of the ports on the intake side of the cylinder.

Lean – Burning less fuel than what is required for good combustion or to be stoichiometric.

Mass Flow – The rate that mass flows through an area of interest.

Opposed Piston Engine – An engine with two pistons facing each other that are within the same cylinder but attached to separate crankshafts.

Port Swirl Angle – The angle that the ports are slanted to increase the swirl within the cylinder (a 0° angle would imply no slanting of the ports). See Figure 1.1 for a clear visual definition.

Port Tumble Angle – The angle that the ports are slanted to increase the tumble within the cylinder (a 0° angle would imply no slanting of the ports). See Figure 1.1 for a clear visual definition.

Rich – Burning more fuel than what is required for good combustion or to be stoichiometric.

Scavenging – The time during an engine cycle when both the intake ports and exhaust ports are open.

Short-circuiting – “Short-circuiting is the loss of fresh charge to the exhaust during the gas-exchange process” (Ausserer et al, 2017, p2).

Swirl – The horizontal rotations of the flow within the cylinder.

Tumble – The vertical rotations of the flow within the cylinder.

Two-Stroke – Two-stroke engines fire every time that the piston completes the compression part of the engine cycle.

ABSTRACT

Two-stroke, opposed piston engines have gained recent attention for their improved thermal efficiency relative to the conventional inline or V-configuration. One advantage of two-stroke, opposed piston engines is a reduction in heat losses since there is no cylinder head. Another advantage is improved gas exchange via uniflow scavenging since the exhaust and intake ports may be located near bottom dead center of the exhaust and intake pistons, respectively. One challenge with the design of two-stroke engines is promoting turbulence within the cylinder. Turbulence is important for mixing air and fuel in the cylinder and for increasing flame speed during combustion.

This work investigates the flow and turbulence through two-stroke, opposed piston engines using computational fluid dynamics (CFD). Specifically, the role of intake manifold and intake port geometry on turbulence within the cylinder was investigated by systematically modifying the engine geometry. Turbulence was then quantified using three metrics: circulation around the cylinder axis (swirl), circulation normal to the cylinder axis (tumble), and volume average turbulent kinetic energy (TKE) within the cylinder.

Increasing the swirl angle from 0 degrees to 10 degrees increased the in-cylinder swirl by a factor of 3. Increasing the swirl angle also increased the volume average TKE by a range of 7.6% to 36.5% across the three cylinders of the engine. A reverse tilt angle of 15 degrees increased tumble circulation near the piston face but decreased tumble circulation by a factor of 3 near the center of the cylinder. The next step for research on this would be to apply more geometric manipulations to the manifold of the swirl engine design to balance the mass flow rate for each port. Following the redesign of the manifold the next step is to perform a dynamic CFD test to verify the mass flow has been balanced under a dynamic scenario.

CHAPTER 1. INTRODUCTION

The automotive or transportation sector has been working on improving engine efficiency for vehicles for many years. The reason that the transportation sector is trying to achieve lower emissions is because of emissions regulations. Those regulations stem from the Paris Agreement which was an agreement developed by the UN to decrease the greenhouse gas emissions to decrease the chance of global warming past 2°C. According to McGlade and Ekins (2015) the cumulative allowance of CO_2 emissions for 2011 to 2050 needs to be limited to 1,100 gigatonnes so that the global warming has a better chance at staying under 2°C. Luderer et al. (2018) said that the top three sectors for producing CO_2 emissions are buildings, transportation, and industry or manufacturing, respectively.

Reducing the emissions produced by running engines is a logical way to reduce the CO_2 being produced by the transportation sector. Current passenger and heavy-duty vehicles are commonly configured as four-stroke engines which have power strokes once every four strokes. However, two-stroke engines have a power stroke every two strokes which means that there is less energy lost to moving the piston from bottom dead center to top dead center. Current engines are also designed to have cylinder heads to hold the valves and serve as the combustion chamber. The cylinder heads are a source of heat loss for four-stroke engines. An interesting engine configuration to combat this heat loss is to have an opposed piston engine so that the heat that would be lost to the cylinder head is retained and contributes to producing useful work. Opposed piston engines are typically configured as two-stroke engines because there is no need for valves especially now that direct injection is easier to configure. Two-stroke, opposed piston engines are, therefore, a viable solution for decreasing the transportation sectors CO_2 emissions and to improve overall engine efficiency.

One issue associated with two-stroke engines is short circuiting. Short circuiting is when an engine exhausts unburnt fuel through the exhaust ports as the fresh air and fuel are filling the cylinder. A couple of ways to decrease the amount of short circuiting in two-stroke engines is to use direct injection and to design the engines to have higher trapping efficiency. Trapping efficiency is an engines ability to keep air and fuel in the cylinder when the intake and exhaust

ports open. Achieving one-hundred percent trapping efficiency is not possible or desirable because exhaust gases do need to leave the cylinder after combustion to restart the cycle.

1.1 Problem

The interest of this project is modeling air flow through a two-stroke, opposed piston engine. Opposed piston engines with multiple cylinders are almost always configured to be a two-stroke because there is no need for a complex valvetrain. The opposed piston configuration is naturally suited for uniflow scavenging gas exchange, whereby the exhaust ports are located at one end of the cylinder and the intake ports are located at the other. However, as with any two-stroke engine, short circuiting will occur where the incoming charge will bypass the cylinder and exit the exhaust ports resulting in a loss of efficiency and an increase of unburned hydrocarbon emissions. Zhang and Zhao said that "researchers had long [recognized] the issue of short-circuiting during the scavenging process in [two-stroke] engines" (2012, p. 2). Two-stroke, opposed piston engines must have the port timing and in cylinder airflow designed correctly or they need to employ other methods to trap the fresh air charge within the cylinder. Improving trapping efficiency will decrease the amount of unburnt fuel that bypasses the cylinder.

One method to keep the fresh air and fuel charge from leaving cylinder to early is to use direct injection in the side of the cylinder wall. By using direct injection, short circuiting is less detrimental since the fluid passing through the cylinder would be mostly air. And, therefore, direct injection would improve trapping efficiency. Unfortunately, direct injection presents new challenges for proper mixing of the air and fuel. Due to the geometry of the opposed piston engine and lack of cylinder head, the location of fuel injectors must be located in the side of the cylinder. Pirault and Flint (2010) said that "Side injection, as is necessary with an OP engine, is probably also viewed as a major negative feature versus the conventional cylinder head central injection trend that allows symmetry of sprays and fuel-to-air mixing". Direct injection is useful for two-stroke opposed piston, engines but as seen in Pirault and Flints work the mixing within the cylinder needs to be improved.

One method for improving mixing is to increase the swirling motion of the flow inside the cylinder. Mattarelli (2017) said that for two-stroke, opposed piston engines "a strong turbulence can be generated within the cylinder, helping the combustion process". Huo et al. (2015) said that

"decent swirl ratio is also required for air/fuel mixing later in the compression stroke". Zhou et al. (2020) found that optimizing the gas exchange parameters, swirl, and tumble, would improve the trapping efficiency which would reduce the amount of fuel used while idling for their direct injection engine. One method for optimizing gas exchange parameters is through geometric changes to the manifolds and ports. Another method for optimizing gas exchange parameters is through adjusting port timing. Port timing is adjusted by physically moving the position of the port on the cylinder wall or by introducing a lead angle on the piston. Exhaust piston lead angle, for example, advances the phase of the exhaust piston relative to the intake piston. The exhaust piston lead angle effectively changes the port timing.

1.2 Purpose

The purpose of this project was to determine the optimal geometries for intake and exhaust manifold and optimal port design for a balanced mass flow to each cylinder and for improved in-cylinder turbulence. The hypothesis for this project is that, by manipulating geometries for the intake manifold and ports, the mass flow rates through each port will balance and the swirl and tumble ratios will increase. The hypothesis will be tested by answering two research questions:

1. How does the geometry of the manifolds effect the balance of the mass flow through each port?
2. How does the intake manifold and port geometries effect the turbulence within the cylinder?

The research questions were evaluated by analyzing flow parameters (such as mass flow rates, circulation, turbulence levels, etc.) which were obtained by post-processing the simulation outputs of a computational fluid dynamics (CFD) model of an opposed piston engine.

1.3 Significance of the Problem & Purpose

The significance of getting good mixing properties for two-stroke opposed piston, engines is important as the engines could be used in heavy-duty vehicles. According to Abani et al. (2017) "Heavy-duty vehicles, currently the second largest source of fuel consumption and carbon emissions are projected to be fastest growing mode in transportation sector in future." The study

conducted by Abani et al. (2017) involved looking at the potential of developing an opposed piston engine for the heavy-duty vehicle industry. Therefore, any methods that can be used to significantly increase the engine efficiency would be crucial as heavy-duty vehicles operate longer and use more fuel than light-duty vehicles.

The significance of good mixing characteristics for two-stroke opposed piston, engines can also be seen in research papers that are focusing more on injector design. For example, Shirvani et al. (2020) found that "By rotating one of the injectors by 45 degrees around its axis, it was found that NOX emission decreased by 20% and gross thermal efficiency (GTE) improved by 0.9%." This shows that there is a need to improve the swirl and tumble in the cylinder to mix the injected fuel with the fresh air. Geometrical changes to the manifolds and ports will improve the mixing parameters further than just changing the injector designs.

1.4 Key Variables & Images for Definitions

1.4.1 Key Variables

Some key variables that were looked at were the flow characteristics (mass flow, swirl, tumble, and turbulence levels) based off changes to both manifold's geometries and the changes of the ports swirl and tumble angles. Mass flow was looked at because that was an easy parameter to compare between the ports of the engine to check if the flow through the engine was balanced. Swirl is a key variable when it comes to mixing the air and fuel within the cylinder which sometimes it is more useful to look at the swirl ratio. Tumble is another key variable for analyzing the mixing abilities of an engine and if not adjusted correctly could contribute to short circuiting. The turbulence level may be quantified by turbulent kinetic energy (TKE) which describes the energy per unit mass carried by turbulent eddies in the cylinder.

1.4.2 Images for Definitions

Figure 1.1 shows two sectional views of a cylinder that has angled ports. Swirl angle is defined as the angle of the port relative to the radial direction of the cylinder. Tilt angle is defined as the angle of the port relative to the plane normal to the axis of the cylinder (labeled as bottom dead center, or BDC, plane in the image). Swirl and tilt angles will be optimized to increase swirl and tumble, respectively.

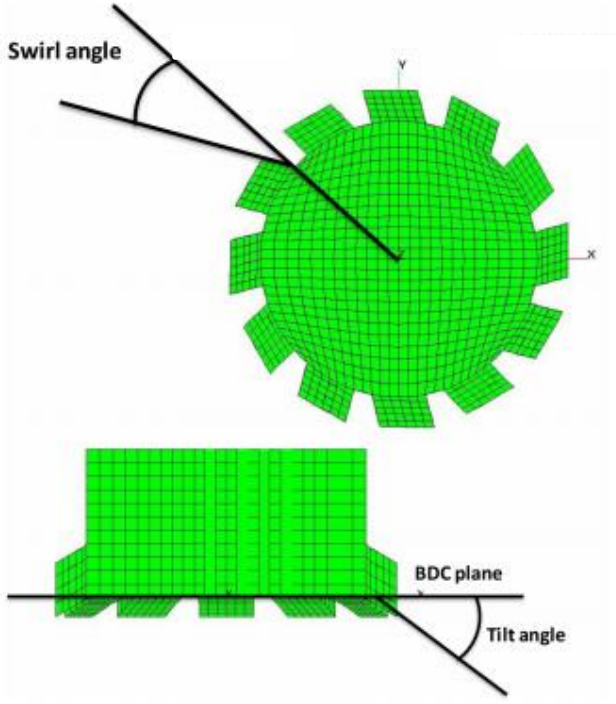

Figure 1.1. Port swirl and tilt angles, Mattarelli et al. (2017)

Figure 1.2 shows a sectional view of a two-stroke engine and describes swirl and tumble motions. Swirl is the rotational flow around the cylinder axis. Tumble is rotational flow around an axis which is perpendicular to the cylinder axis.

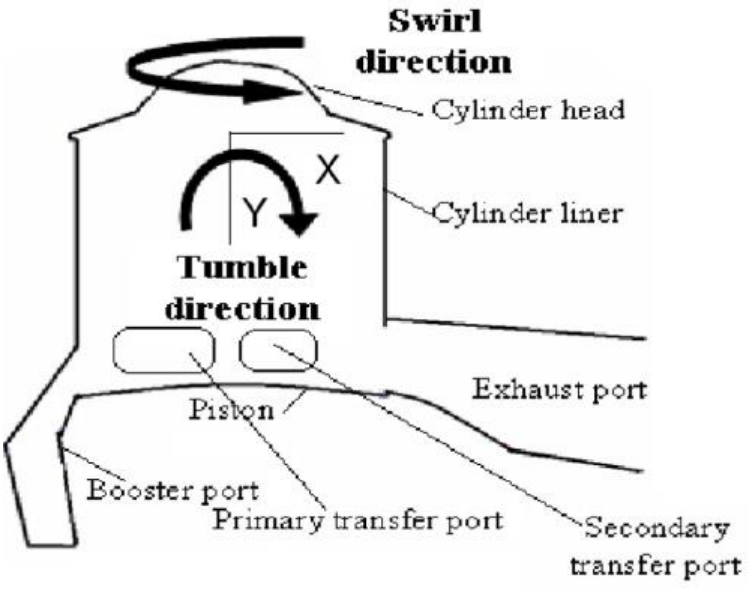

Figure 1.2. Visualization of swirl and tumble, Krishna et al. (2013)

Figure 1.3 shows what Outer Dead Center (ODC), and Inner Dead Center (IDC) are defined as for opposed piston engines. The ODC is the distance from the center of the cylinder to the end of the cylinder which for a conventional engine is equivalent to BDC. The IDC is when the pistons are at the other end of their stroke leaving the piston in the middle of the cylinder which is similar to conventional engines TDC, but for a conventional engine the piston is at the top of its stroke not in the middle of the cylinder.

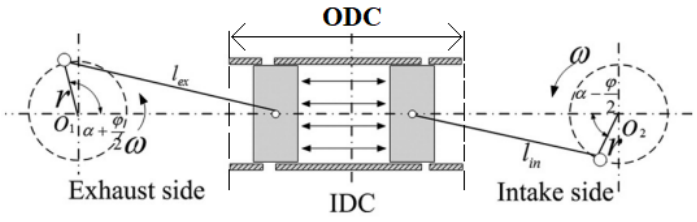

Figure 1.3. Definition of ODC and IDC, adapted from Ma et al. (2015)

1.5 Delimitations, Limitations, & Assumptions

1.5.1 Delimitations

The delimitations of the project are as follows:

- The engine being modeled has three cylinders.
- The simulation will be a static simulation meaning that the pistons will not move.
- All the pistons are at outer dead center.
- The compression ratio for the engine is 12:1.
- The displacement of the engine was designed to be 4.0 L.
- The bore of the engine is 90 mm.
- The stroke of the engine is 210 mm (each piston travels 105 mm).
- The intake manifold pressure is 41 kPa, and the temperature is 300 K.

1.5.2 Limitations

The limitation of this project was that the geometric optimization is conducted using numerical modeling and simulations. Experimental investigation would be preferable but requires unique infrastructure and resources which were not available at the time of this work.

1.5.3 Assumptions

The assumptions made for the steady-state CFD analysis are the following:

- Steady-state simulation
- Turbulence is modeled using the k-epsilon model
- No EGR system
- Air is the working fluid (not considering the introduction of other gaseous species)
- The outlet of the exhaust manifold discharges into an environment at Standard

Temperature and Pressure (STP)

- Ideal gas equation of state
- The properties of air remain constant throughout the engine (Constant viscosity, thermal conductivity, specific heat capacity, etc.)

CHAPTER 2. REVIEW OF LITERATURE

2.1 Search Methodology

2.1.1 Problem Statement

One problem that two-stroke, opposed piston engines have is properly mixing the air charge with the fuel inside of the combustion chamber. Having poorly designed ports or manifolds on a two-stroke engine can result in low swirl and tumble in the cylinder which will result in short circuiting and low flame speed.

2.1.2 Concepts of the Problem

- *Exhaust Manifold Design*
    - This term refers to the geometries of the exhaust manifold and the runners of the exhaust manifold, namely the shape, size, and whether it is tapered.
- *Exhaust Ports Design*
    - This term refers to the shape, size, and angle of the ports on the exhaust side of the cylinder.
- *In-Cylinder Air Flow*
    - This refers to the way that the air flows within the cylinder like swirl and tumble.
- *Intake Manifold Design*
    - This term refers to the geometries of the intake manifold and the runners of the intake manifold, namely the shape, size, and whether it is tapered.
- *Intake Ports Design*
    - This term refers to the shape, size, and angle of the ports on the intake side of the cylinder.

- *Mixing*
    - This term refers to the mixing of air and fuel within the cylinder.
- *Opposed Piston Engine*
    - Opposed piston engine means that the engine has two pistons in the same cylinder that are facing each other.
- *Swirl*
    - Refers to the spiraling motion of the flow in the cylinder.
- *Tumble*
    - Refers to the motion of the flow falling into the bottom of the cylinder.
- *Turbulence*
    - Refers to the unsteadiness of the flow.
- *Two-Stroke*
    - Two-stroke means that the engine will have a power stroke every cycle instead of every other cycle like a four-stroke engine.

2.1.3 Concept Map and Venn Diagram

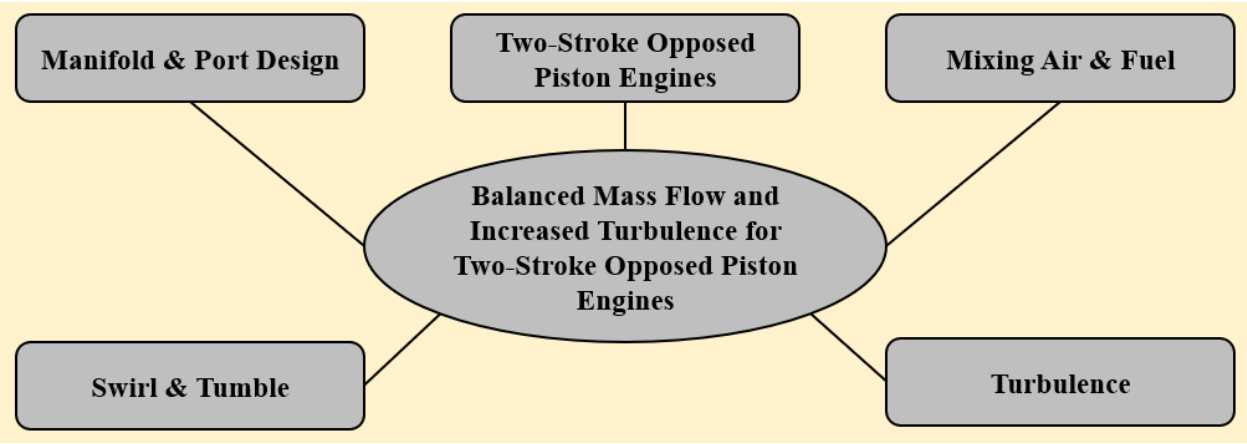

Figure 2.1. Concept map of search terms

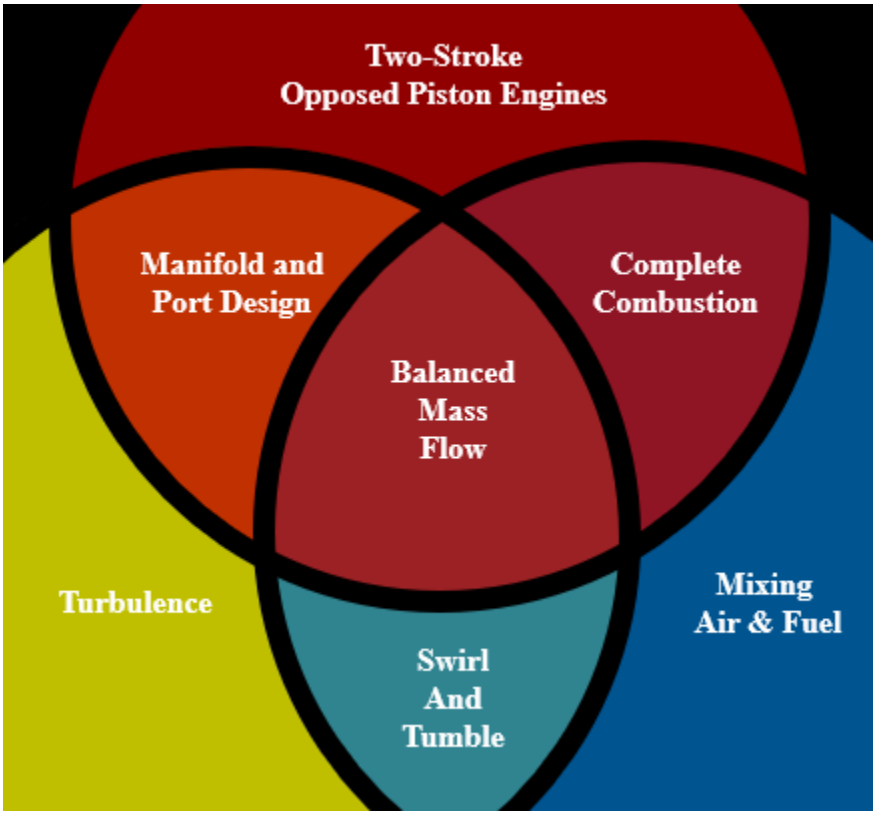

Figure 2.2. Venn diagram that shows how the search terms relate to each other

2.1.4 Most Relevant Databases

Since this project is within the realm of engines that means that the most relevant database to search in would be the SAE Mobilus database. The second most relevant database would be the Dissertations and Theses database. Most of the searches will be conducted in the SAE Mobilus database as it has more relevant information and is more easily found.

2.1.5 Search Characteristics of the Relevant Databases

The contents that are most common for the SAE Mobilus database are technical papers and journal articles. The SAE Mobilus database does not have a thesaurus built into it so knowing what wording to use already or having a thesaurus open in another window in the web browser is helpful. However, the SAE Mobilus database does have a guide on the main page that provides examples of each search function that can be used within the database.

The contents of the Dissertations and Theses database is exactly as it sounds, it is a collection of dissertations and theses on a platform called ProQuest. ProQuest does not have a thesaurus built into it so knowing what wording to use already or having a thesaurus open in another window in the web browser is useful. ProQuest has a button that the user can click which will open a pop-up window with tips on how to use the search engine and explains how the search engine interprets the user input.

2.1.6 Search Strategy

To develop a search strategy, it is important to first establish a target of what is needing to be found. The current state of this thesis is still in the data collection methodology stage so the most useful results would contain some CFD methodology and results for modeling the flow through an engine or engine components. The search strategy that will be used is start broad and narrow down by combining searches as seen below in the following list of steps. Following the list is a Venn diagram that shows the method used for searching more efficiently.

Steps for searching in the SAE Mobilus database:

1. Search “two-stroke AND opposed AND piston AND engine”
2. Search “turbulence”
3. Search “mixing AND air AND fuel”
4. Search “two-stroke AND opposed AND piston AND engine AND turbulence”
5. Search “two-stroke AND opposed AND piston AND engine AND mixing AND air AND fuel”
6. Search “turbulence AND mixing AND air AND fuel”
7. Search “two-stroke AND opposed AND piston AND engine AND mixing AND air AND fuel AND turbulence”
8. Filter results down to any that have been published since 2015
9. Look through the remaining results to find the useful sources.

Note: that in between steps one needs to check the number of results. If there are too many then move to next step. If there are not very many consider rewording the search terms.

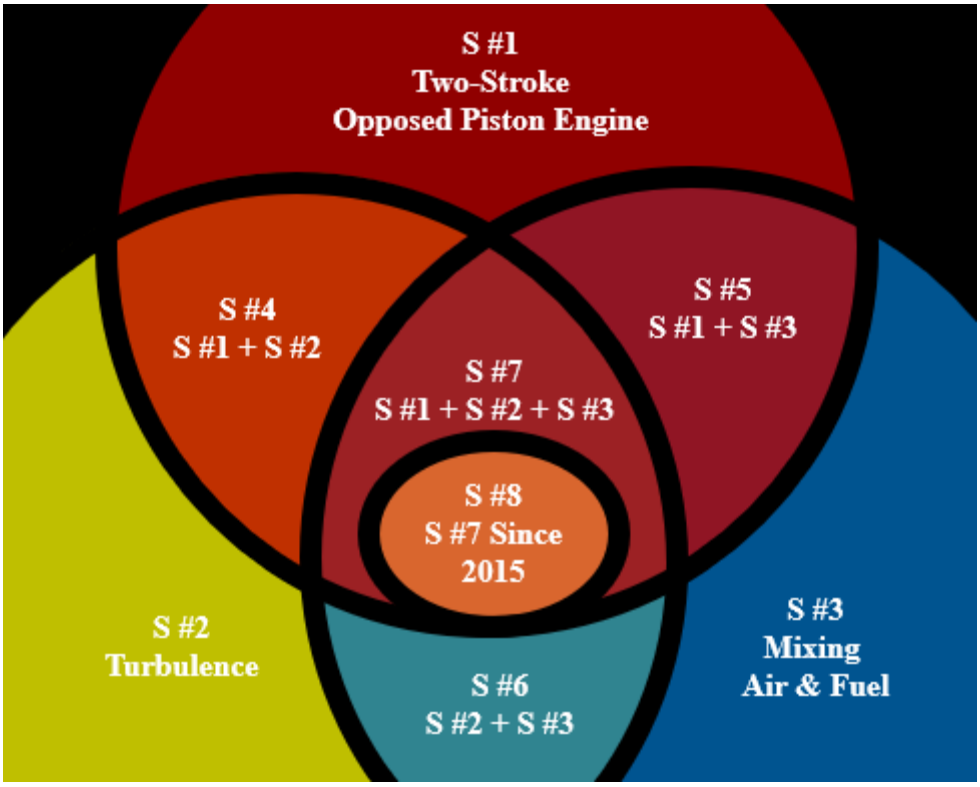

Figure 2.3. Venn diagram that shows how the searches have been assembled

2.1.7 Results from Search Strategy

The results of this search strategy can be seen in Table 2.1. Table 2.1 shows the search number in the left most column, the search terms that were used for that search on the second to left column titled "Search Term(s), the number of results generated from the search in the middle column, the number of useful sources in the column second from the right, and lastly the name of the folder to which the useful results were saved.

Table 2.1. Sample search results gained from search methodology

S#	Search Term(s)	# Of Results	Useful
1.	Two-Stroke Opposed Piston Engine	**467**	
2.	Turbulence	**13,844**	
3.	Mixing Air and Fuel	**16,454**	
4.	Two-Stroke Opposed Piston Engine AND Turbulence	**184**	
5.	Two-Stroke Opposed Piston Engine AND Mixing Air and Fuel	**257**	
6.	Turbulence AND Mixing Air and Fuel	**5,186**	
7.	Two-Stroke Opposed Piston Engine AND Mixing Air and Fuel AND Turbulence	**137**	
8.	Two-Stroke Opposed Piston Engine AND Mixing Air and Fuel AND Turbulence (2015 to 4/6/2021)	**37**	**12**

Database: SAE Mobilus April 6, 2021

2.1.8 Review of the Search Results

This search strategy was effective as it narrowed the number of results from 467 to just 37 and of the 37 there were 12 useful ones that all appeared on the first page of the results. Doing this search produced some material that had not be previously found so it will take a little bit of time to read the new information and further evaluate the usefulness of it and to see if the new information overlaps much. If 37 results seem like too many to look through there are more filters that could have been used to cut down the results further. The Venn diagram was a useful tool to aid in the search process and helped to clarify the search strategy.

2.2 Review of the Literature Problem

Zhang and Zhao did a project in 2012 where they looked at the combustion process of an engine that can run as either a two-stroke or a four-stroke engine. In the paper Zhang and Zhao (2012) claimed that "short-circuiting is a common issue for two-stroke engine operation." Later

in the paper they also talk about how to measure the emissions created from running the engine rich.

Krishna et al performed an in-cylinder flow analysis on a two-stroke engine in 2013. Krishna et al (2013) said that two-stroke engines were phased out because of their lower than ideal efficiency. The emissions of using a low efficiency engine likely had something to do with the phase out as well. However, according to Krishna et al (2013) "they are again becoming popular because of adaptation of direct fuel injection technology to them." The reason that Krishna et al said this was because with direct injection it is possible to inject fuel into the cylinder after the ports are closed. The issue that this presents is that the injectors will now need to be oversized to overcome the pressure that the cylinder is applying to the air in the cylinder once the ports are closed.

Ausserer et al (2017) said the that two-stroke engines have a significant loss because "the intake and exhaust processes have significant overlap, which leads to the first loss pathway measured in this study — short-circuiting." Ausserer et al (2017) laid out the factors that affect how much an engine short-circuits as "a number of engine design factors, including scavenging layout, port design [11], fuel-injection strategy, and tuning of the exhaust and/or intake runner." This shows that intake and exhaust manifold design are relevant areas to try to improve as they usually contain a good portion of the runners.

Understanding the flow path inside an engine cylinder is important to improve the fuel efficiency through designs of the components. Nemati et al (2020) looked at the scavenging process in a large marine engine and said that "having a better understanding of this process and the associated flow pattern is crucial." Nemati et al (2020) explain that it is not possible to physically measure the flow path by saying that "this is not achievable solely by experimental tests for large engines during engine operation due to the difficulties of measuring the flow field inside the cylinder." Therefore, it is important to use CFD and a good model for the CFD to get a good understanding of the flow inside of the engine before arbitrarily making changes to the engine.

2.3 Review of the Literature Purpose and Significance

Krishna et al showed that if the two-stroke engines cannot have improvements made to their efficiency then they will not be used by saying. "Previously, two-stroke engines were widely

used because of high power density and potentially lower mechanical losses as compared to their four-stroke counter parts [1]. However, due to their low efficiency and high emissions, they were faced out" (Krishna et al, 2013, p1). This also shows that most of the efforts in researching the two-stroke engines are spent trying to optimize the two-stroke process to improve efficiency so that they will meet today's emissions standards.

Ausserer et al (2017) said that "for an 85% efficient electric motor, a 5% ICE efficiency is the breakeven point [6], where both motor and engine are assumed to have the same specific power." The size of the motor that is being discussed is relevant for this claim. The application that Ausserer et al are refereeing to is the remotely piloted aircraft area so the engines will be smaller, but they are still two-stroke engines. As Ausserer et al pointed out that there is a point where the power versus efficiency of engines or electric motors are equal in which case the deciding factor is typically emissions driven.

According to Nemati et al (2020) "scavenging which is one of the key processes in the two-stroke marine engines, has a direct effect on fuel economy and emissions." This makes sense since scavenging is the period in an engine cycle where both the intake and exhaust are open. "This process is responsible for fresh air delivery, removing the combustion products from the cylinder, cooling the combustion chamber surfaces and providing a swirling flow for better air-fuel mixing" (Nemati et al, 2020, p1). This shows that having good swirl is not only necessary for combustion but also for better fuel efficiency which will reduce emissions.

2.4 Review of the Literature Methodology

Zhang and Zhao developed a new way to measure the rate of short circuiting in a two-stroke engine during 2012. "The cycle-resolved air short-circuiting rate is derived from instantaneous measurement of the carbon dioxide concentration near an exhaust valve using a [Combustion] fast-response non-dispersive infrared [analyzer]" (Zhang and Zhao, 2012, p1). Unfortunately, this method involves having a physical engine that one could run to get data from where the project being proposed will be simulated on a computer.

Srivastava did a project for a Ph.D. from Michigan State University in 2015 that involved modeling and simulating the spray of injectors in an opposed piston engine. Srivastava used Large-Eddy Simulation (LES) to simulate the spray of an injector in the cylinder of the engine. Srivastava

(2015) did this by using "the two-phase filtered mass density function (FMDF) model, which is an Eulerian-Lagrangian subgrid-scale probability density function (PDF) model for LES of two-phase turbulent reacting flows." Some of the variables that Srivastava (2015) looked at were "the effects of various geometric parameters, operating conditions and spray parameters on the flow evolution, turbulence, spray and combustion in the engine." Srivastava (2015) looked at each of these variables by using "three sets of simulations were carried out for the opposed piston engine: non-reacting flows without spray, non-reacting flows with spray and reacting flows with spray and combustion." The useful case that was tested that is similar to the proposed project is the non-reacting flow simulations that Srivastava conducted as that is similar to the proposed topic.

Krishna et al (2013) did a CFD analysis on a single cylinder two-stroke engine by using a software called STAR-CFD. Krishna et al (2013) said that the goal of their study was to "find out the best turbulence model which predicts the fluid flow field inside the cylinder of a two-stroke engine." The turbulence models that Krishna et al (2013) looked at in their study were "viz. standard k-ε, Chen k-ε and RNG k-ε." As a result of the study that Krishna et al (2013) performed they found that the "RNG k-ε turbulence model best predicts the in-cylinder flow fields in a two-stroke engine."

Some potential results seen from using CFD to try to improve the overall efficiency of an engine can be seen by the example that Ausserer et al gave in their paper. "For example, rigorous computational fluid dynamics (CFD) has been used to reduce short-circuiting by 30% in a 70 cm3 displacement two-stroke engine" (Ausserer et al, 2017, p3). This is not from just changing the geometries of the intake and exhaust manifold but from many factors including the geometries of the ports, the injector timing, and the piston design. Ausserer et al say that "short-circuiting is typically quantified and reported using the trapping efficiency, delivery ratio, and charging efficiency." So, it will be important to see which geometry changes will improve the trapping efficiencies the most.

Nemati et al (2020) did a CFD test on a large two-stroke marine engine using a couple of models. "The simulations are conducted using both Unsteady Reynolds Averaged Navier Stokes (URANS) and Large Eddy Simulation (LES) turbulence models" (Nemati et al, 2020, p1). The results of the CFD models that were run were swirl and tumble velocities. Nemati et al (2020)

validated their results by using “the experimental results obtained from Particle Image Velocimetry (PIV) tests [1].”

CHAPTER 3. RESEARCH METHODOLOGY

3.1 Introduction

The problem addressed by this research is the poor airflow characteristics for mixing fuel and air (mass flow, swirl, tumble, TKE, etc.) within the cylinders of a three-cylinder, two-stroke opposed piston, engine. Having good airflow within the cylinder is critical for having combustion of the fuel within the cylinder. Part of having good airflow for each cylinder requires the mass flow rate to be the same for each cylinder. Another part to having good airflow within the cylinder requires the mixing parameters (swirl, tumble, TKE, etc.) to be the same for each cylinder for a given mass flow rate.

The purpose of this research was to determine the flow characteristics through an opposed piston engine to see the effects of changing geometries of the ports and the manifolds. This will help to guide future research as to how to design the ports for the engine to have good swirl and tumble. This study will also provide understanding on how the manifolds effect the flow through the ports and the cylinder of the engine. The initial hypothesis is that the swirl and tumble can be improved by changing the geometry of the manifolds in addition to the geometry of the ports.

To test this hypothesis, a series of Three-Dimensional (3D) CAD models were made in Autodesk Inventor and were developed for analyzing the flow through the designs using a CFD analysis in ANSYS Fluent. Therefore, this project will generate at least three 3D CAD models of an opposed piston engine with intake and exhaust manifolds, CFD analyses, and a report of the findings.

3.2 Research Type

Four 3D models of opposed piston engines were developed to use CFD analyses for determining a good combination of port geometry and manifold design. Therefore, the project is quantitative research since the CFD analysis will produce numerical data. There will be a few different modifications made to the model to vary the port geometries and the manifold geometries. Also, the model will be analyzed as a static model that has the pistons at ODC (recall Figure 1.3 on page 23).

3.3 Scope

The scope of the research was to perform CFD simulations on a static model making geometric changes between each analysis. The first CFD was done to an engine that has no geometrical changes and was a baseline model. For the second CFD test the intake manifolds were tapered to balance the mass flow for the cylinders. The third CFD test looked at the results of angling the ports to improve swirl within the cylinder. A fourth CFD test involved angling the ports again to improve in-cylinder tumble.

3.4 Data Collection

The key variables that were looked at in this study are the swirl, tumble, and mass flow for each cylinder. Some other variables that were looked at were the dimensions of the ports, the angle of the ports, the angle of the manifolds, and the tapering of the manifolds. The instrumentation used to measure the key variables and the results of altering the other variables was a program called Ansys Fluent.

After gaining data from CFD models the swirl and tumble were calculated using Tecplot which is a post processing software. Swirl was quantified by calculating the circulation within the cylinder. To find circulation, vorticity was calculated first. Vorticity was calculated using Tecplot and was quantified as Z Vorticity. Tecplot calculates Z vorticity using the right-hand rule where the direction of Z vorticity is always coming out of or into the page no matter what variables are appearing on the axis. After calculating vorticity, the circulation is calculated by performing a scalar integral on the vorticity data. Circulation is the integral of vorticity over an area. Figure 3.1 shows the intake port section of cylinder three with velocity vectors plotted on top of the vorticity contour plot. The axes for Figure 3.1 are unitless numbers. The contour plot in the top right of Figure 3.1 shows high vorticity values by coloring them red and low vorticity areas are denoted in green. Despite having regions of high vorticity, the circulation calculated for this region is fairly low since the flow is not swirling strongly around the cylinder's axis. The calculated circulation for this example is 6.937 m^2/s.

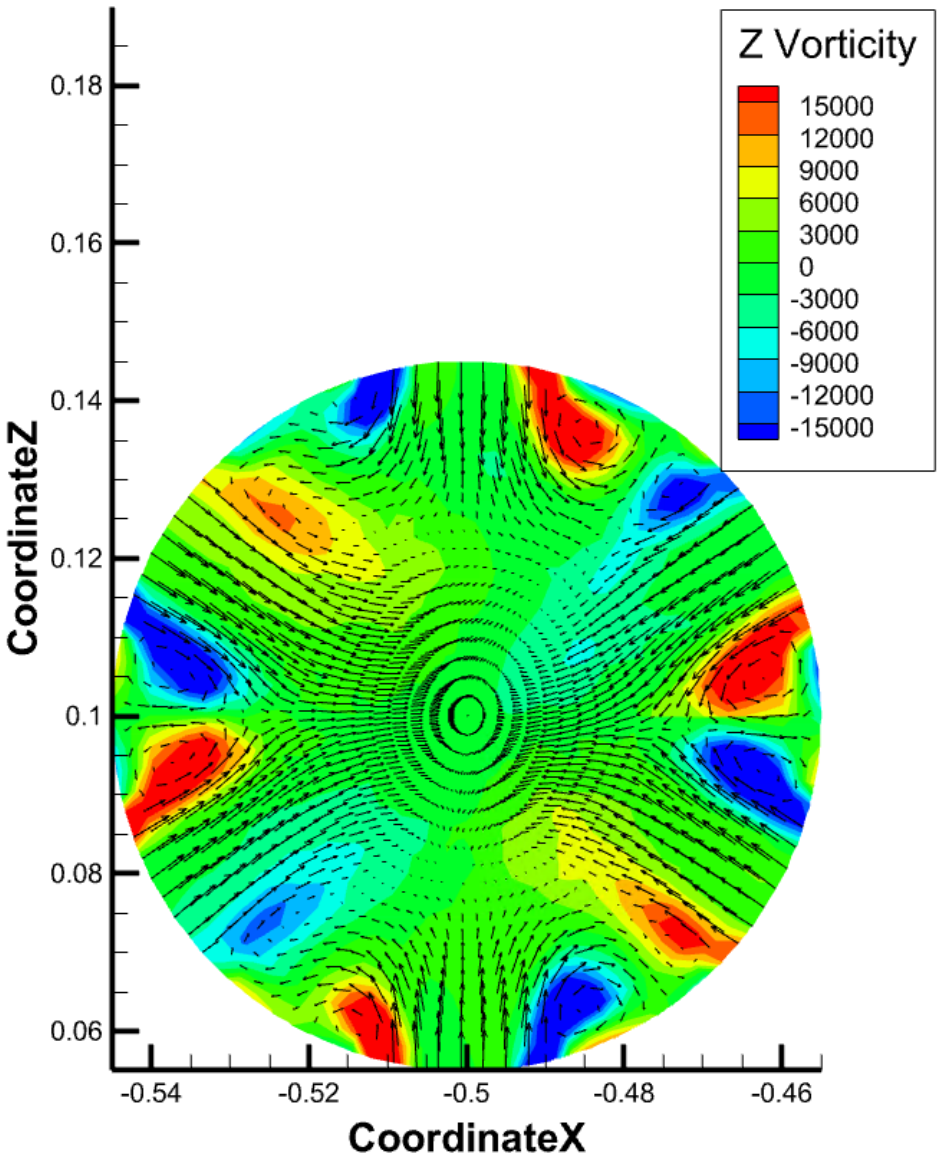

Figure 3.1. Vorticity contour plot over plotted with velocity vectors

The workflow for the research project is shown in Figure 3.2. The methods for gathering the data for the study was to first start with a model that essentially has a straight path for the air to flow through within the engine to establish a baseline. The next step was to taper the intake manifold runners to see if the flow has increased velocity going into the cylinder. Then, a new intake manifold was made so that the manifold runners can somewhat angle the flow entering the cylinder to test how much swirl can be generated from just the runners being angled. Then, the same step was done to the intake manifold again but with am emphases on improving the tumble

within the cylinder. Single changes will continue to be made to the model until all cases have been tested.

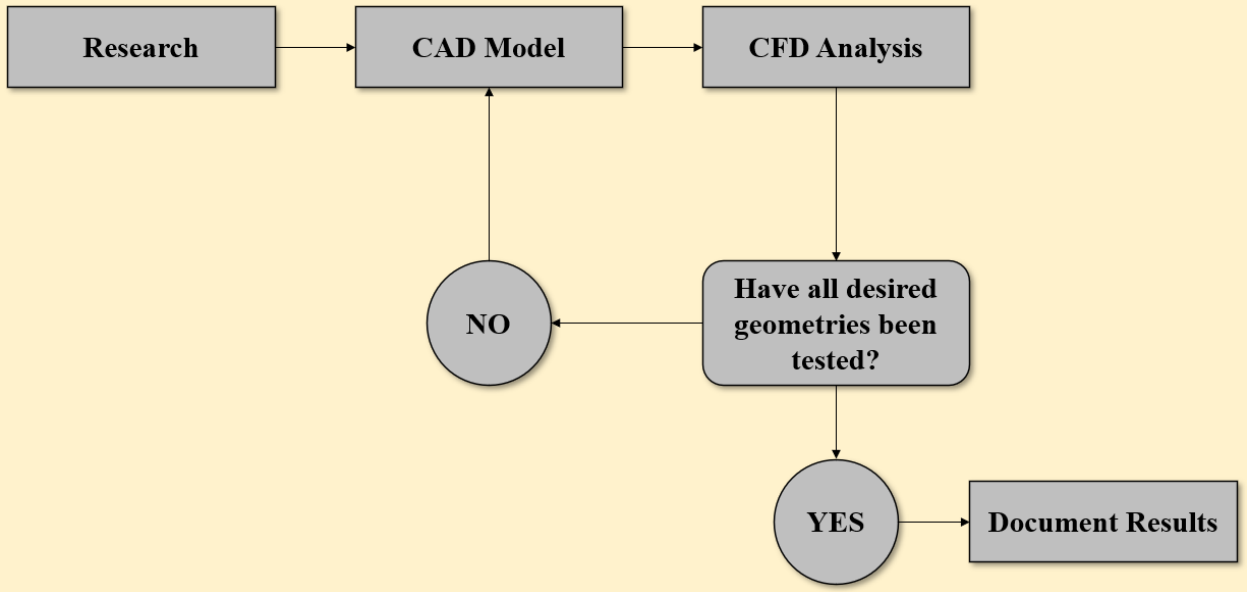

Figure 3.2. General flow of proposed work

3.5 Data Analysis

The CFD simulations produced velocity and pressure fields which were analyzed to understand the flow path in the manifolds and the cylinder. Integrating the mass flow rate (per unit area) across the face of each port determined whether the ports and cylinders are receiving a uniform mass flow. After looking at these two aspects for each sample collected from the CFD, a comparison of the results was performed against the other configurations of the engine and against other published results. The comparison involved looking at the velocities of the swirl and tumble, the mass flow through the cylinder, and also if the optimal changes are in line with other published results of a similar engine. The first step in performing the comparison was to establish a baseline for the flow through the engine. To establish a baseline flow through the engine a CFD was done to a model of the engine that had no geometrical modifications made to the ports or manifolds. Meaning that the flow will enter the cylinder without the ports or manifolds being tapered or angled. By doing this it was easier to determine which modifications improve certain flow characteristics like swirl and tumble or hinder the flow characteristics within the cylinder.

To quantify swirl the circulation was calculated. Circulation is calculated by taking the integral of the vorticity over a surface area as shown by equation 3.1. The circulation is Γ, the variable for the vorticity is ω, and A is the area.

$$\Gamma = \iint \omega \cdot dA \tag{3.1}$$

Quantifying tumble is similar to swirl where circulation is calculated. However, the tumble characteristic involves calculating circulation on a vertical plane through the engine whereas swirl is circulation on a horizontal plane through the engine. Therefore, to calculate swirl the X and Z vorticity components are integrated over an area. Tumble is like swirl but uses the X and Y vorticity components. Figure 3.3 is a better visualization of swirl and tumble integral areas.

Figure 3.3 is an isometric drawing of a vertical axis plane and a horizontal axis plane through half of one of the engine cylinders. The horizontal axis is the ZX plane and has cyan arrows to show the orientation of circulation for swirl. The vertical axis is the XY plane and has dark blue arrows to show the orientation of circulation for tumble.

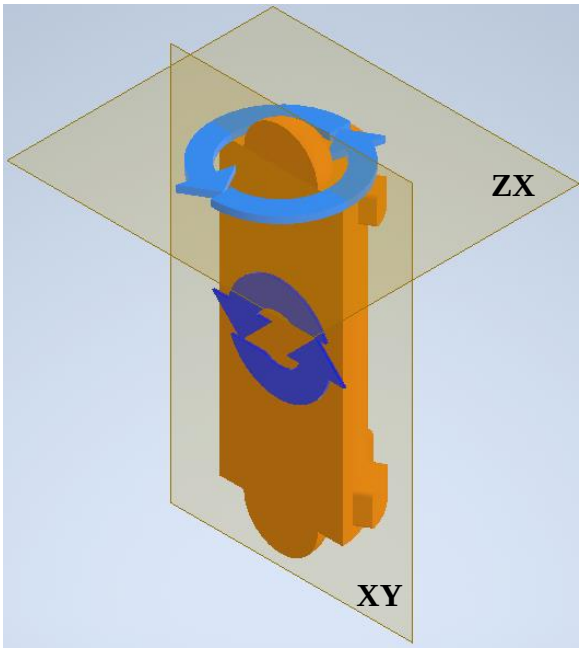

Figure 3.3. Swirl and tumble area representation.

Figure 3.3 shows that the swirl integral takes place on the ZX plane which means that the Z and X component vorticities are needed for the integral. The XY vorticity components are needed for tumble since the dark blue arrows are oriented on the XY plane.

CHAPTER 4. RESULTS

4.1 Baseline Design

4.1.1 Geometric Model

Figure 4.1 shows the internal geometry of the first design of the opposed piston engine. The blue components in Figure 4.1 shows the intake manifold and intake ports. The orange components in Figure 4.1 represent the cylinders and a portion of the intake and exhaust ports. The red component in Figure 4.1 represents exhaust ports, exhaust manifold, and an exhaust collector.

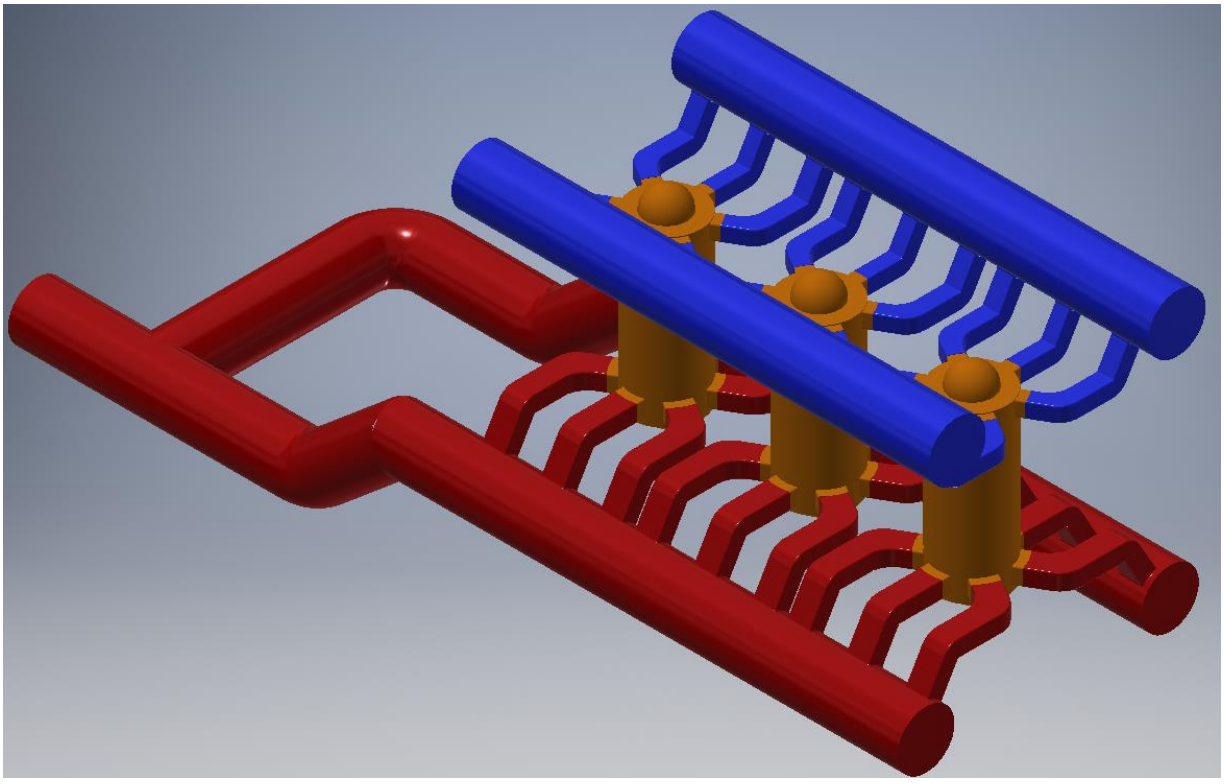

Figure 4.1. CAD model for the baseline design of the baseline opposed piston engine

Figure 4.1 shows the baseline design with straight ports and non-tapered manifolds. This design is expected to produce a low swirl flow due to the angle of the ports. However, the mass flow balance, swirl, and TKE levels are unknown. Establishing a baseline model is important for being able to determine what effect each change will have on the flow characteristics.

4.1.2 Mesh and Boundary Conditions

The element order for the mesh was linear and the element size was 67.553 mm. The mesh had a growth rate of 1.2 and a max size of 135.11 mm. The mesh was setup to not use adaptive sizing. The mesh defeature size was set to 0.33776 mm. The mesh curvature minimum size and normal angle were 0.67553 mm and eighteen-degrees. The inflation layers were set to have a maximum of 10 layers with a 1.2 growth rate. The baseline design mesh had 14,618,346 total elements. The rest of the settings used to generate the mesh are in appendix A.

According to the Ansys 2020 help manual, changing the element size will change the minimum element size for the mesh. The minimum element size is calculated by using the specified element size with the CFD min size factor which defaults to 0.01. Therefore, just because the element size was set to 67.553 mm does not mean that a 67.553 mm element size will be present in the mesh.

Tetrahedrons were used for the shape of the elements for the mesh of the baseline engine design. According to Frei (2013) tetrahedrons can mesh any geometry including complex ones and for most cases making tetrahedrons the first element shape to try. Another element shape that can be considered for use in CFD is hexahedrons. According to Montazerin et al. (2015) the hexahedral mesh and the mesh made up of tetrahedrons that they worked with had similar results for their CFD study. The solution for the tetrahedral mesh converged so tetrahedrons were used as the element shape.

Figure 4.2 shows an isometric view of the computational mesh for the baseline design. The mesh size is easier to see in Figure 4.4 which has a close-up view of a cross sectional view of an intake manifold runner. The unstructured mesh used tetrahedral elements and inflation layers were used on the walls to capture the large velocity gradients in the boundary layer.

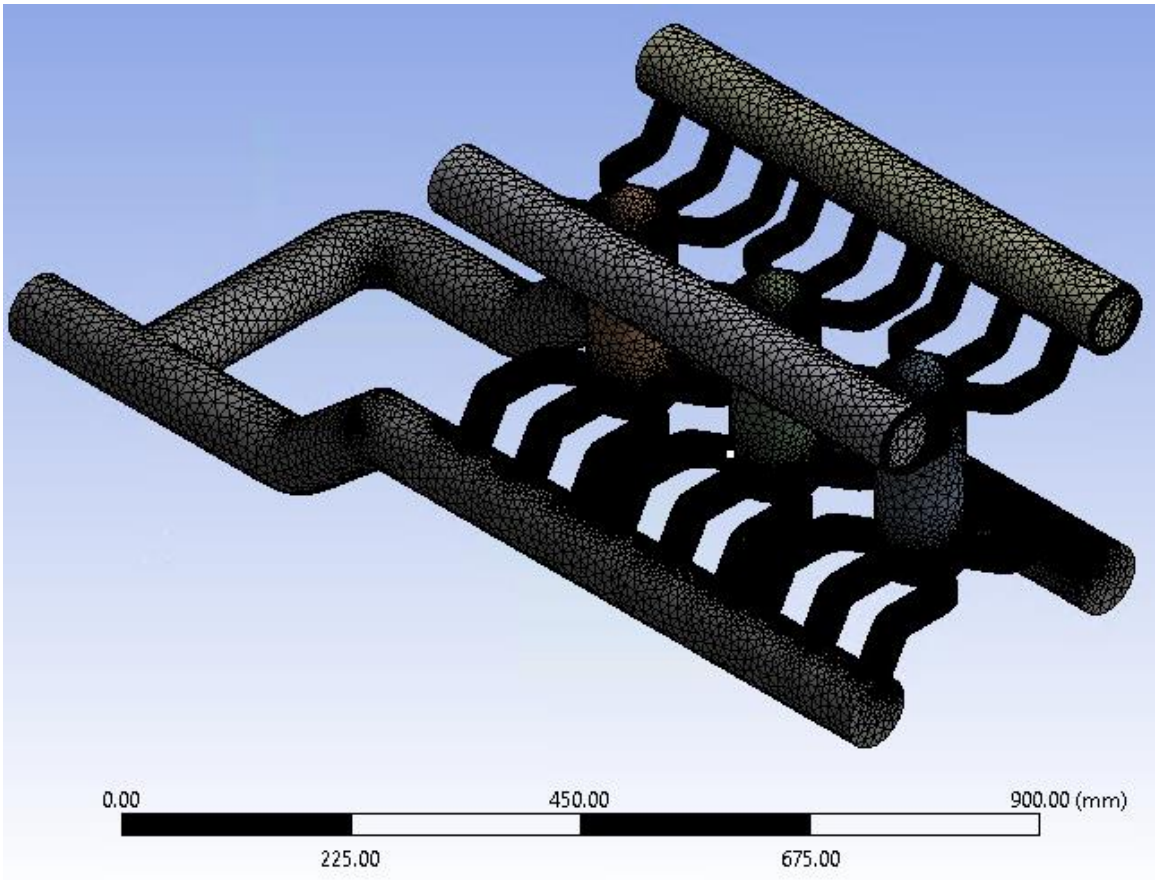

Figure 4.2. Isometric view of the meshed model for the baseline opposed piston engine

Figure 4.3 shows the right half of the meshed engine cut down the middle. The bottom left corner of Figure 4.3 shows the inflation layer within the exhaust manifold. Figure 4.3 also shows detail of the mesh inside of the cylinders. Figure 4.4 shows a section of an intake manifold runner close-up so that the inflation layers are easier to see.

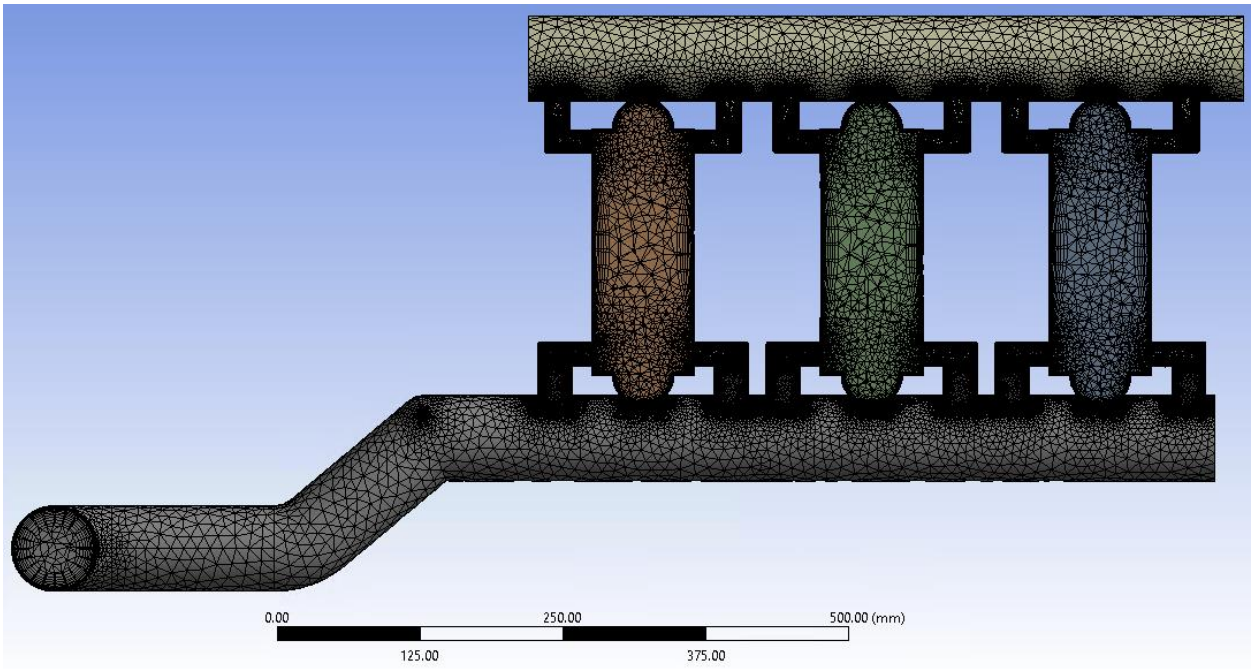

Figure 4.3. Section view of the meshed model for the baseline opposed piston engine

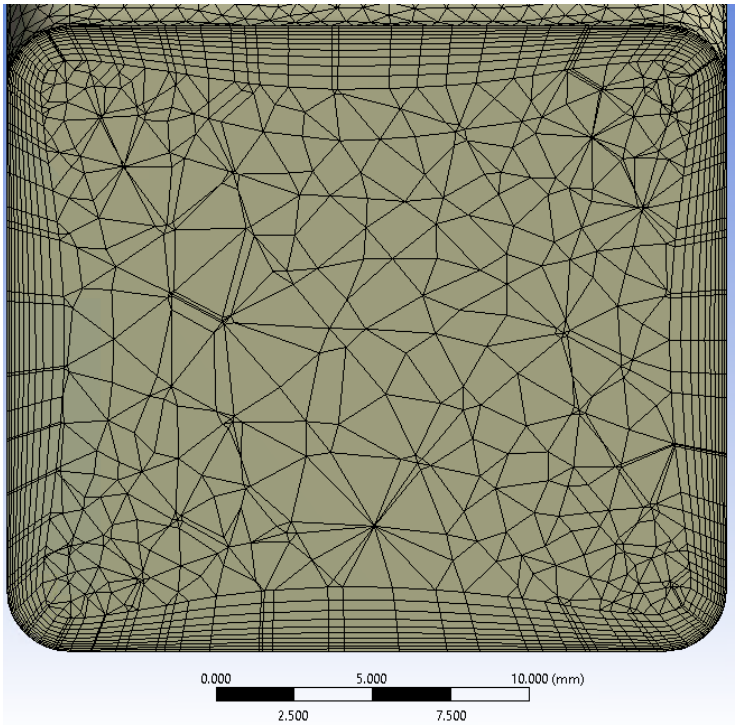

Figure 4.4. Section view of the meshed intake manifold runner for the baseline opposed piston engine

As seen from Figure 4.4, the layers become thinner closer to the walls. The inflation layer grows as new layers are added outward from the wall boundaries. The growth rate was 1.2 for the baseline mesh. The inflation layer blends with the size of the elements in the core of the mesh. Figure 4.4 shows that the corners of the port had smaller elements in the core of the mesh and the inflation layer adjusted by shrinking the height of the layers automatically.

Figure 4.5 and Figure 4.6 show the model boundary conditions. Figure 4.5 shows the wall boundaries, highlighted in red. Wall boundaries are automatically assigned an adiabatic (zero heat flux across the wall), impermeable (zero mass flux through the walls), and no-slip condition (zero velocity at the wall). The letter tags seen in Figure 4.5 label the walls of each object. For example, letter tag A is the left intake manifold as shown by the legend in the top left corner of Figure 4.5.

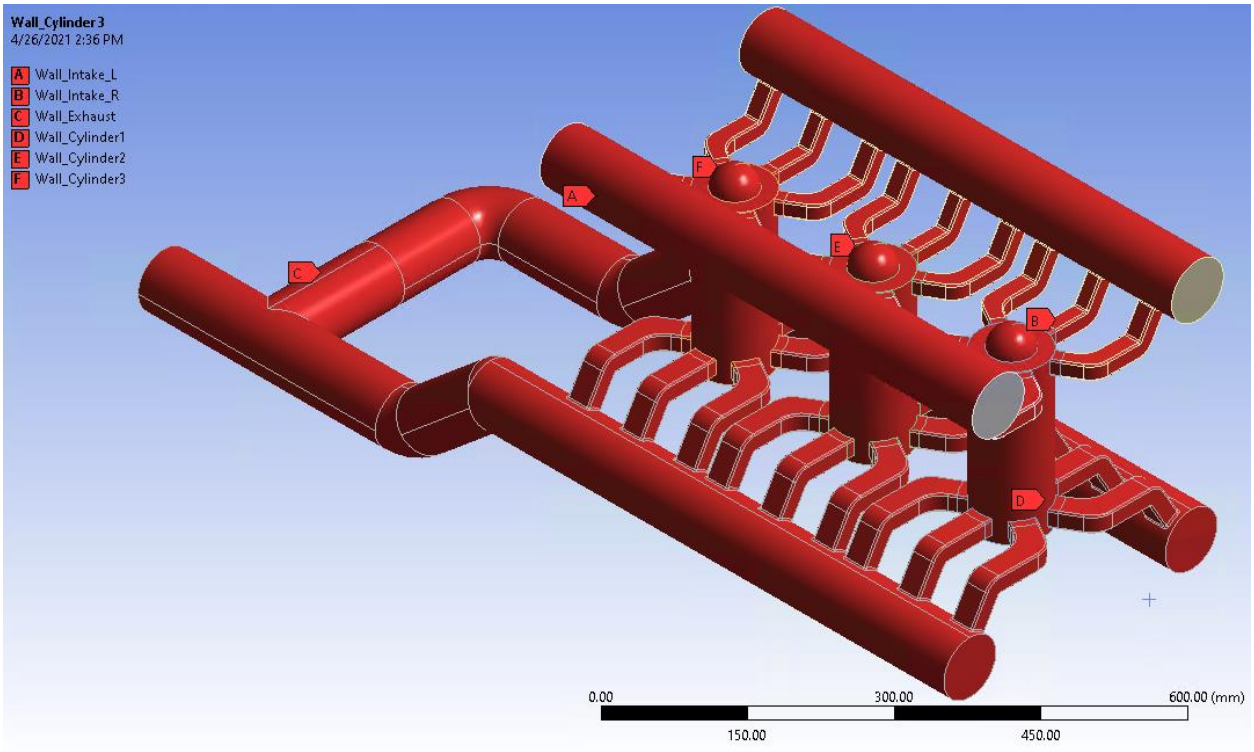

Figure 4.5. Baseline engine wall boundary conditions

Figure 4.6 shows the boundary conditions for the pressure inlet and pressure outlet. The left side of Figure 4.6 shows the inlets and they are labeled with the letter tag B. The middle of Figure 4.6 shows the legend for the letter tags. The right side of Figure 4.6 shows the pressure outlet on the backside of the engine.

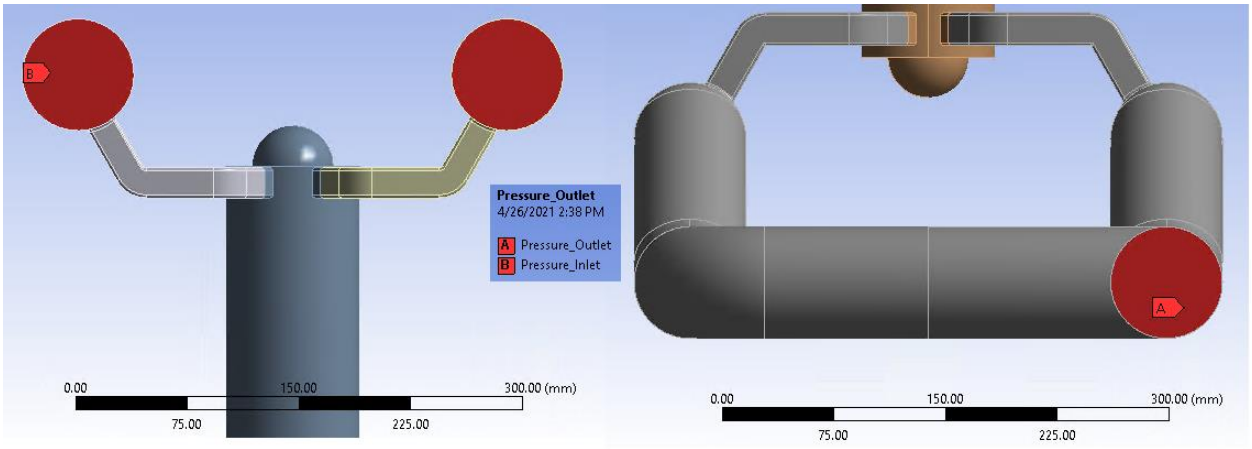

Figure 4.6. Baseline inlet and outlet boundary conditions

The pressure applied to the inlets was 41.4 kPa (6 psi) gage pressure to simulate a modest turbo or super charger for the engine. Two-stroke opposed piston, engines commonly have either a turbo or a super charger to help keep up with the airflow demand of the two-stroke engine. The pressure applied to the outlet was atmospheric pressure, zero gage pressure.

4.1.3 Mesh Sensitivity Analysis

Determining the mesh size was done by creating three different meshes with different element sizes. Table 4.1 shows the different settings used for the three different meshes used in the analysis. The full settings for the fine mesh can be seen in Appendix A and the settings for the coarse and medium meshes can be seen in Appendix B. The coarse mesh used an element size of 92.5 mm, resulting in an overall element count of 9.5 million. The medium mesh used an element size of 80 mm, resulting in an overall element count of 11.8 million. The fine mesh used an element size of 67.5 mm, resulting in an overall element count of 14.6 million.

Table 4.1. Mesh element sizing options used for sensitivity analysis

Mesh	**Coarse**	**Medium**	**Fine**
Element Size	92.5 mm	80 mm	67.553 mm
Maximum Layers	10	10	10
Inflation Growth Rate	1.2	1.2	1.2
Elements	9,544,304	11,778,934	14,618,346

When creating the different meshes for each case the inflation layers and inflation growth rate for the cells were held constant for each case. The only property changed by the user was the element size. The rest of the values that changed were the program default values that were based on the element size. The inflation layers are the cell regions close to edges or complicated features. Figure 4.4 is a cross section on one of the intake manifold runners which shows the inflation layers around the edges of that face.

As seen by Table 4.1 the coarse mesh had the least number of elements which allows it to compile quickly. One downside to using less elements is that the output is less accurate as to what is really happening in the flow field. The fine mesh had the most elements and took the longest to compile but will provide more accurate results than the coarse mesh will. To determine an acceptable mesh size to be used, the mass flow rates through the ports were looked at to determine which model would produce the most accurate results while reducing computing time.

Figure 4.7 shows the mass flow rate in kilograms per second on the vertical axis. Figure 4.7 also shows the port number for each mesh size in the gray and yellow shaded regions along the horizontal axis. The legend on the right of Figure 4.7 shows that the mas flow rate for cylinder one fine mesh is blue, medium mesh is orange, and gray is coarse.

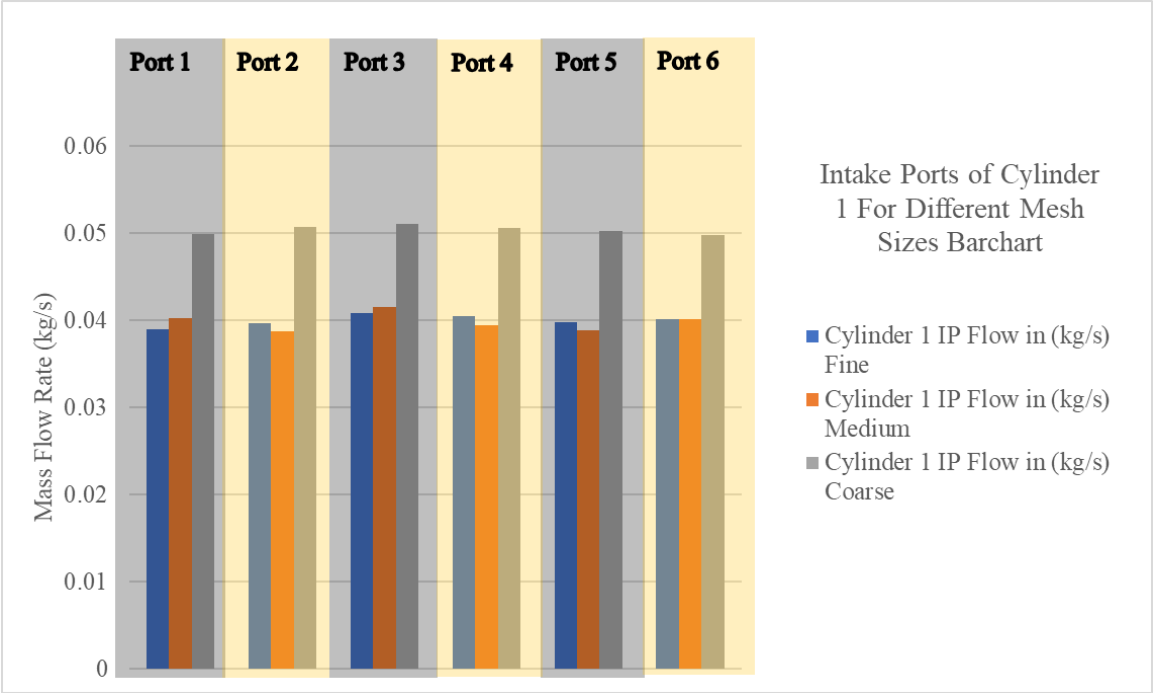

Figure 4.7. Cylinder one intake port mass flow rates for three mesh sizes

The results of plotting the mass flow rates for each intake port for cylinder one shows that the coarse mesh mass flow results are much higher than the other two meshes. As seen by the orange and blue bars in Figure 4.7, the medium and fine mesh mass flow rates through the ports are identical for cylinder one. The results seen in Figure 4.7 show that the fine mesh produced accurate enough results since the mass flow rates did not change drastically between the medium and fine mesh for cylinder one.

Figure 4.8 is formatted similarily to Figure 4.7 but shows the results for cylinder two instead of one. Figure 4.8 shows the mass flow rate in kilograms per second on the vertical axis. The gray and yellow shaded regions on Figure 4.8 are highlighting the ports for each mesh size. The right side of Figure 4.8 shows that the fine mesh is blue, medium mesh is orange, and the coarse mesh is gray.

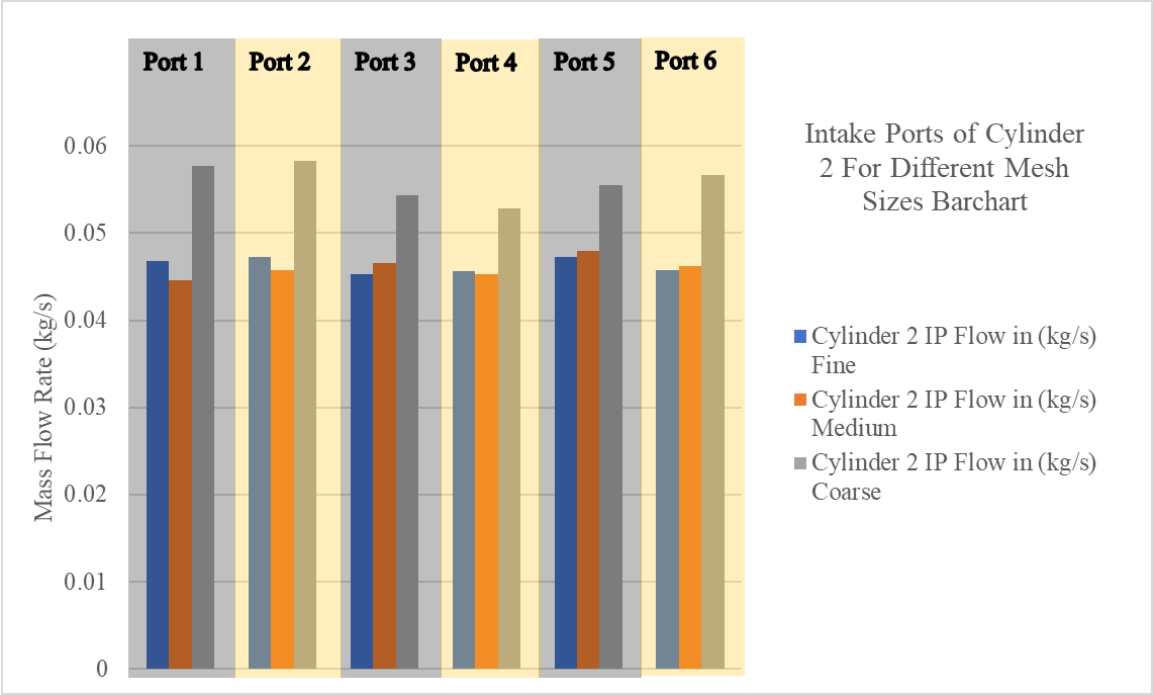

Figure 4.8. Cylinder two intake port mass flow rates for three mesh sizes

The results of plotting the mass flow rates for each intake port for cylinder two shows that the coarse mesh mass flow results are again much higher than the other two meshes. Figure 4.8 shows that the medium and fine mesh mass flow rates through the ports are about the same. Figure 4.8 shows that the mass flow rates did not change much between the medium and fine mesh for cylinder two. Therefore, just like the results from Figure 4.7 showed, the fine mesh settings were determined to be fine for use with future models.

Figure 4.9 shows the results for cylinder three mass flow rates for each port of the three different meshes. Figure 4.9 shows the mass flow rate in kilograms per second on the vertical axis. The gray and yellow shaded regions on Figure 4.9 separate the bars into sections that show the mass flow rates for each of the ports for each mesh size. Figure 4.9 shows the fine mesh in blue, medium mesh in orange, and the coarse mesh in gray.

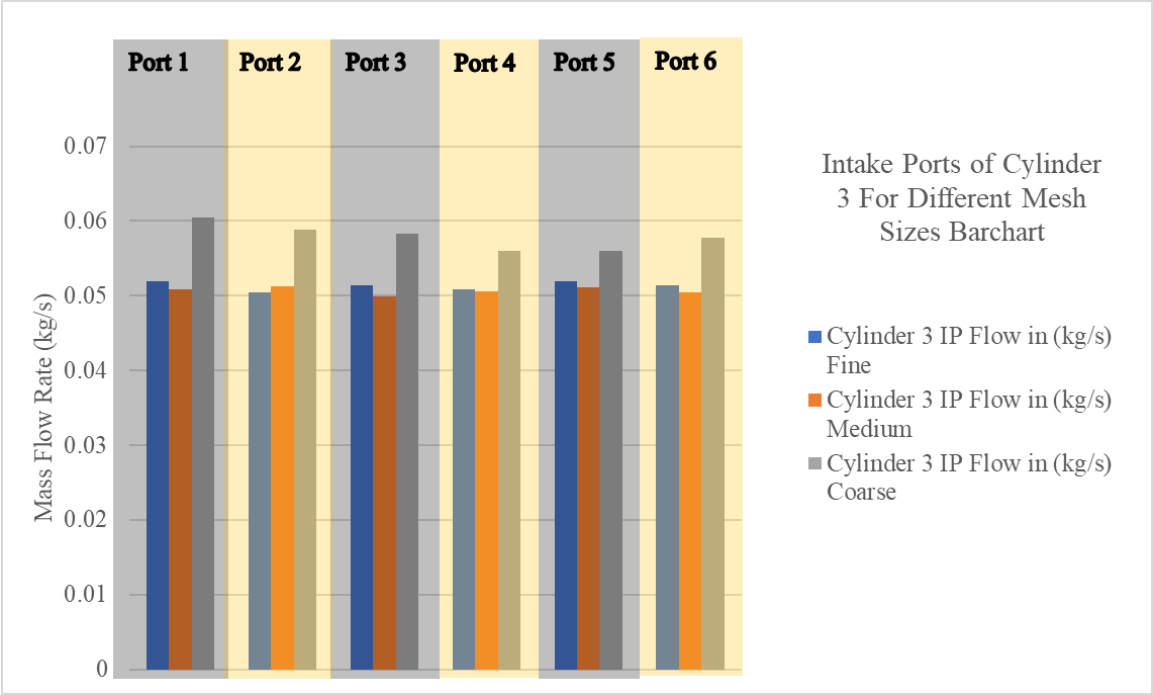

Figure 4.9. Cylinder three intake port mass flow rates for three mesh sizes

The results of plotting the mass flow rates for each intake port for cylinder three shows that the coarse mesh mass flow results are closer to the other two meshes but still higher than the other two meshes. Figure 4.9 shows that the medium and fine mesh mass flow rates through the ports have similar mass flow rates. Figure 4.9 shows that the mass flow rates did not change much between the medium and fine mesh for cylinder three. Therefore, just like the results from Figures 4.7 and 4.8 showed, the fine mesh settings were determined to be fine for use with future models.

Figure 4.10 is comprised of three sections. The first section, the top, is the exhasut mass flow rates for the ports of cylinder one for three different mesh sizes. The second section, the middle, is the exhasut mass flow rates for the ports of cylinder two for three different mesh sizes. Lastly, the third section, the bottom, is the exhasut mass flow rates for the ports of cylinder three for three different mesh sizes. The vertical axis for each of the sections is the mass flow rates in kilograms per second. Each section shows the mass flow rates results for the coarse mesh in gray, the medium mesh in orange, and the fine mesh in blue.

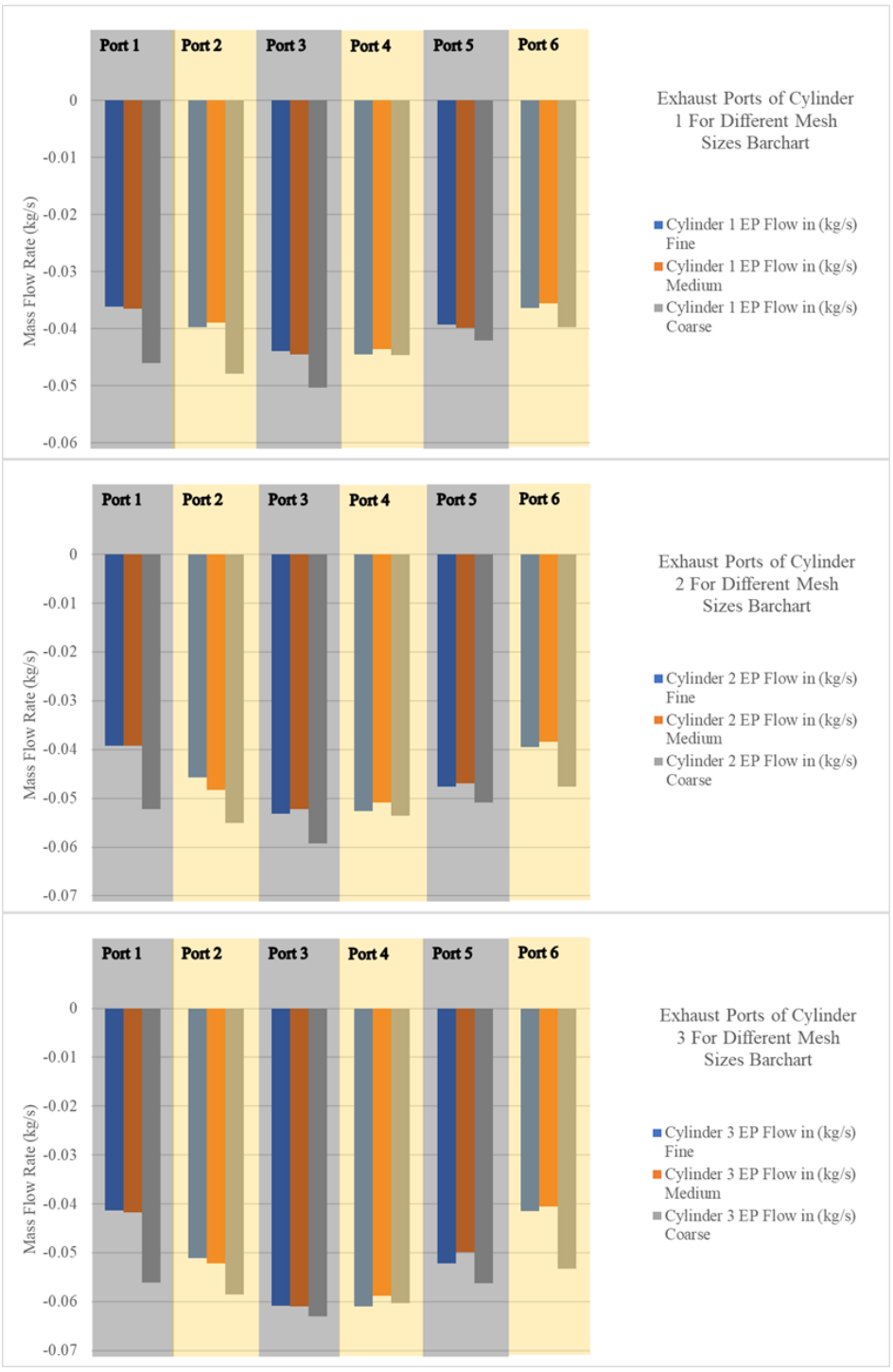

Figure 4.10. Cylinders one, two, and three exhaust port mass flow rates for three mesh sizes

Figure 4.10 shows that the flow rates through the exhaust ports of each of the cylinders has a negative flow rate which implies that the mass is flowing out of the cylinder. Figure 4.10 also shows that medium and fine mesh sizes have roughly the same flow rates just like what Figures 4.7 through 4.9 showed. Therefore, the fine mesh was chosen as the mesh size to use for the rest of the engine designs since there was not a big difference between the fine and medium mesh flow rates.

Table 4.2 shows the section of the engine in the leftmost column. The second to the left column of Table 4.2 specifies the intake port (IP) or the exhaust port (EP). The third column from the left of Table 4.2 shows the difference of the coarse and medium mesh mass flow rates as a percentage. The rightmost column of Table 4.2 shows the difference of the medium and fine mesh mass flow rates as a percentage. The EP Total and IP Total rows at the bottom of Table 4.2 shows the difference of the total mass flow rate through the exhaust and intake manifolds as a percentage.

Table 4.2. Percent difference of the mass flow rates for each port from coarse to fine mesh sizes

		Difference of Coarse to Medium (%)	Difference of Medium to Fine (%)
Cylinder 1	EP 1	-23.2	-1.0
	EP 2	-20.5	2.0
	EP 3	-12.4	-1.2
	EP 4	-2.3	2.2
	EP 5	-5.3	-1.5
	EP 6	-10.9	2.1
	IP 1	21.5	3.2
	IP 2	26.7	-2.3
	IP 3	20.5	1.7
	IP 4	25.0	-2.7
	IP 5	25.6	-2.4
	IP 6	21.5	0.1
Cylinder 2	EP 1	-28.3	-0.2
	EP 2	-13.1	-5.5
	EP 3	-12.5	1.7
	EP 4	-5.4	3.6
	EP 5	-7.9	1.3
	EP 6	-21.3	2.6
	IP 1	25.8	-4.8
	IP 2	24.1	-3.5
	IP 3	15.5	2.7
	IP 4	15.3	-0.8
	IP 5	14.8	1.3
	IP 6	20.4	0.8
Cylinder 3	EP 1	-29.2	-0.9
	EP 2	-11.5	-1.9
	EP 3	-3.2	-0.3
	EP 4	-2.5	3.4
	EP 5	-12.1	4.5
	EP 6	-27.0	2.2
	IP 1	17.2	-1.9
	IP 2	13.9	1.4
	IP 3	15.5	-3.0
	IP 4	10.2	-0.7
	IP 5	9.1	-1.5
	IP 6	13.5	-1.9
Change in total flow	EP Total	-13.4	0.8
	IP Total	18.4	-0.8

Table 4.2 shows that the difference of mass flow rates between the coarse and medium mesh was between 2% to 30%. Table 4.2 also shows that the difference between mass flow rates for the medium and fine mesh was under 5% for all but one of the ports. The only port that had a percent difference larger than 5% for the difference of medium and fine was exhaust port two for cylinder two. The difference of the total mass flow rate of the manifolds for the medium and fine mesh were under 1%. Therefore, the fine mesh settings were deemed acceptable for gathering data since increasing the fineness of the mesh would just increase the computation time and not impact the mass flow significantly.

4.1.4 Balance of Mass Flow

Figure 4.11 shows the mass flow of air through each of the intake and exhaust ports. The intake ports have a positive mass flow rate (top side of the bar chart), and the exhaust ports have a negative mass flow rate (bottom side of the bar chart). Figure 4.11 uses different colored bars for each cylinder as seen in the legend from the right side of Figure 4.11. Across the top of Figure 4.11 are labels sectioning of the different ports, one through six.

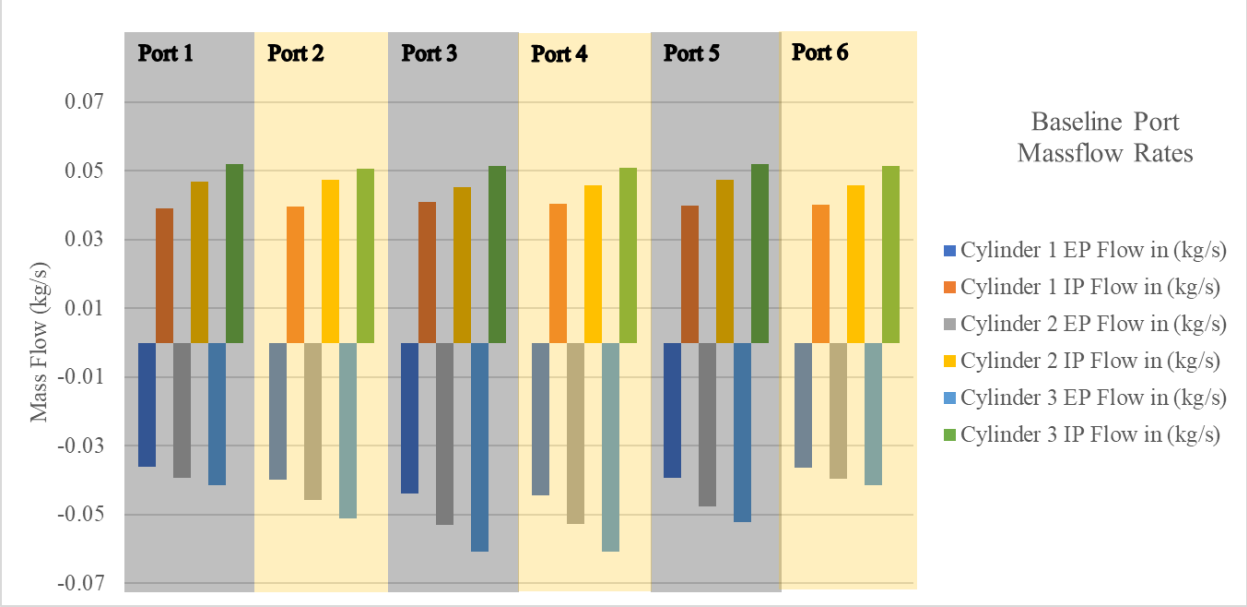

Figure 4.11. Baseline mass flow through each port of cylinders one, two, and three

Figure 4.11 shows cylinder three has the highest mass flow rate followed closely by cylinder two. Cylinder one has the lowest mass flow rate according to Figure 4.11 so this shows the need to redesign the manifolds for balanced mass flow rates through the engine. Tapering the intake manifold will decrease the volume of the flow path through the manifold for cylinders one and two thus, equalizing the flow.

Figure 4.12 shows the velocity magnitude extracted from three sections of the engine model. The order of the sections is top to bottom so the intake ports, middle of the cylinder, and exhaust ports are displayed in that order. Each section of Figure 4.12 also has three circular contour plots for cylinders three, two, and one, respectively.

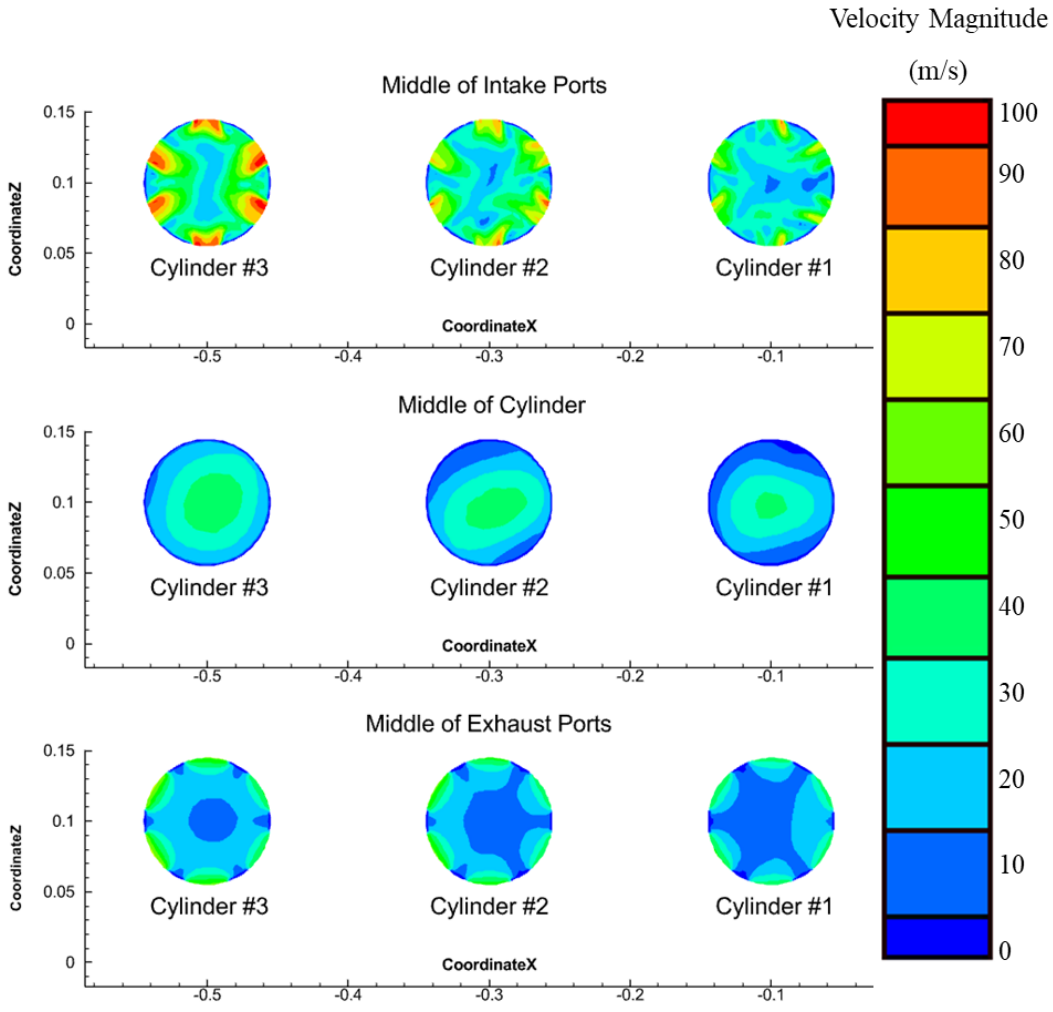

Figure 4.12. Baseline velocity magnitude (m/s) for different sections of the cylinder

Figure 4.12 shows the magnitude of the flow velocity through the engine. From the intake ports of cylinder three contour plot it is observed that the flow entering cylinder three is at higher a velocity than the other three cylinders. Higher flow velocities in cylinder three correspond to the higher mass flow rates observed in Figure 4.11. The exhaust ports show that cylinder three has a higher velocity exiting the ports compared to cylinders two and one. The exhaust ports for cylinder two show that more flow is going through the piston on the side close to cylinder three. However, rather than the velocity being higher for the side closest to cylinder three, the exhaust ports of cylinder one has a higher velocity close to the front of the engine.

Figure 4.13 shows the velocity magnitude for a vertical (XY) plane section of cylinders one, two, and three. The order of the cylinders from left to right is cylinder three, two, and one. On the right side of Figure 4.13 is the color bar for the contour plot which shows the values of the velocity magnitude within the cylinder on the XY plane.

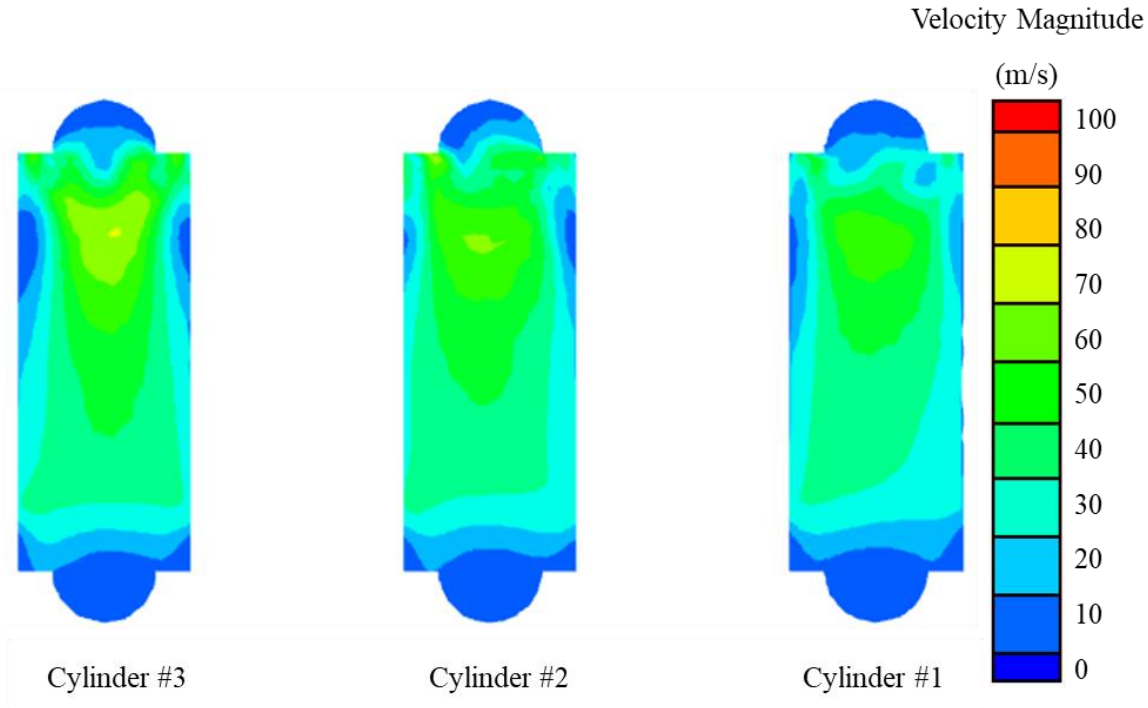

Figure 4.13. Baseline velocity magnitude (m/s) on the XY plane for cylinders one through three

Figure 4.13 shows that the flow has higher velocity in cylinder three than the other two cylinders. Figure 4.12 showed that cylinder three had the highest velocity into the cylinders from the intake ports plane but Figure 4.13 shows the flow path from top to bottom of the cylinders. Figure 4.13 shows that the cylinders experience the highest velocity magnitudes in the center of each cylinder.

4.1.5 Swirl Circulation

Figure 4.14 shows Y-vorticity contour plots. Figure 4.14 is laid out similarly to Figure 4.12 where it has three sections that are separated by each section of the engine. The labels for each section appear above the contour plot. The three sections are from top to bottom the intake ports, middle of the cylinder, and exhaust ports. Like Figure 4.12, each section of Figure 4.14 has three sections of contour plots for cylinders three, two, and one, respectively.

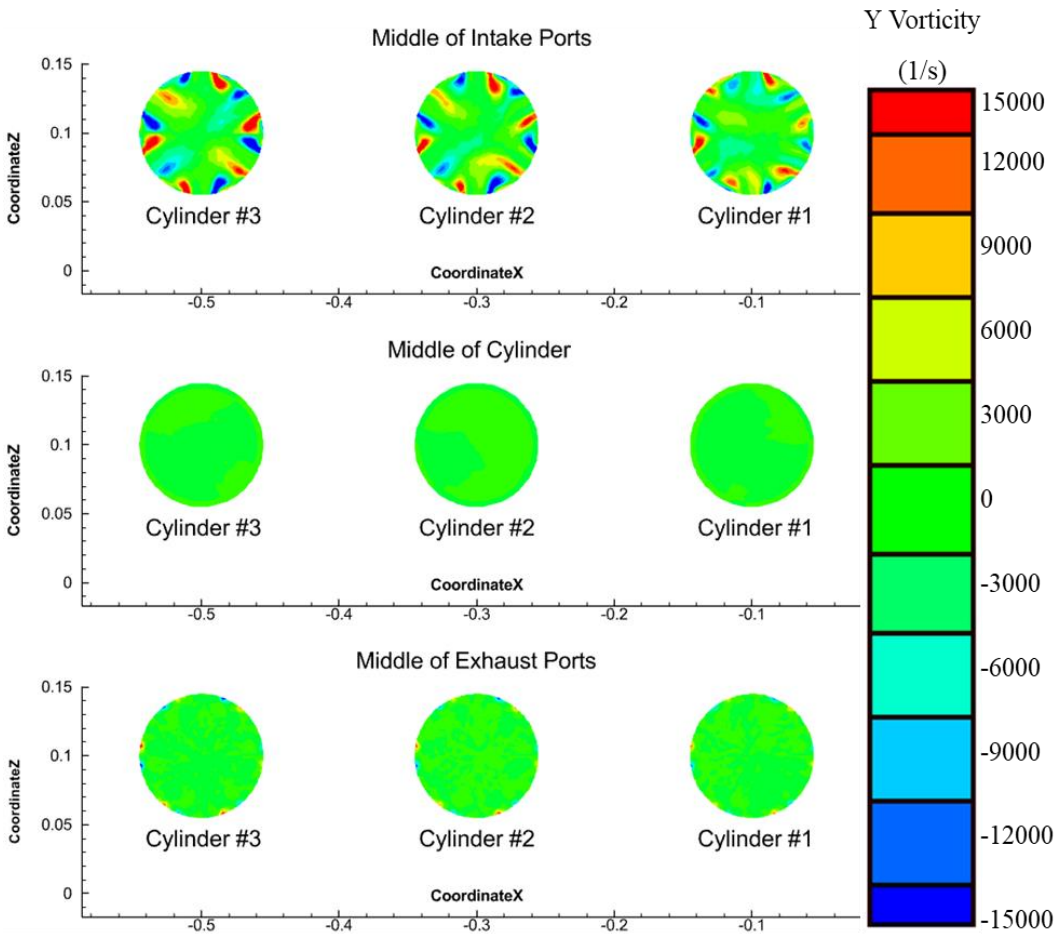

Figure 4.14. Baseline vorticity for the three different sections for cylinders one through three

Figure 4.14 shows that, for the baseline design, there are regions of high Y-vorticity at the plane of the intake ports. However, the Y-vorticity is nearly zero at the middle of the cylinder and at the exhaust ports. Near the intake ports, the regions of high Y-vorticity are caused by the shear-force as the high momentum fluid passes through the port and into the cylinder.

When integrating the Y-vorticity over each cylinder, it was found that there is little-to-no circulation which indicates that there is little-to-no-swirl. Table 4.3 shows the swirl calculated for each cylinder section. The left column of Table 4.3 shows each section of the engine. The middle column shows the cylinder number. The right column shows the value of swirl calculated for each cylinder section.

Table 4.3. Baseline swirl values for the three sections of the engine

Section	Cylinder	Swirl (m^2/s)
Middle of the intake ports	1	-0.1
	2	0.1
	3	0
Midway through the cylinder	1	0
	2	0
	3	0
Middle of the exhaust ports	1	0
	2	0
	3	-0.1

Table 4.3 shows that the swirl is low, on the order of 1E-3 to 1E-1 m^2/s, for each of the three cylinders. The swirl results seen from Table 4.3 were expected because the ports are straight and aligned with the radial direction of the cylinder (zero swirl angle). Modifying the ports to have non-zero swirl angle strengthens the swirling motion in the cylinder which was observed from the results of the swirl engine design.

4.1.6 Tumble Circulation

Figure 4.15 shows the Z-vorticity contour plot for cylinders three, two, and one from left to right. The cylinders all have a label underneath the contour plot identifying each cylinder. Like Figure 4.13, Figure 4.15 is based on the XY plane which is a vertical plane through the center of the engine. The right portion of Figure 4.15 shows the color bar values for the contour plot.

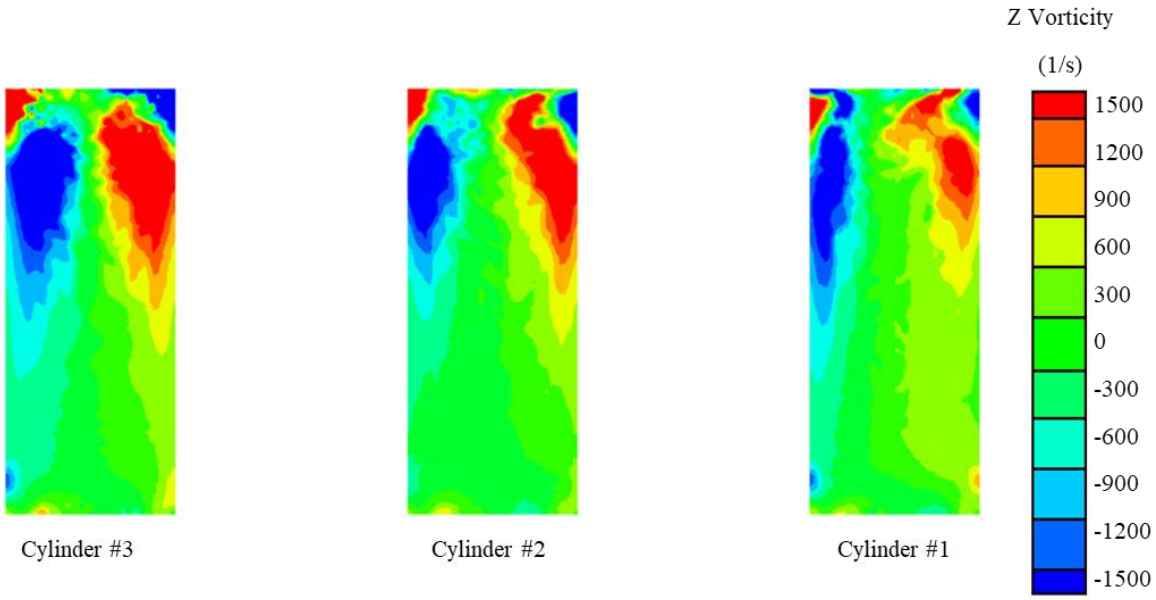

Figure 4.15. Baseline vorticity on the XY plane for cylinders one through three

Figure 4.15 shows what the in-cylinder tumble looks like. Figure 4.15 shows regions of high Z-vorticity on the right side of the cylinder and negative vorticity regions on the left side. The vorticity was calculated over a rectangular area within the cylinder. The rectangular area was two and a half millimeters way from the cylinder walls centered in the cylinder to filter out high vorticity due to wall shear stress. Figure 4.16 shows the original data plane followed by a rectangular region that matches the dimensions of the cylinder except for the circular region of the piston.

Similar to Figure 4.15, Figure 4.16 shows the Z-vorticity contour plot for the cylinders. However, Figure 4.16 shows the original data plane on the top and a rectangular zone that has the data interpolated on to it from the original data plane on the bottom. The right portion of Figure 4.16 shows the color bar values for the contour plot.

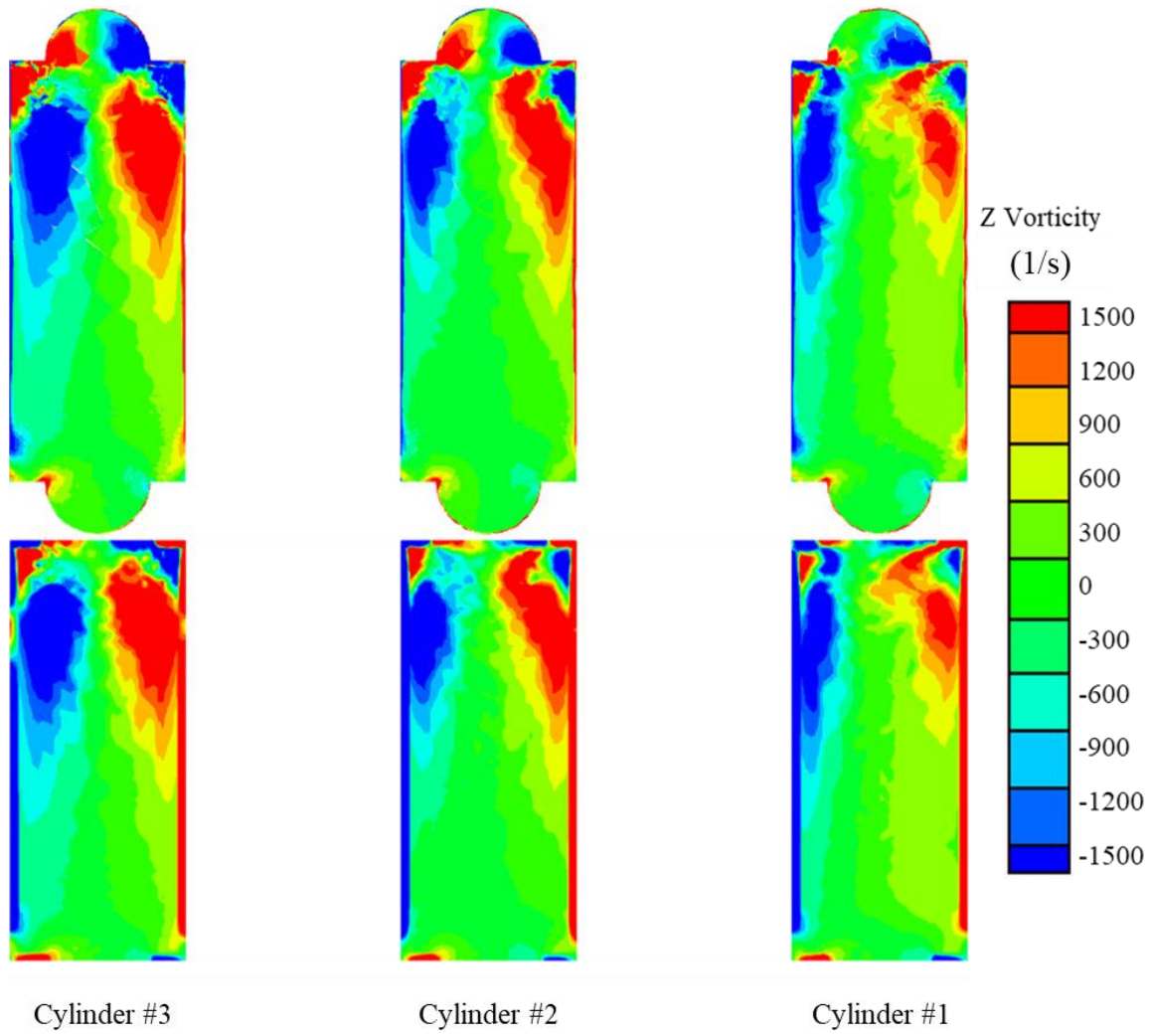

Figure 4.16. Baseline vorticity plot comparison of actual data to interpolated data

Figure 4.16 shows that the Z-vorticity near the walls of the cylinder is exaggerated in the interpolated data zones compared to the original data plane. Therefore, the rectangular zones that are two and a half millimeters away from the cylinder walls, shown in Figure 4.15, were chosen for calculating the tumble over.

When integrating the Z-vorticity over each cylinder, it was observed that because of the positive and negative circulations within the cylinder the overall tumble appeared to be very low. Therefore, to get around this issue two rectangular regions were created within the cylinder to calculate the positive circulation, the right side, and the negative circulation, the left side, so that

the values would not cancel each other out. Table 4.4 shows the cylinder number in the left column, the rectangular section in the middle column, and the tumble value in the right column.

Table 4.4. Baseline tumble values for cylinders one, two, and three

Cylinder	Rectangular Region Location	Tumble (m^2/s)
1	Left	-3.7
	Right	4.6
2	Left	-4.0
	Right	4.4
3	Left	-6.0
	Right	5.3

Table 4.4 shows that the tumble has a larger magnitude than the swirl for the baseline engine design. The baseline engine design did not have any intentional design characteristics to increase swirl. Therefore, it is expected that by adding a tilt angle to the ports the tumble values will increase from these baseline values. Lastly, Table 4.4 shows that the tumble values were close in magnitude between the left and the right rectangles for each of the rectangular regions.

4.1.7 Turbulent Kinetic Energy (TKE)

The volume average TKE was calculated to determine the amount of TKE within each cylinder of the engine design. Table 4.5 shows the cylinder number in the column on the left and the volume average TKE in the column on the right.

Table 4.5. Baseline volume average TKE for cylinders one, two, and three

Cylinder	Volume Average TKE (m^2/s^2)
1	225
2	313
3	435

Table 4.5 shows that the cylinder with the highest TKE was cylinder three. This is expected since cylinder three had the most mass flow to it. The volume average TKE was calculated using just the cylinders volume so the following Figures of TKE contour plots show more TKE than what was calculated in the average for Table 4.5.

Figure 4.17 is a contour plot that shows the TKE on the XY plane of the middle of each cylinder. The cylinders are ordered from left to right three, two, and one. The color bar on the right of Figure 4.17 shows the values for each color in m^2/s^2 on the contour plot.

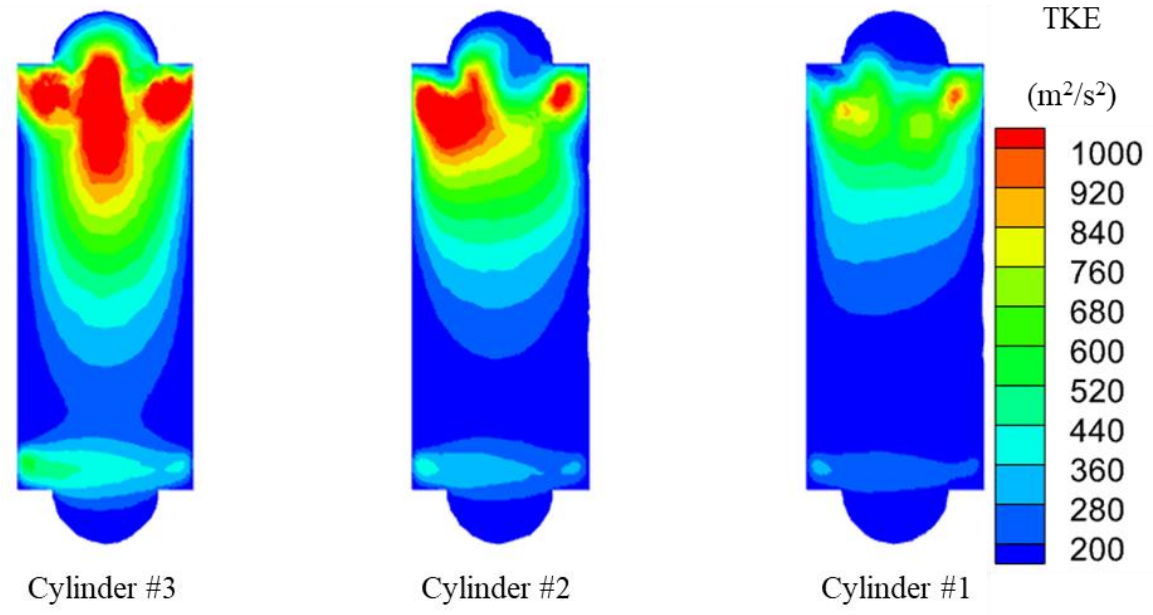

Figure 4.17. Baseline TKE on the XY plane for the middle of each cylinder

Figure 4.17 shows that cylinder three has the highest TKE values. Cylinder three having the most TKE makes sense since it also had the most mass flow rate into the cylinder. Figure 4.17 shows the areas on the XY plane in the cylinders that are experiencing the highest flow energy.

Figure 4.18 is a contour plot of TKE on the ZX plane for the middle of the intake ports of each cylinder. The cylinders are ordered from left to right three, two, and one. The color bar on the right of Figure 4.18 shows the values for each color in m^2/s^2 on the contour plot.

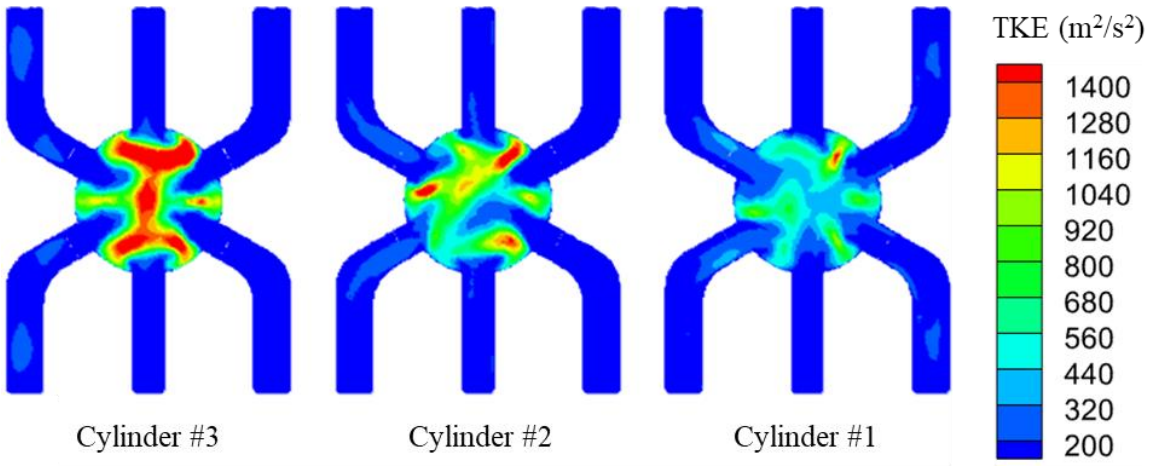

Figure 4.18. Baseline TKE on the ZX plane of the middle of the intake ports for each cylinder

Figure 4.18 shows that intake ports do not have uniform TKE values across each cylinder. Cylinder three has the highest TKE in the center of the cylinder while the other cylinders are experiencing higher TKE in other regions of the cylinder. Figure 4.18 shows the regions of the ZX plane in the middle of the intake ports of the cylinders that are experiencing the highest flow energy.

Figure 4.19 is a contour plot of TKE on the ZX plane for the middle of each cylinder. The cylinders are ordered from left to right three, two, and one. The color bar on the right of Figure 4.19 shows the values for each color in m^2/s^2 on the contour plot.

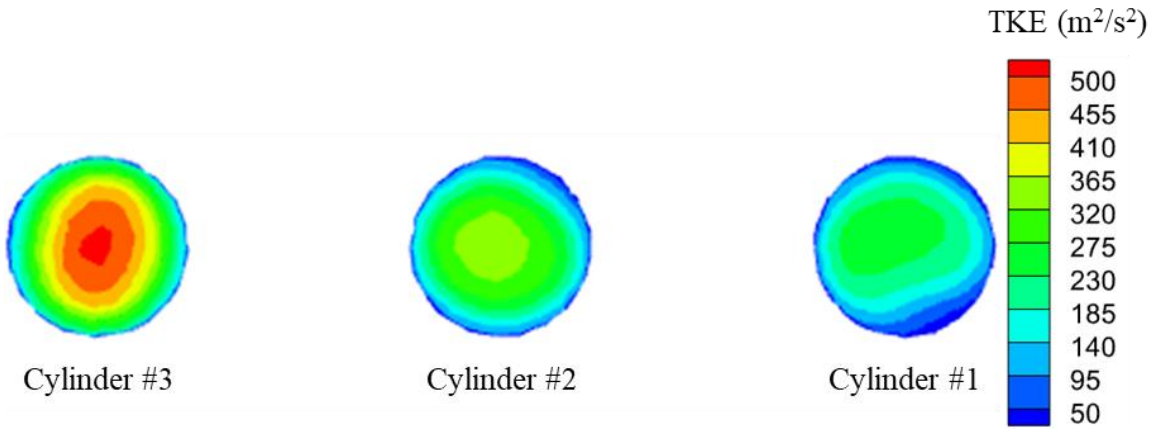

Figure 4.19. Baseline TKE on the ZX plane of the middle of the cylinders

Figure 4.19 shows the regions within the middle of the cylinder that are experiencing the highest flow energy. Similar to Figures 4.17 and 4.18, the highest TKE is in the center of the cylinders. Figure 4.19 shows that the cylinders experience TKE from the center out to the cylinder walls.

Figure 4.20 is a contour plot of TKE on the ZX plane for the middle of the exhaust ports for each cylinder. The cylinders are ordered from left to right three, two, and one. The color bar on the right of Figure 4.20 shows the values for each color in m^2/s^2 on the contour plot.

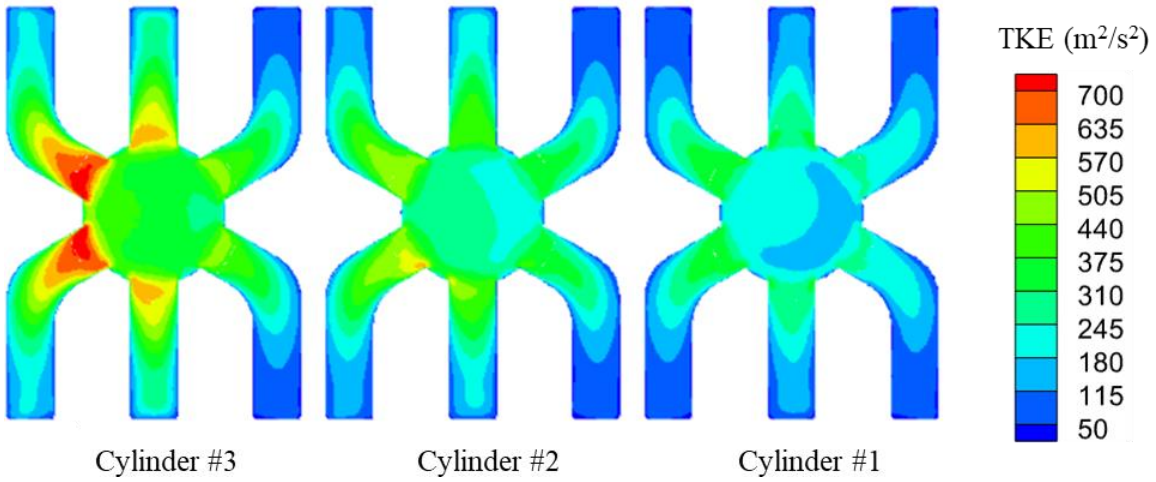

Figure 4.20. Baseline TKE on the ZX plane of the middle of the exhaust ports for each cylinder

Figure 4.20 shows the regions on the ZX plane of the exhaust ports that are experiencing the highest flow energy. Figure 4.20 shows that the exhaust ports furthest from the inlets of the intake manifold are experiencing the highest TKE. The two exhaust ports experiencing the highest TKE are exhaust ports three and four. Back in Figure 4.11 the mass flow through ports three and four are the highest so it makes sense that they experience the highest TKE.

Figure 4.21 is a contour plot of TKE on the YZ plane for the middle of cylinder one. The color bar on the right of Figure 4.21 shows the values for each color in m^2/s^2 on the contour plot. The top of Figure 4.21 is the intake side of the cylinder and the exhaust is the bottom of Figure 4.21.

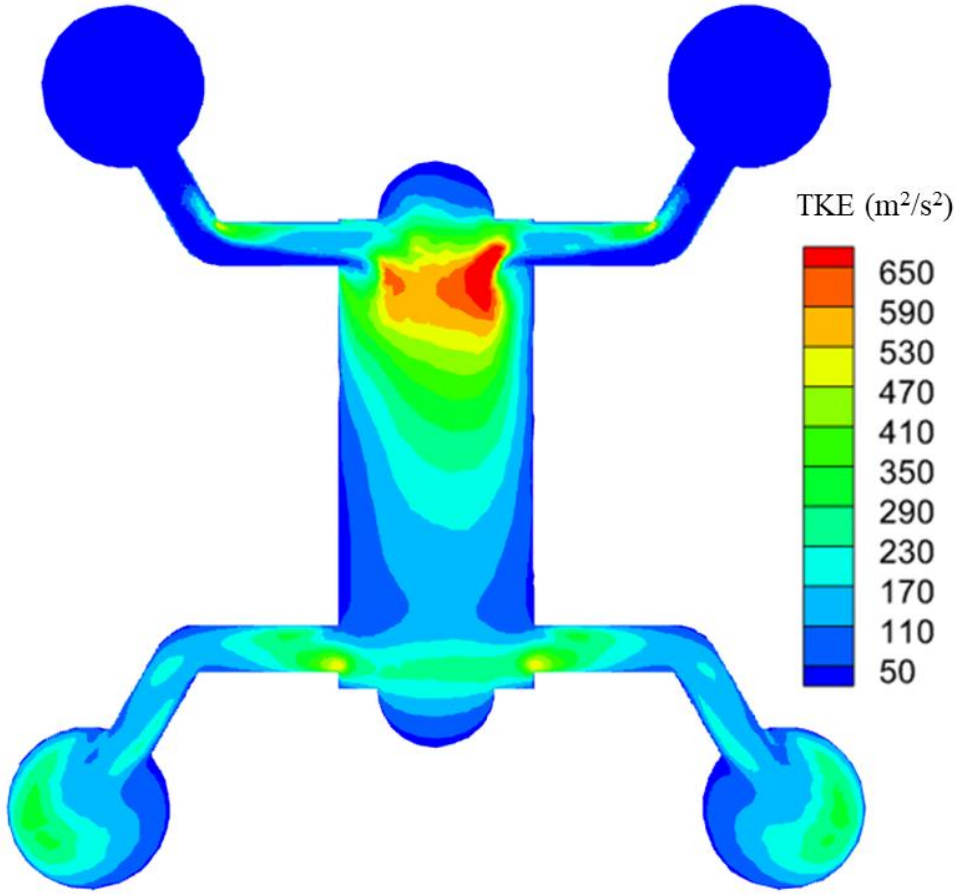

Figure 4.21. Baseline TKE on the YZ plane of the middle of cylinder one

Figure 4.21 shows that there are regions in the intake manifold runners that are experiencing higher TKE near the bends in the runners. Figure 4.21 also shows that the exhaust manifold and runners are experiencing higher TKE values. Figure 4.21 shows that the intake side of the cylinder experiences higher TKE than the exhaust side of the cylinder.

Figure 4.22 is a contour plot of TKE on the YZ plane for the middle of cylinder two. The color bar on the right of Figure 4.22 shows the values for each color in m^2/s^2 on the contour plot. The top of Figure 4.22 is the intake side of the cylinder and the exhaust is the bottom of Figure 4.22.

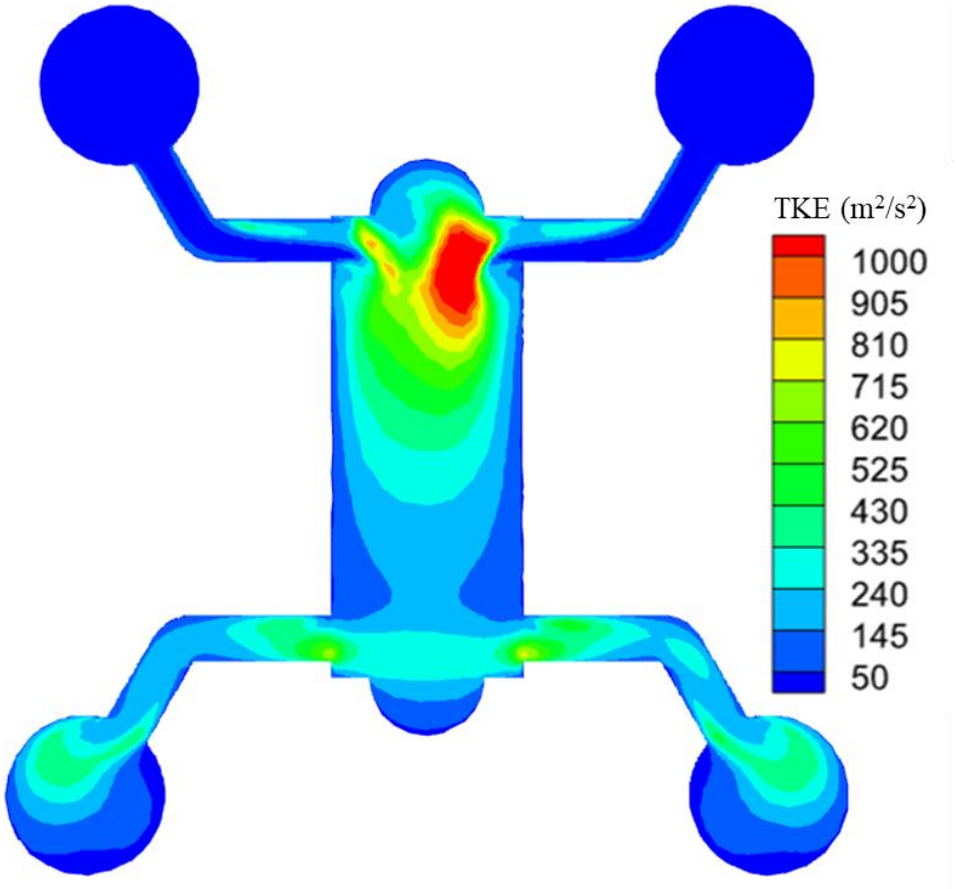

Figure 4.22. Baseline TKE on the YZ plane of the middle of cylinder two

Figure 4.22 shows that the regions in the intake manifold runners for cylinder two that are experiencing higher TKE are lower than that of cylinder one. The scale of the color bar is different for the contour plot of cylinders one and two. However, the magnitude of TKE experienced in cylinder two compared to the magnitude of the TKE in the cylinder two intake manifold runners is greater than that of cylinder one. Therefore, the TKE experienced near the bends of the intake manifold becomes less significant as the mass flow rate increases.

Figure 4.23 is a contour plot of TKE on the YZ plane for the middle of cylinder three. The color bar on the right of Figure 4.23 shows the values for each color in m^2/s^2 on the contour plot. The top of Figure 4.23 is the intake side of the cylinder and the exhaust is the bottom of Figure 4.23.

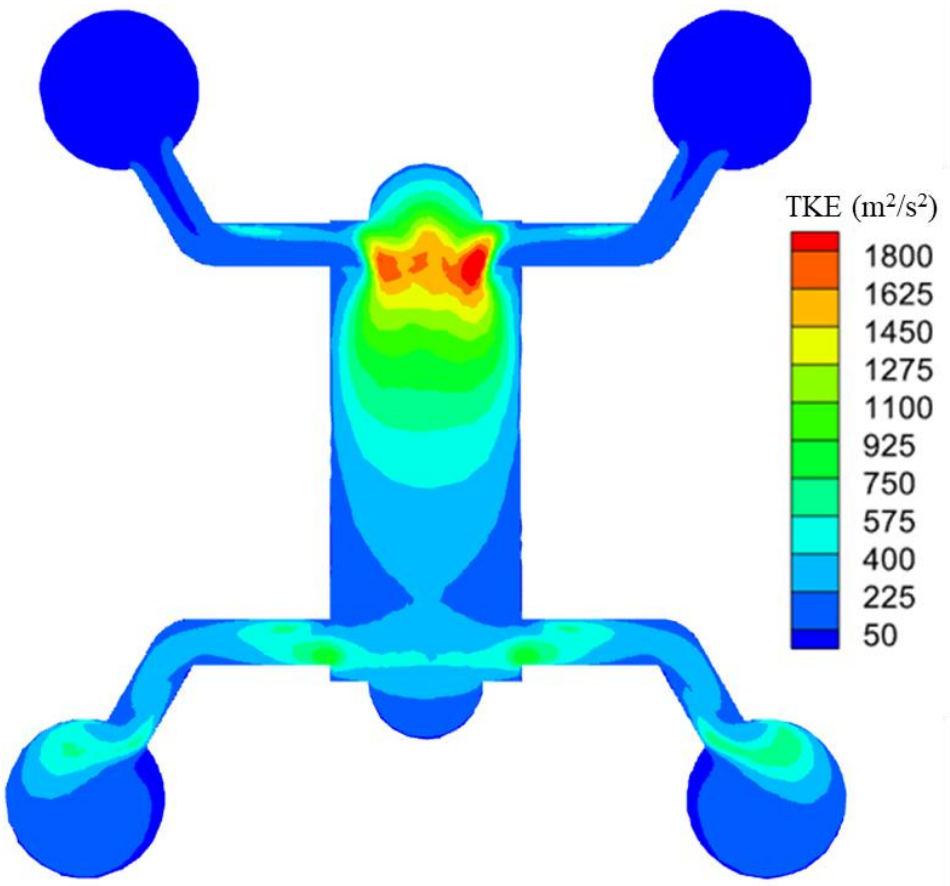

Figure 4.23. Baseline TKE on the YZ plane of the middle of cylinder three

Figure 4.23 shows a continuation of the trend seen from Figure 4.22 where the difference between the magnitude of TKE within the cylinder to the bends in the runners have increased. The scale of the color bar is higher for cylinder three than for cylinder two. Figure 4.23 shows that the highest TKE is occurring at the top of cylinder three near the intake ports.

4.1.8 Baseline Design Summary

The first engine model was made to create a baseline for cylinder and port mass flow rate, swirl, tumble, and TKE. The mass flow was highest for cylinder three which showed that the flow was not balanced. The baseline engine showed that the swirl was lowest for cylinder three which was also the cylinder with the highest mass flow. However, cylinder three did have the highest tumble and TKE.

4.2 Tapered Design

The goal for the second design of the engine was to balance the mass flow rates for each of the ports. It was hypothesized that by tapering the intake manifold the flow would become balanced. However, the desired results were not observed for this design. It is further hypothesized that in order to achieve a balanced mass flow for each of the ports that the physical size of the ports would need to vary from port to port.

4.2.1 Geometric Model

Figure 4.24 shows the internal geometry for the tapered intake manifold design of the opposed piston engine. The blue components in Figure 4.24 shows the intake manifold and intake manifold runners. The orange components in Figure 4.24 represent the cylinders and a portion of the intake and exhaust ports. The red component in Figure 4.24 represents exhaust manifold runners, exhaust manifold, and an exhaust collector.

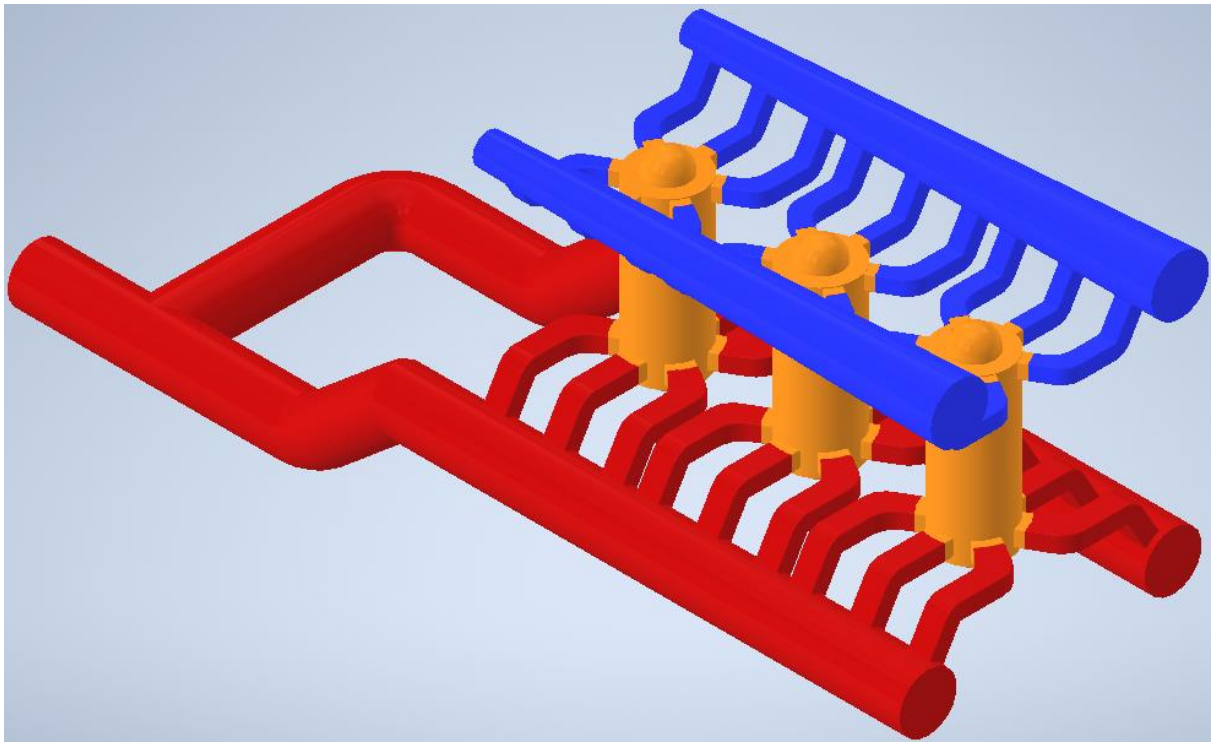

Figure 4.24. CAD model for the tapered manifold opposed piston engine

Figure 4.24 shows the tapered intake manifold design with straight ports. This design was expected to produce a more balanced mass flow rate to each of the cylinders. Like the baseline model, this model was not designed for improving swirl, tumble, or TKE.

4.2.2 Mesh and Boundary Conditions

Figure 4.25 is an isometric view of the mesh for the tapered intake manifold design. The scale is located at the bottom of Figure 4.25. The top of the model in Figure 4.25 is the tapered intake manifold. The runners from the intake and exhaust manifolds have a smaller mesh size than most of the other regions which makes them appear as black sections. The exhaust manifold is the bottom component in Figure 4.25. The cylinders are in between the intake and exhaust manifolds in Figure 4.25.

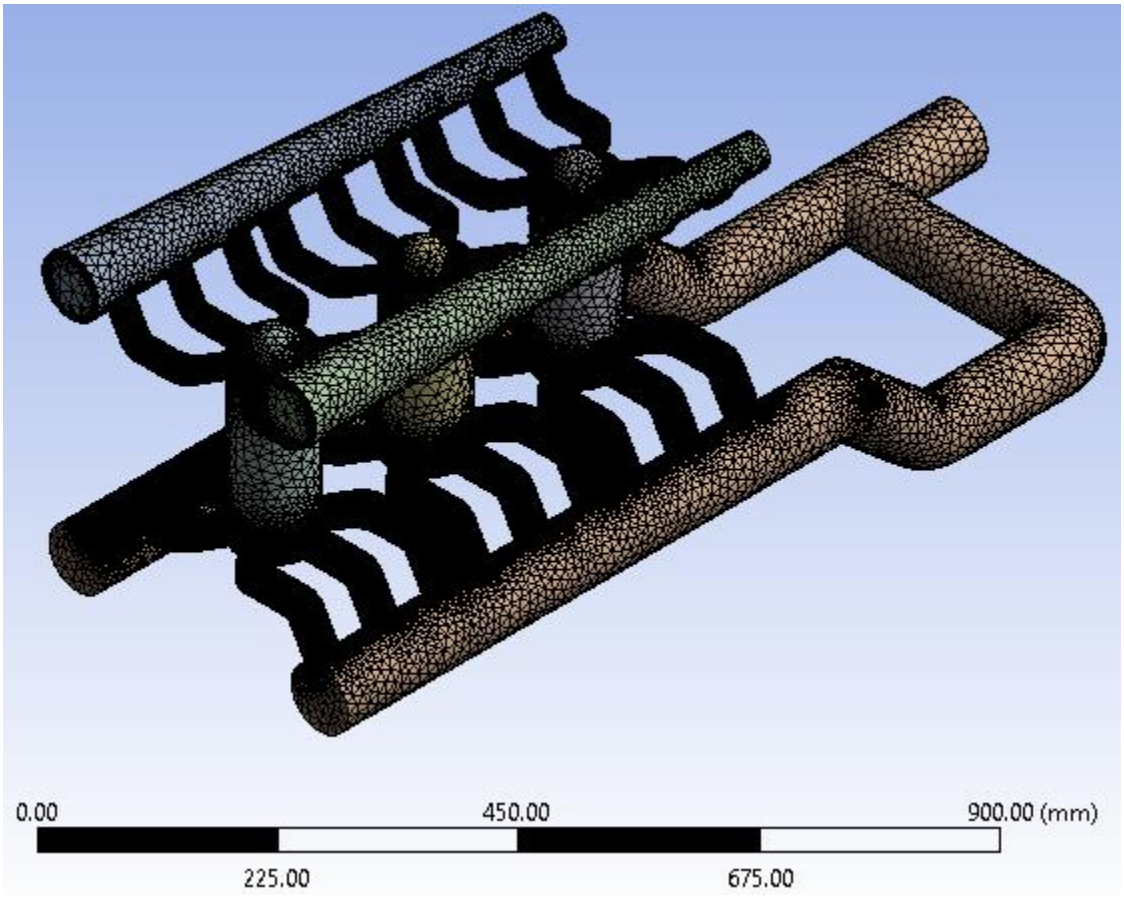

Figure 4.25. Isometric view of the meshed tapered manifold opposed piston engine

The element size for the mesh seen in Figure 4.25 was set to the same size and sizing constraints as the baseline model. The mesh for the tapered model used tetrahedral elements and inflation layers just like the baseline model. The meshing software automatically resizes the elements to be smaller in complex geometry regions which is why the runners for the intake and exhaust manifolds appear to be black. The mesh for the tapered manifold design had 14,580,224 total elements.

Figure 4.26 shows the right half of the meshed tapered manifold engine cut down the middle. The inflation layers for the mesh can be seen in the bottom left corner of Figure 4.26 which is a cross section of a portion of the exhaust manifold. The scale bar is at the bottom of Figure 4.26 to show how long the model is in millimeters.

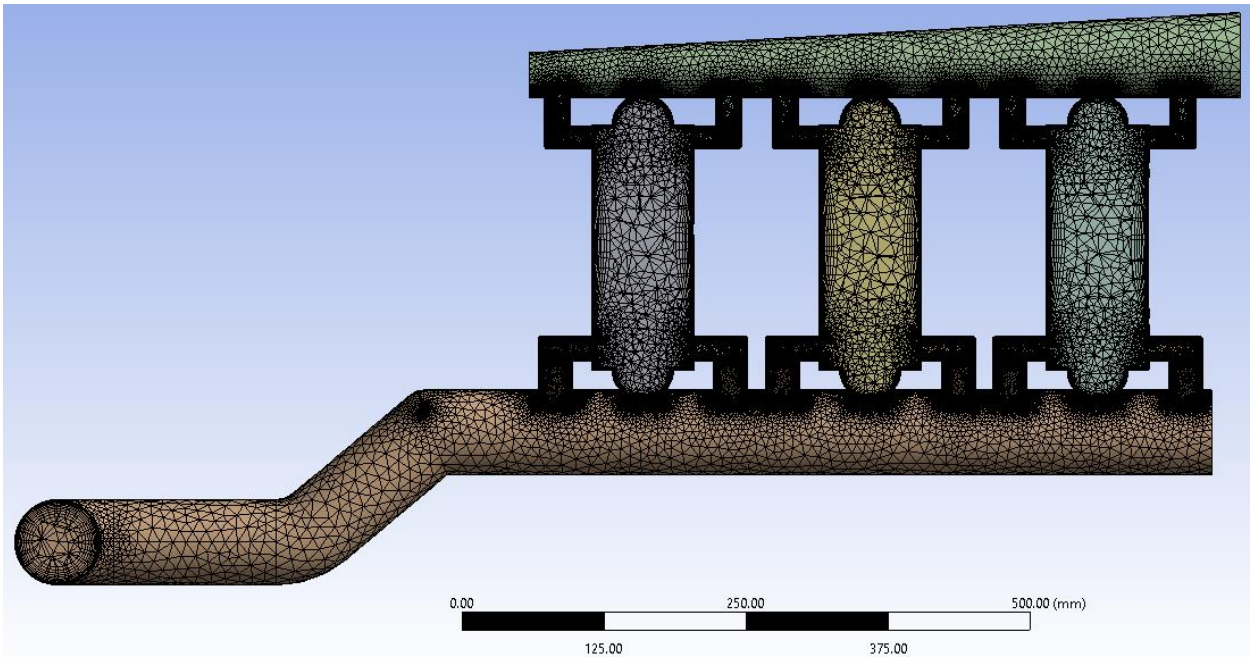

Figure 4.26. Section view of the meshed tapered manifold opposed piston engine

Figure 4.26 shows the taper for the intake manifold and the element sizes decreasing from cylinder one to three, moving from right to left. Figure 4.26 also shows the detail of the mesh inside of the cylinders. The meshing software also decreases the size of the elements near the walls to get more accurate results near the walls.

Figure 4.27 is a cross sectional view of one of the intake manifold runners. Figure 4.27 has the scale bar under the cross-sectional view of the runner. The scale bar is ten millimeters which is half the length or width of the port size.

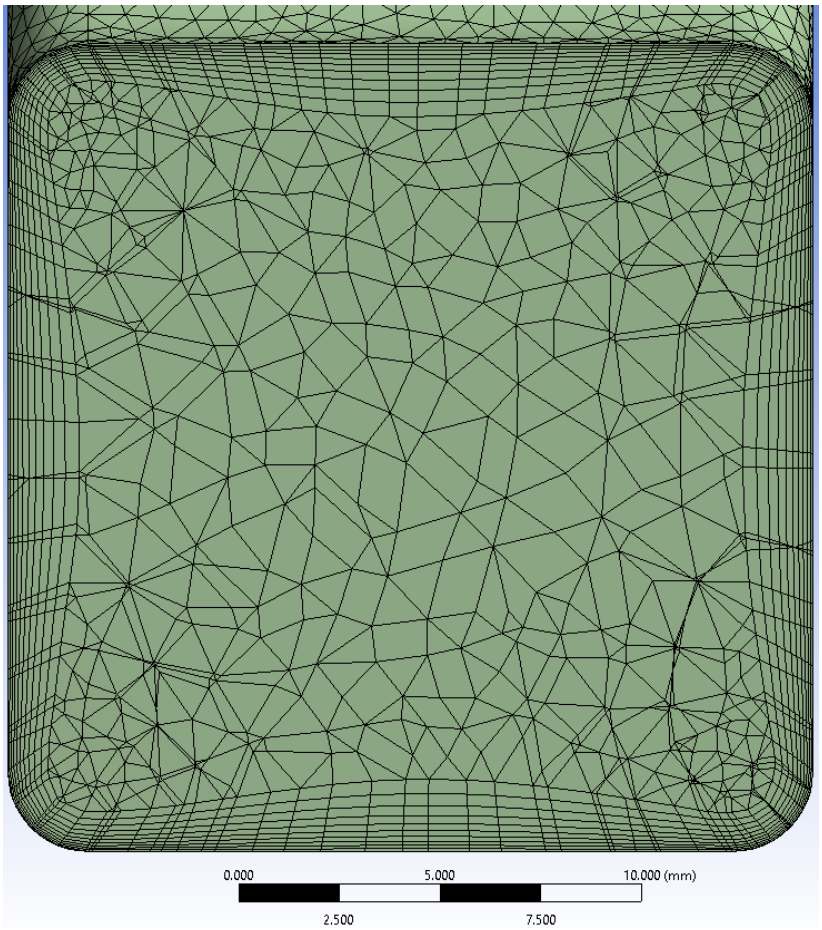

Figure 4.27. Section view of the meshed tapered manifold intake runner for the opposed piston engine

Figure 4.27 shows a close-up of the inflation layers of an intake manifold runner so that the elements are easier to see. Figure 4.27 shows that the layers become thinner closer to the walls. The inflation layers for the mesh of the tapered manifold design had the same settings as for the baseline design. Figure 4.27 shows that the corners of the ports have smaller elements than the center area of the intake ports.

Figures 4.28 and 4.29 show boundary conditions for the tapered manifold design. Figure 4.28 shows the wall boundaries, highlighted in red. The wall boundaries were setup the same as the baseline model. The letter tags seen in Figure 4.28 label each component of the model and correspond to the names in the list in the top left corner of Figure 4.28.

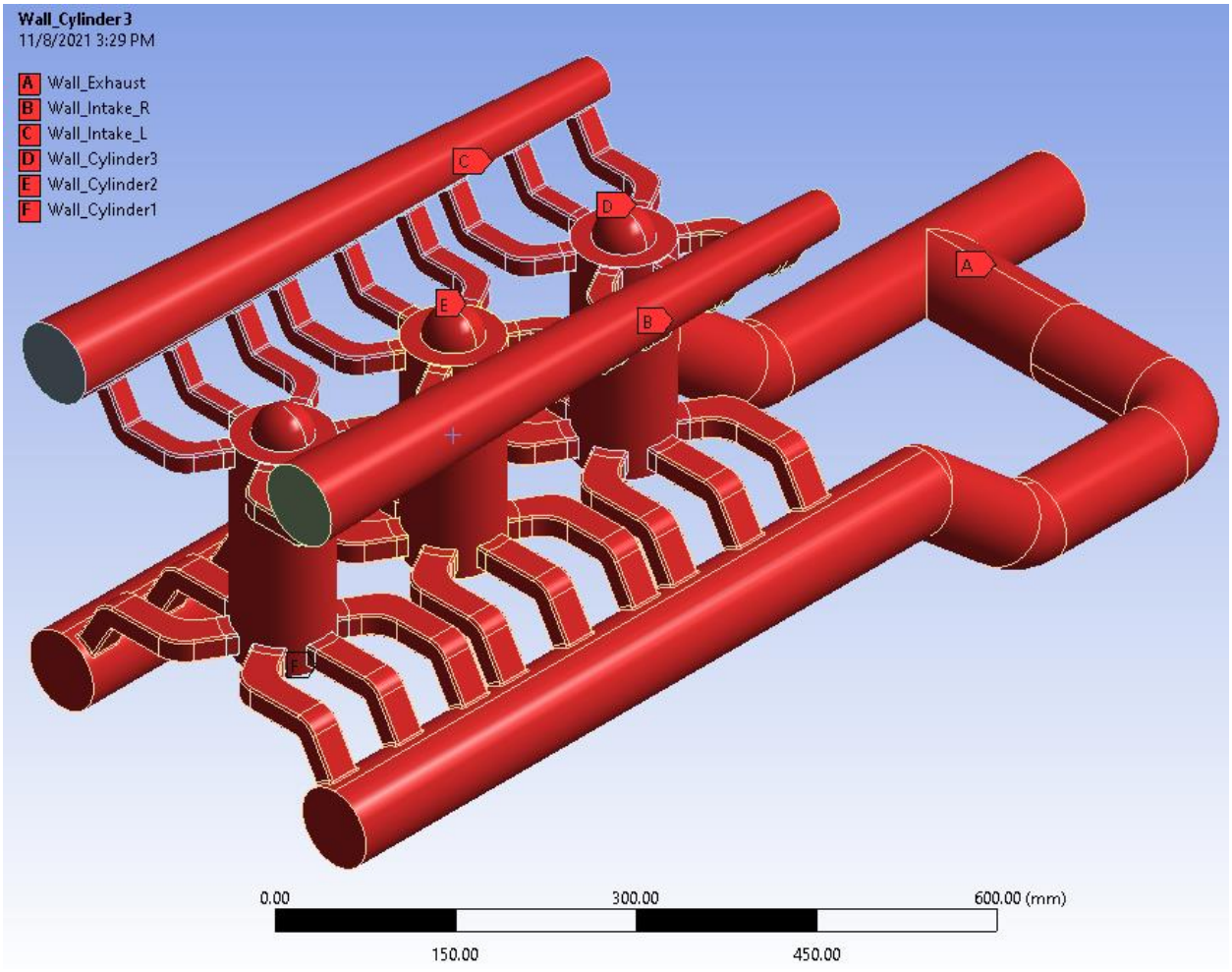

Figure 4.28. Tapered model wall Boundary conditions

Figure 4.28 shows the different components of the model by name using the letter tags. The unselected areas in Figure 4.28, the non-red areas, are the pressure inlets to the model. By selecting all the outer surfaces and naming them as walls, Fluent will simulate the flow inside of those boundaries.

Figure 4.29 shows the pressure inlet and outlet boundary conditions. The left side of Figure 4.29 shows the pressure inlets labeled with the letter tag A. The middle of Figure 4.29 shows the legend for the letter tags. The right side of Figure 4.29 shows the pressure outlet on the backside of the engine with the letter tag B.

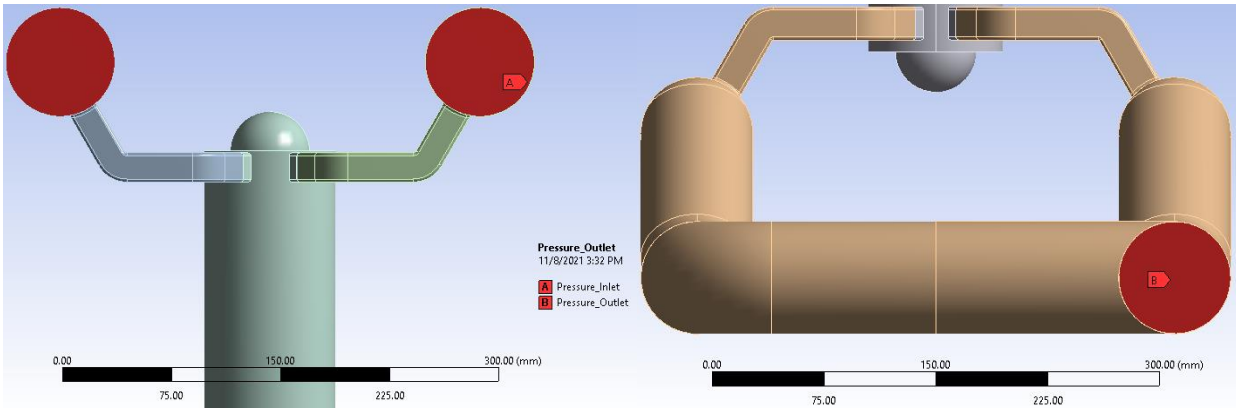

Figure 4.29. Tapered model inlet and outlet boundary conditions

The same pressure as the baseline model was applied to the inlets which was 41.4 kPa (6 psi) gage pressure. The pressure applied to the outlet was atmospheric pressure, zero gage pressure. The temperature of the pressure inlet and outlet was 320 Kelvin and 300 Kelvin.

4.2.3 Balance of Mass Flow

Figure 4.30 shows the mass flow of air through each of the intake and exhaust ports. The intake ports have a positive mass flow rate (top side of the bar chart), and the exhaust ports have a negative mass flow rate (bottom side of the bar chart). Figure 4.30 uses different colored bars for each cylinder as seen in the legend on the right side of Figure 4.30. Across the top of Figure 4.30 are labels inside shaded rectangles to label the different ports, one through six for each cylinder.

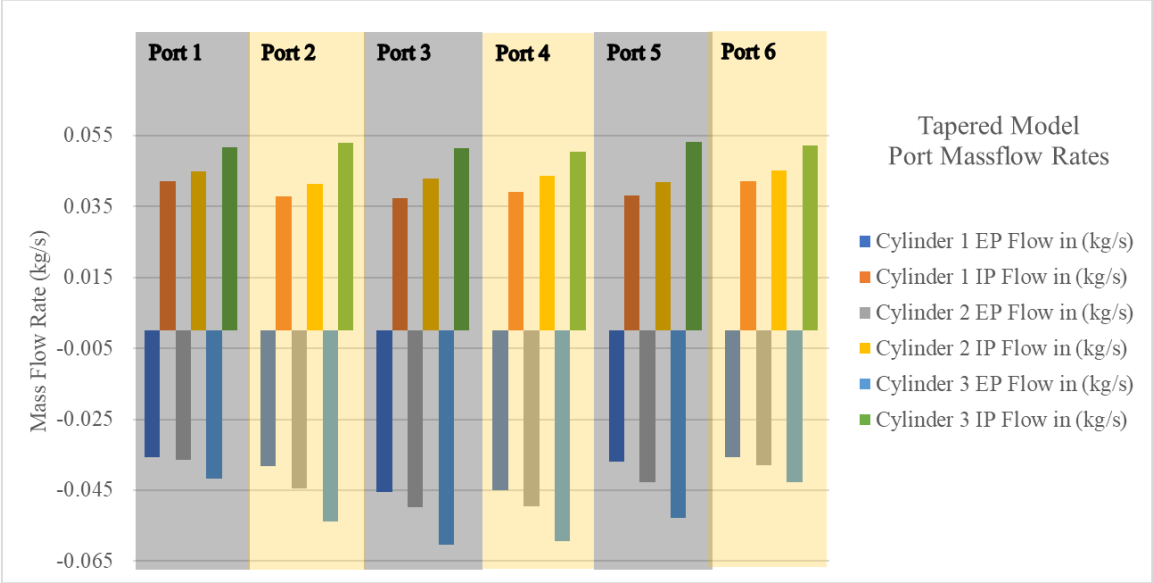

Figure 4.30. Tapered model mass flow through each port of cylinders one, two, and three

Figure 4.30 shows that cylinder three has the highest mass flow rate even with the tapered manifold. Cylinder one and two have mass flow rates that are closer to the same than the baseline model. However, the cylinder three mass flow rate was even higher for the tapered manifold model than for the baseline model. Tapering the intake manifold was expected to reduce the mass flow rate to cylinder three because of the decreased volume of the flow path through the manifold. Therefore, the ports cross sectional area in the manifold would need to be decreased to further attempt to reduce the mass flow rate in order to balance the mass flow rate. The alternative to reducing port size for cylinder three is to increase the port size for the other two cylinders.

Figure 4.31 shows the velocity magnitude in m/s extracted from three sections of the engine model. The order of the sections is top to bottom intake ports, middle of the cylinder, and exhaust ports. Each section of Figure 4.31 also has three circular contour plots for cylinders three, two, and one, from left to right. The color bar on the right of Figure 4.31 shows the values for velocity magnitude.

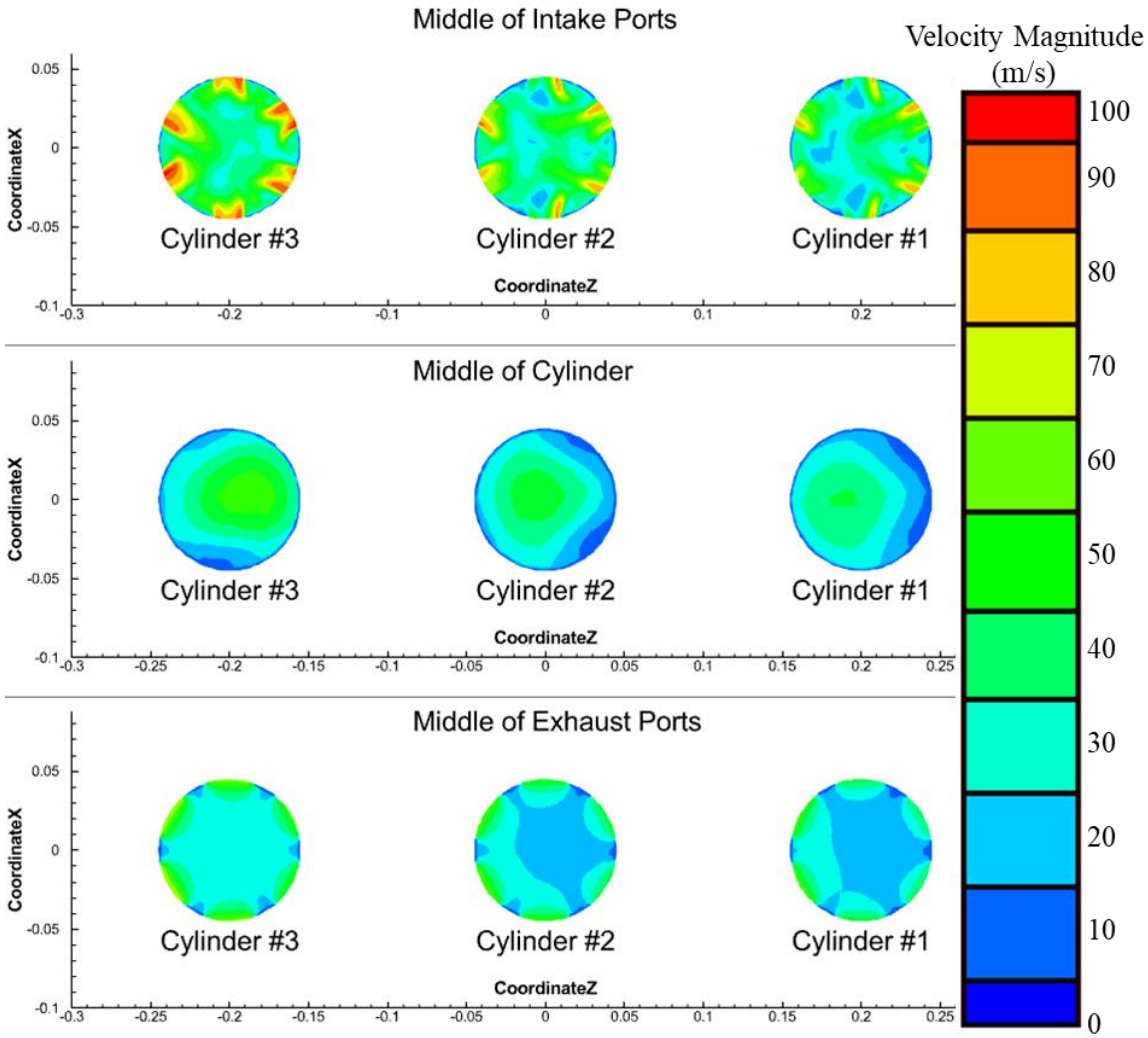

Figure 4.31. Tapered model velocity magnitude (m/s) for different sections of the cylinder

Figure 4.31 shows the magnitude velocity of the flow through three sections of the engine. From the intake ports of cylinder three contour plot it is observed that the flow entering cylinder three is at higher a velocity than the other three cylinders. Higher flow velocities in cylinder three correspond to the higher mass flow rates observed in Figure 4.30. The exhaust ports show that cylinder three has a higher velocity exiting the ports compared to cylinders two and one. The exhaust ports for cylinder two show that more flow is going through the piston on the side close to cylinder three. However, rather than the velocity being higher for the side closest to cylinder three, the exhaust ports of cylinder one has a higher velocity close to the front of the engine.

Figure 4.32 shows the velocity magnitude for the middle of the cylinders one, two, and three. The order of the cylinders from left to right is cylinder three, two, and one. On the right side of Figure 4.32 is the color bar for the contour plot which shows the values of the velocity magnitude for the plane in the middle of the cylinders.

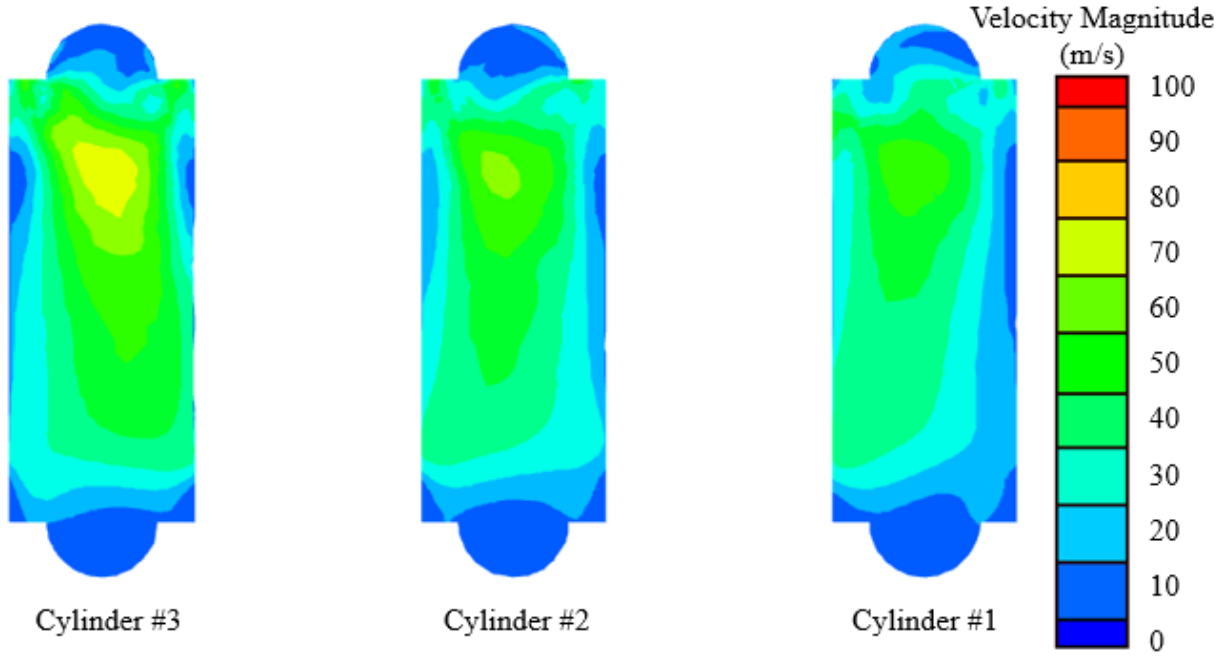

Figure 4.32. Tapered model velocity magnitude (m/s) on the XY plane for cylinders one through three

Figure 4.32 shows that the flow has higher velocity in cylinder three than the other two cylinders. Figure 4.31 showed that cylinder three had the highest velocity into the cylinders from the intake ports plane but Figure 4.32 shows the flow path from top to bottom of the cylinders. Figure 4.32 shows that the cylinders experience the highest velocity magnitudes in the center of each cylinder near the intake ports. The velocity magnitude through cylinder three for the tapered manifold design is higher than the baseline model.

4.2.4 Swirl Circulation

Figure 4.33 shows Y-vorticity contour plots with units of 1/s. Figure 4.33 is laid out similarly to Figure 4.31 where it has three sections that are separated by each section of the engine. The labels for each section appear above the contour plot. The three sections are from top to bottom the intake ports, middle of the cylinder, and exhaust ports. Like Figure 4.31, each section of Figure 4.33 has three sections of contour plots for cylinders three, two, and one, respectively.

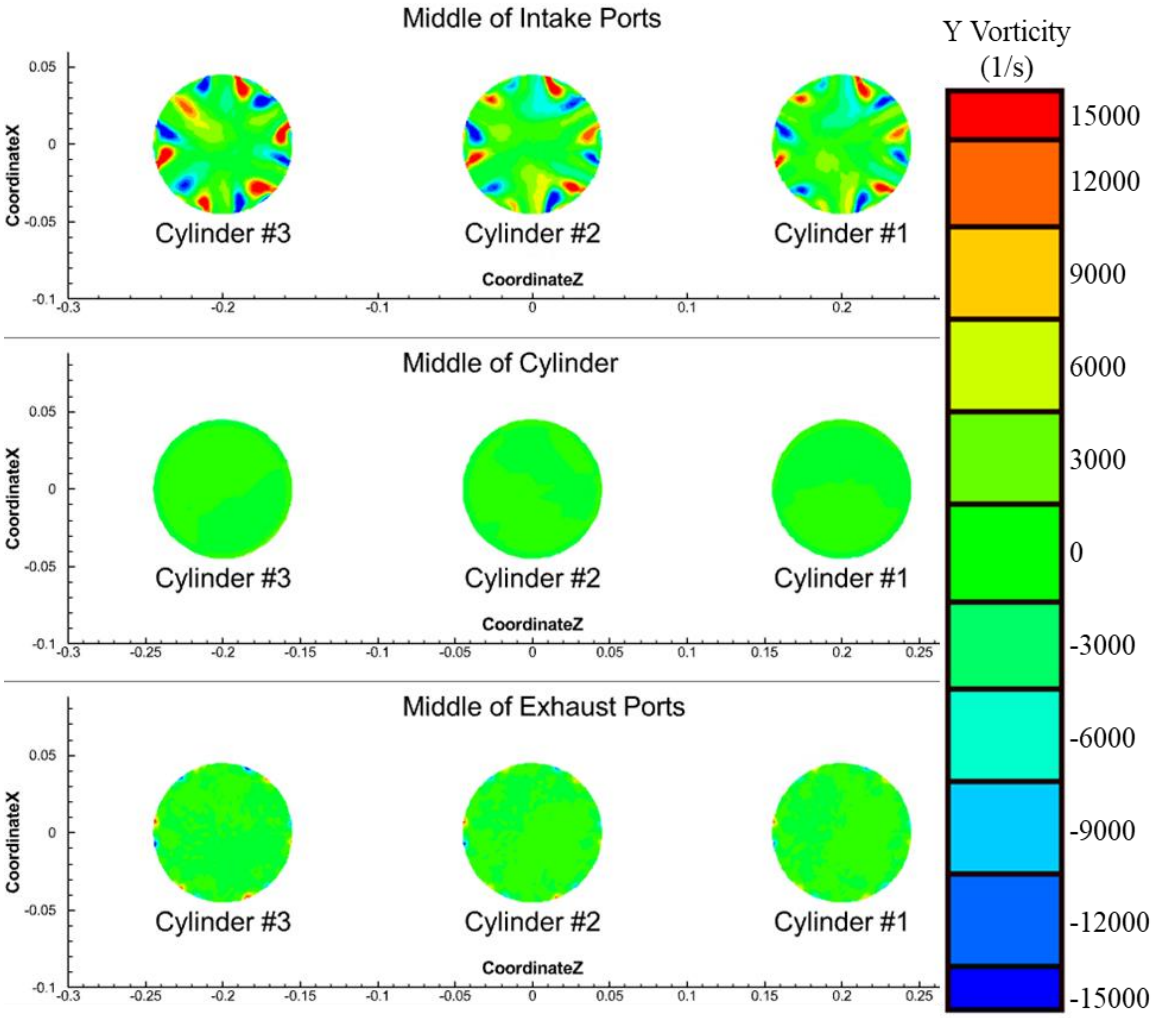

Figure 4.33. Tapered model vorticity for the three different sections for cylinders one through three

Figure 4.33 shows the swirl circulation for the tapered manifold design. Figure 4.33 also shows that there are regions of high Y-vorticity near the walls of the intake ports in the cylinders. The Y-vorticity is nearly zero at the middle of the cylinder and at the exhaust ports just like for the baseline design.

Table 4.6 shows the swirl calculated for each cylinder section. The left column of Table 4.6 shows each section of the engine. The second column from the left shows the cylinder number. The third column from the left shows the value of swirl in m^2/s for the baseline design. The last column shows the value of swirl in m^2/s for the tapered manifold design. The highlighted numbers in red for Table 4.6 represent a decrease in swirl magnitude compared to the baseline design. The numbers highlighted in green for Table 4.6 represent an increase of swirl magnitude from the baseline design.

Table 4.6. Comparison of swirl values for the three sections of the baseline and tapered design

Section	Cylinder	Swirl (m^2/s) Baseline	Swirl (m^2/s) Tapered
Middle of the intake ports	1	-0.1	0
	2	0.1	0
	3	0	-0.2
Midway through the cylinder	1	0	0
	2	0	0
	3	0	0
Middle of the exhaust ports	1	0	0.1
	2	0	0.1
	3	-0.1	-0.1

Integrating the Y-vorticity over each cylinder showed that there is little-to-no circulation which indicates little-to-no-swirl. Table 4.6 shows that the swirl was lower for most places in the cylinder for the tapered manifold design compared to the baseline design. There were portions of the tapered manifold design that had the swirl going in the opposite direction than that of the baseline design.

4.2.5 Tumble Circulation

Figure 4.34 shows the Z-vorticity in 1/s contour plot for cylinders three, two, and one from left to right. The cylinders all have a label underneath the contour plot identifying each cylinder. Like Figure 4.32, Figure 4.34 is based on a vertical plane through the center of the engine. The right portion of Figure 4.34 shows the color bar values for the contour plot.

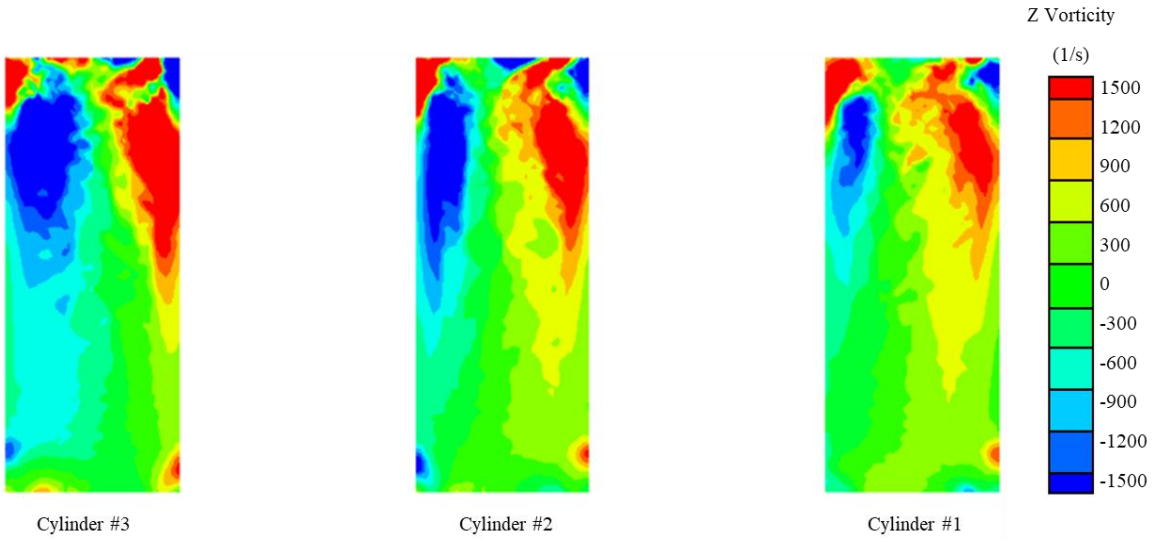

Figure 4.34. Tapered model vorticity on the XY plane for cylinders one through three

Figure 4.34 shows the in-cylinder tumble regions with red being positive tumble and blue being negative tumble. The smaller rectangular regions were used for Figure 4.34 because of the reasons discussed on page 62. The tapered manifold design produced tumble in the same direction as the baseline model and roughly the same amount.

The left column of Table 4.7 shows the cylinder number. The second column from the left shows the cylinder number. The third column from the left shows the value of tumble in m^2/s for the baseline design. The last column shows the value of tumble in m^2/s for the tapered manifold design. The highlighted numbers in red for Table 4.7 represent a decrease in tumble magnitude compared to the baseline design. The numbers highlighted in green for Table 4.7 represent an increase of tumble magnitude from the baseline design.

Table 4.7. Comparison of tumble values for the three sections of the baseline and tapered design

Cylinder	Rectangular Region Location	Tumble (m^2/s) Baseline	Tumble (m^2/s) Tapered
1	Left	-3.7	-0.7
	Right	4.6	6.0
2	Left	-4.0	-4.1
	Right	4.4	6.2
3	Left	-6.0	-7.3
	Right	5.3	4.8

The magnitude for tumble increased for all but two regions of the tapered manifold design in comparison to the baseline design. The baseline engine and tapered manifold designs did not have any intentional design characteristics to increase tumble. Lastly, Table 4.7 shows that the tumble values for the tapered manifold design were increasing in magnitude from cylinder one to cylinder three.

4.2.6 Turbulent Kinetic Energy (TKE)

The volume average TKE was calculated to determine the amount of TKE within each cylinder for both the baseline and tapered manifold engine designs. Table 4.8 shows the cylinder number in the column on the left. The middle column shows the volume average TKE in m^2/s^2 for the baseline design. The right column shows the volume average TKE in m^2/s^2 for the tapered manifold design. The highlighted numbers in red for Table 4.8 represent a decrease in TKE compared to the baseline design. The numbers highlighted in green for Table 4.8 represent an increase in TKE from the baseline design.

Table 4.8. Comparison of volume average TKE for the baseline and tapered designs of cylinders one through three

Cylinder	Volume Average TKE Baseline (m^2/s^2)	Volume Average TKE Tapered (m^2/s^2)
1	225	231
2	313	271
3	435	359

Table 4.8 shows that the cylinder with the highest TKE was cylinder three for both the baseline and the tapered manifold design. The TKE for cylinder one of the tapered manifold design increased from the value of the baseline design. The TKE for cylinders two and three of the tapered manifold design decreased from the values of the baseline design.

Figure 4.35 is a contour plot that shows the TKE on a vertical plane through the middle of each cylinder. The cylinders are ordered from left to right three, two, and one. The color bar on the right of Figure 4.35 shows the values for each color in m^2/s^2 on the contour plot.

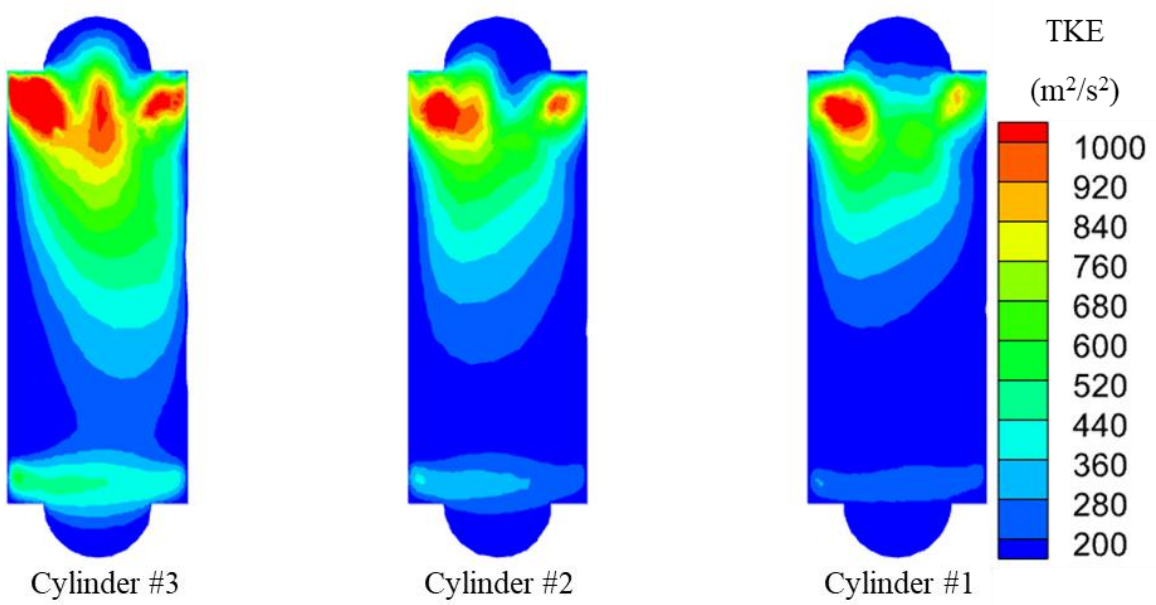

Figure 4.35. Tapered model TKE on a vertical plane for the middle of each cylinder

Figure 4.35 shows that cylinder three has the highest TKE values just like for the baseline design. The regions in the cylinder that had the highest values of TKE were near the intake ports of the cylinders. The TKE was lower for each cylinder except for two regions near the intake ports of cylinder one when comparing the tapered design to the baseline design.

Figure 4.36 is a contour plot of TKE on the ZX plane for the middle of the intake ports of each cylinder. The cylinders are ordered from left to right three, two, and one. The color bar on the right of Figure 4.36 shows the values for each color in m^2/s^2 on the contour plot.

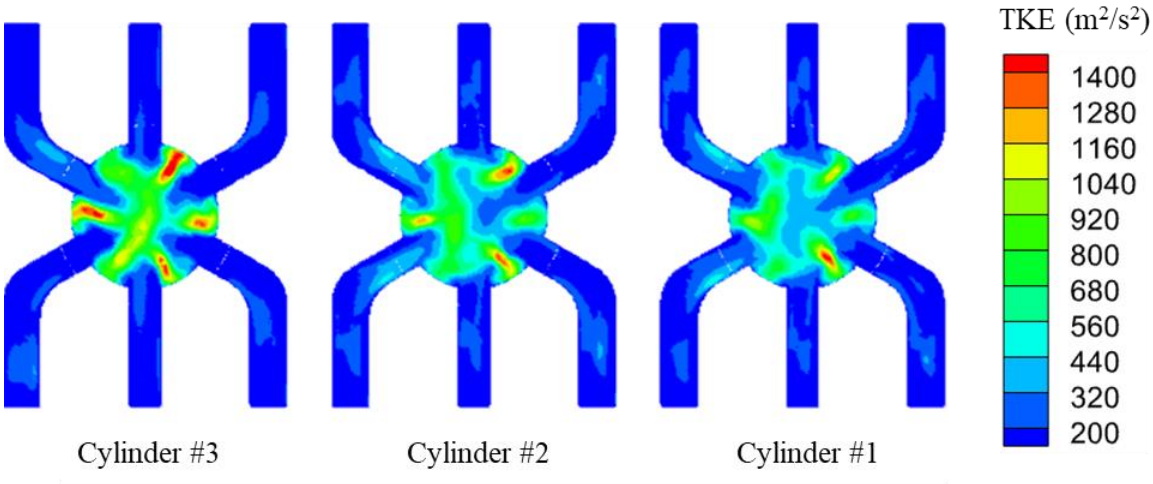

Figure 4.36. Tapered model TKE on the ZX plane of the middle of the intake ports for each cylinder

Figure 4.36 shows the regions of TKE for the tapered manifold design on the ZX plane. Figure 4.36 shows that the TKE for the intake ports of the cylinders are closer for the tapered design than the baseline design. However, Cylinder three still has the highest TKE out of all three cylinders.

Figure 4.37 is a contour plot of TKE on the ZX plane for the middle of each cylinder. The cylinders are ordered from left to right three, two, and one. The color bar on the right of Figure 4.37 shows the values for each color in m^2/s^2 on the contour plot.

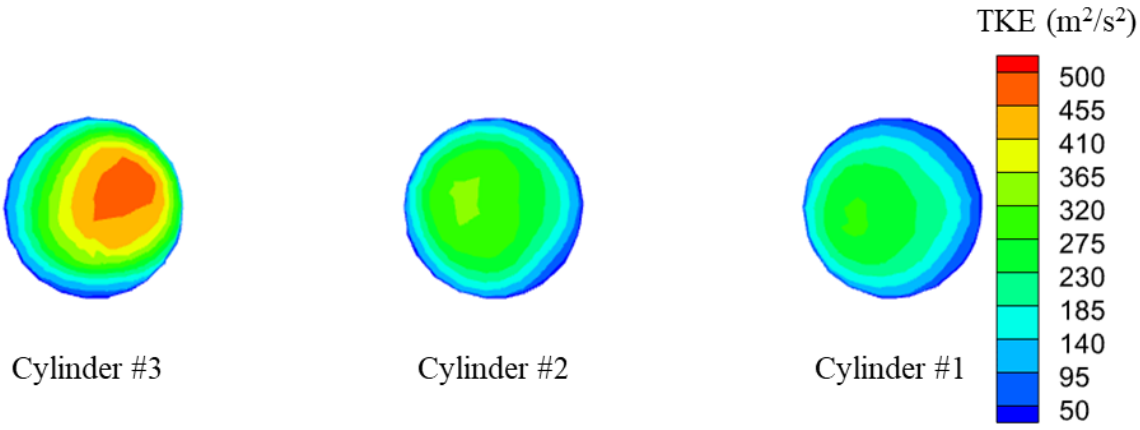

Figure 4.37. Tapered model TKE on the ZX plane of the middle of the cylinders

Figure 4.37 shows the region of higher TKE in cylinder three has shifted further to the right than the where it was for the baseline design. Just like the Figures 4.35 and 4.36 showed, the highest TKE is in the center of the cylinders for each cylinder. Figure 4.37 shows that the each of the regions that experience higher TKE from the baseline design have shifted slightly to the left for cylinders one and two for the tapered manifold design.

Figure 4.38 is a contour plot of TKE on the ZX plane for the middle of the exhaust ports for each cylinder. The cylinders are ordered from left to right three, two, and one. The color bar on the right of Figure 4.38 shows the values for each color in m^2/s^2 on the contour plot.

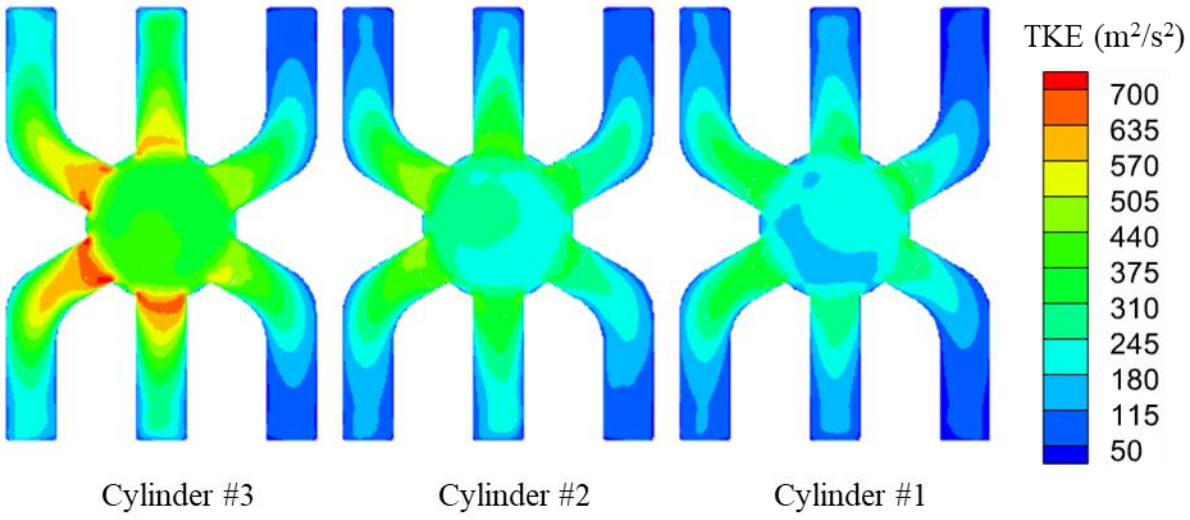

Figure 4.38. Tapered model TKE on the ZX plane of the middle of the exhaust ports for each cylinder

Figure 4.38 shows the regions on the ZX plane of the exhaust ports that are experiencing the highest flow energy. The two exhaust ports experiencing the highest TKE are exhaust ports three and four which the ones that are the furthest from the inlet of the intake manifold. Back in Figure 4.30 the mass flow through ports three and four are the highest so it makes sense that they experience the highest TKE. The exhaust ports had bigger regions of higher TKE for the tapered manifold design than the baseline design when comparing Figure 4.38 to Figure 4.20.

Figure 4.39 is a contour plot of TKE on the YZ plane for the middle of cylinder one. The color bar on the right of Figure 4.39 shows the values for each color in m^2/s^2 on the contour plot. The top of Figure 4.39 is the intake side of the cylinder and the exhaust is the bottom of Figure 4.39.

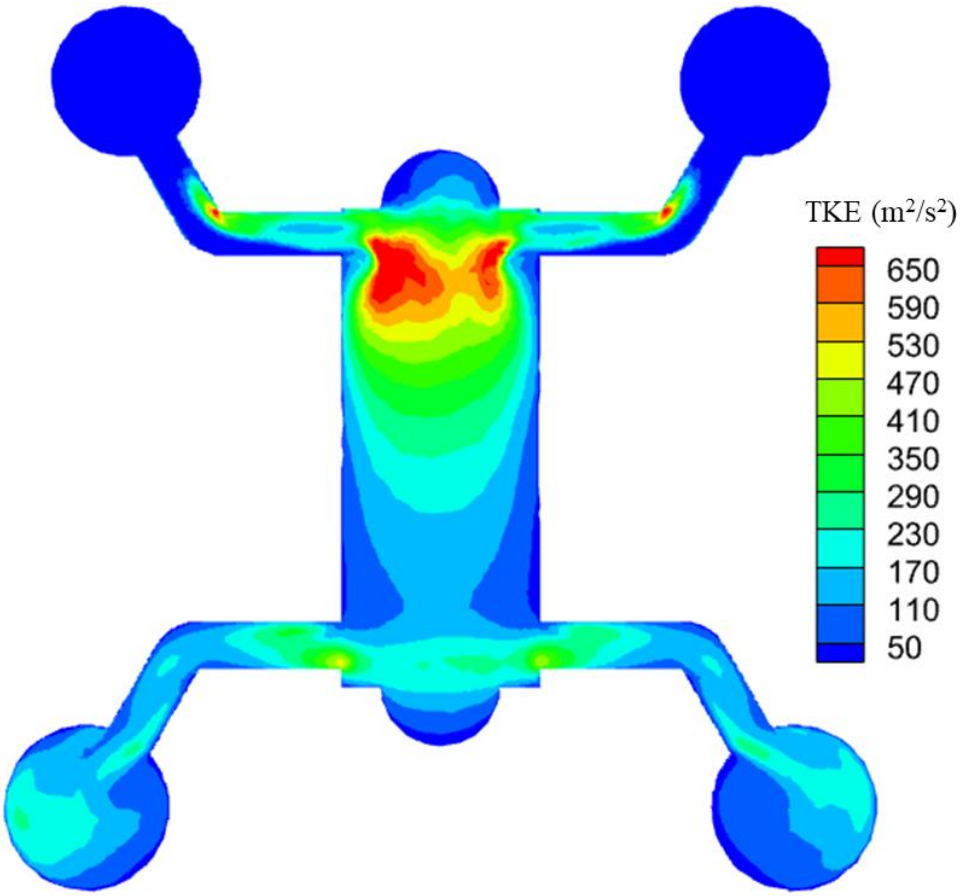

Figure 4.39. TKE on the YZ plane of the middle of cylinder one for the tapered manifold design

Just like with the baseline design Figure 4.39 shows that there are regions in the intake manifold runners that are experiencing higher TKE near the bends. The diameter of the circles for the intake manifold are slightly smaller than the exhaust manifold circle diameter because of the taper. Figures 4.40 and 4.41 show the change of intake manifold diameter more noticeably than Figure 4.39. Lastly, just like for the baseline design Figure 4.39 shows that the intake side of the cylinder experiences higher TKE than the exhaust side of the cylinder.

Figure 4.40 is a contour plot of TKE on the YZ plane for the middle of cylinder two. The color bar on the right of Figure 4.40 shows the values for each color in m^2/s^2 on the contour plot. The top of Figure 4.40 is the intake side of the cylinder and the exhaust is the bottom of Figure 4.40.

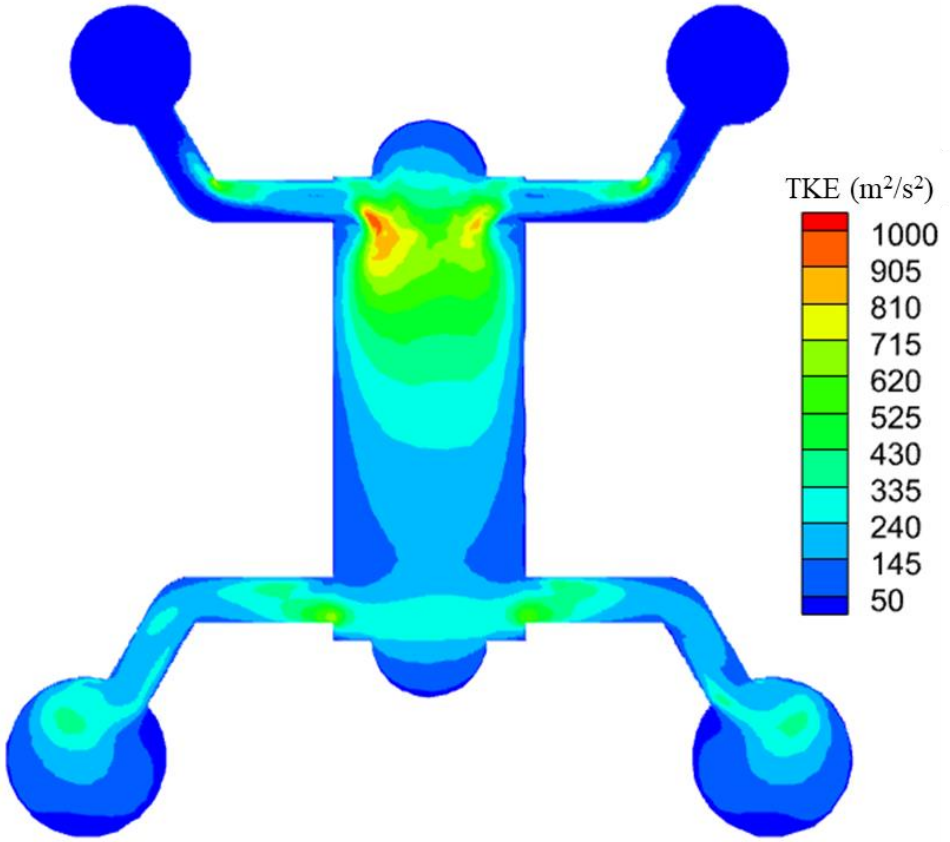

Figure 4.40. TKE on the YZ plane of the middle of cylinder two for the tapered manifold design

Figure 4.40 has the same color bar values as Figure 4.22 to compare the regions of higher TKE for the tapered design to the baseline design. The tapered model had lower TKE than the values seen from Figure 4.22 of the baseline model. Figure 4.40 shows that the intake manifold circles have decreased from the size that they were in Figure 4.39 because of the taper.

Figure 4.41 is a contour plot of TKE on the YZ plane for the middle of cylinder three. The color bar on the right of Figure 4.41 shows the values for each color in m^2/s^2 on the contour plot.

The top of Figure 4.41 is the intake side of the cylinder and the exhaust is the bottom of Figure 4.41.

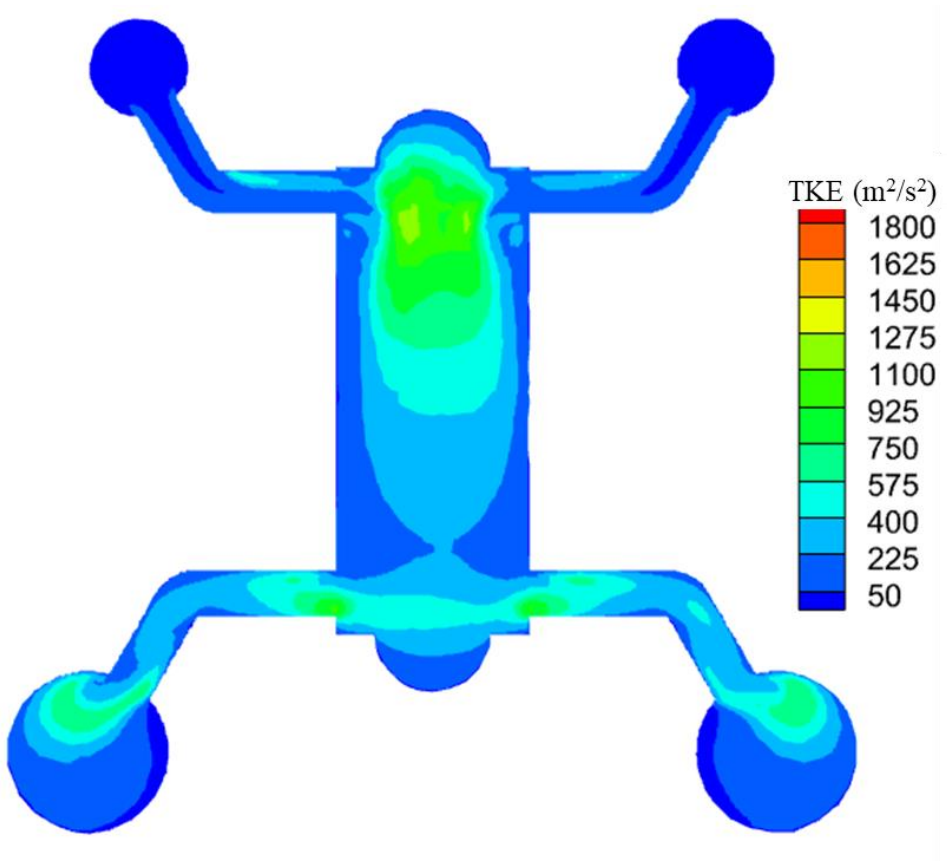

Figure 4.41. TKE on the YZ plane of the middle of cylinder three for the tapered manifold design

Figure 4.41 shows that the TKE has decreased in the YZ plane of cylinder three for the tapered manifold design compared to the baseline design, seen in Figure 4.23. The scale of the color bar in Figure 4.41 is the same as the one for Figure 4.23. Figure 4.41 shows that the highest levels of TKE are experienced towards the center of the cylinder up near the intake ports.

4.2.7 Tapered Manifold Design Summary

As mentioned in the beginning of section 4.2 the goal of the tapered design was to balance the mass flow rates to each of the intake ports. Section 4.2.3 showed that tapering the manifolds did not achieve a balanced mass flow rate across the ports. Therefore, to balance the mass flow restrictions are port size reductions would need to be implemented to further attempt to balance

the mass flow rates. The CFD analysis for this model was done using a static condition meaning that all the pistons stayed open and did not move. The results could be different if performing a dynamic CFD test. The three things mentioned for trying to achieve a balanced mass flow rate fell outside of the scope of the project. Dynamic CFD testing was outside of the scope of the project primarily due to the computational time requirements of dynamic CFD modeling.

4.3 Swirl Design

The goal for the third engine design is to increase the swirl in each cylinder in comparison to the baseline design. An angle of ten degrees was used for the swirl angle for the ports. Figure 1.1 shows how the angle of the ports is defined. Only the intake manifold runners were angled.

4.3.1 Geometric Model

Figure 4.42 shows the internal geometry of the opposed piston engine that has an intake manifold designed to increase swirl. The blue components in Figure 4.42 shows the intake manifold and intake manifold runners. The orange components in Figure 4.42 represent the cylinders and a portion of the intake and exhaust ports. The red component in Figure 4.42 represents exhaust manifold runners, exhaust manifolds, and an exhaust collector.

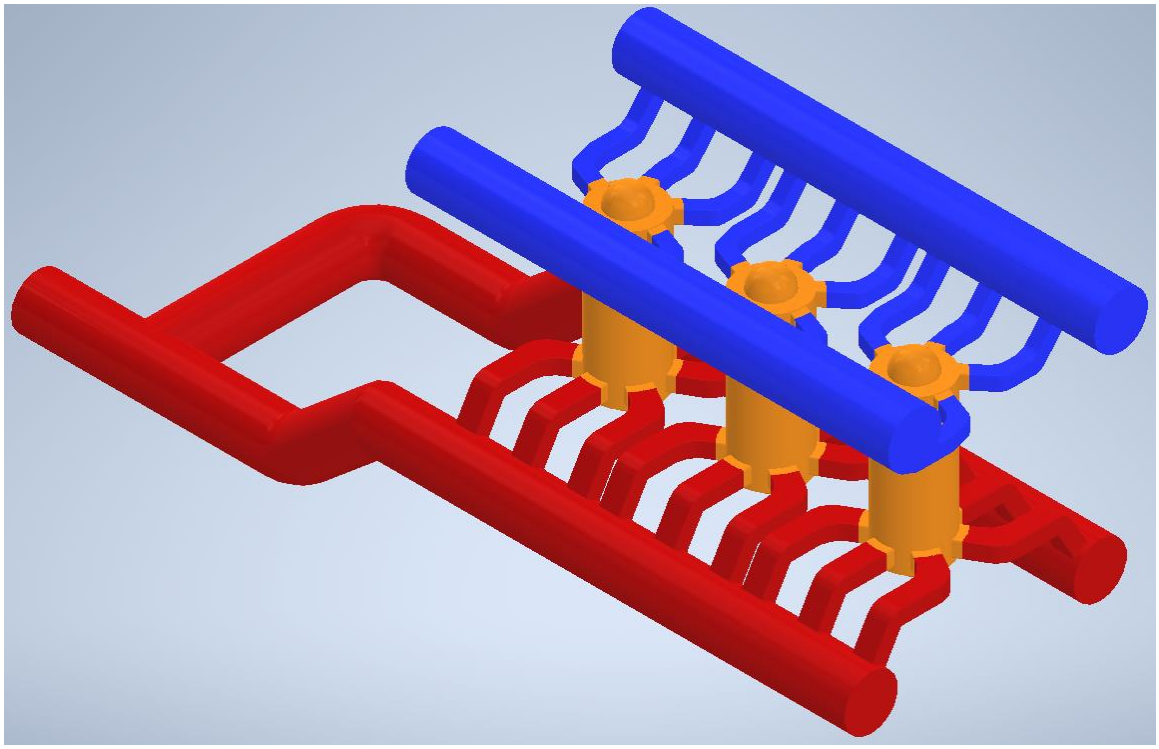

Figure 4.42. CAD model for the swirl opposed piston engine

Figure 4.42 shows the swirl design with ports that have been angled to increase swirl without tapered manifolds. This design is expected to produce higher swirl than the baseline design swirl values to the angle of the ports. However, no methods were implemented to balance the mass flow rates of the ports or to increase tumble.

Figure 4.43 is a top-down view of the intake manifold for the swirl design. The top of Figure 4.43 is the right half of the intake manifold, and the bottom is the left half. The orange portions of Figure 4.43 are the cylinders for the engine.

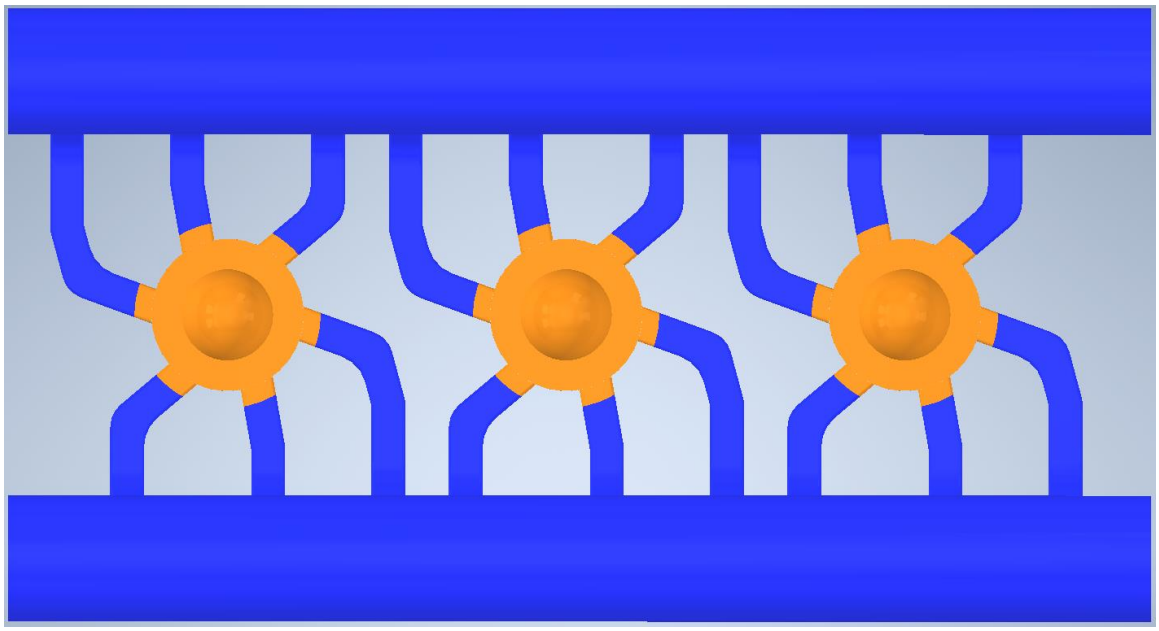

Figure 4.43. Top down view of the intake manifold for the swirl opposed piston engine

The manifolds for the swirl design had to be made slightly long than the baseline designs manifold. The angle of the ports made the intake manifold runners longer than the baseline designs. The bends in the manifold runners for the swirl design were done using the same dimensions as the baseline design. The angle of the ports seen in Figure 4.43 were made to create swirl in a counterclockwise direction.

4.3.2 Mesh and Boundary Conditions

Figure 4.44 is an isometric view of the mesh for the swirl design. The scale is located at the bottom of Figure 4.44. The top of the model in Figure 4.44 is the tapered intake manifold. The runners from the intake and exhaust manifolds have a smaller mesh size than most of the other regions which makes them appear as black sections. The exhaust manifold is the bottom component in Figure 4.44. The cylinders are in between the intake and exhaust manifolds in Figure 4.44.

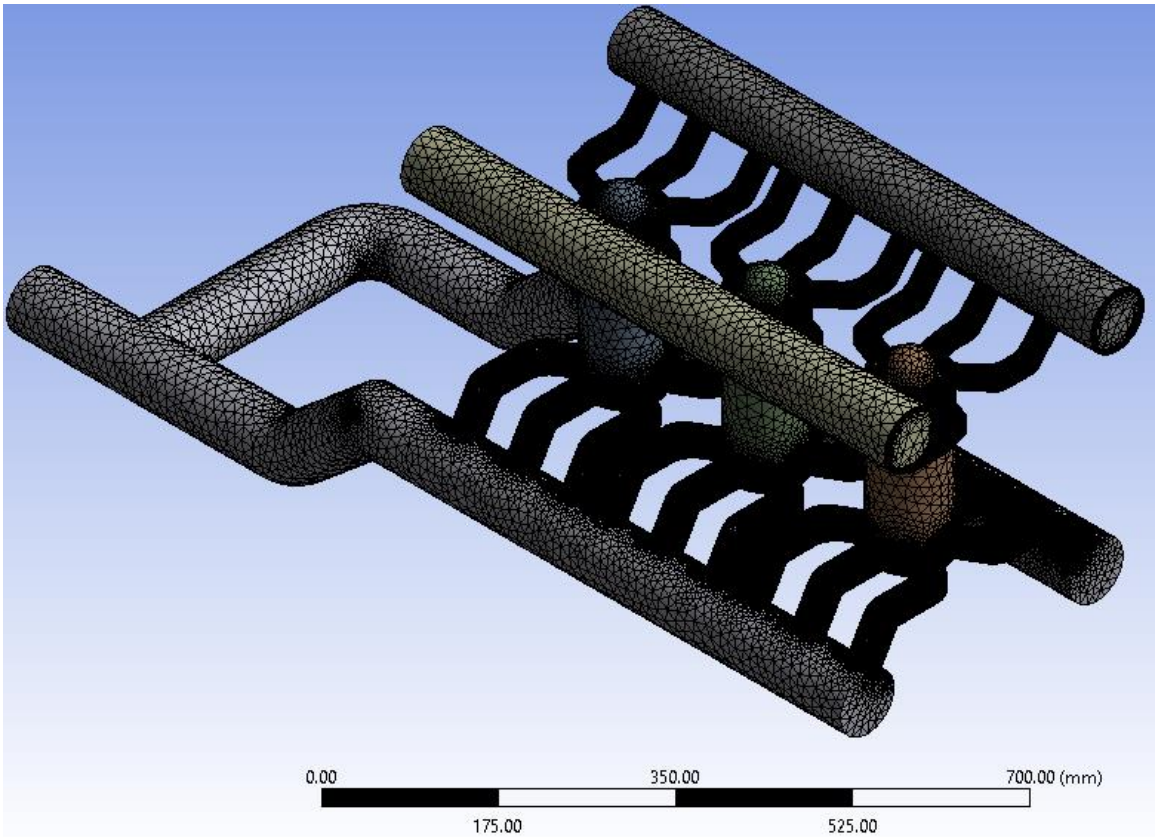

Figure 4.44. Isometric view of the mesh for the swirl opposed piston engine design

The element size for the mesh seen in Figure 4.44 was set to the same size and sizing constraints as the baseline model. The mesh for the swirl model used tetrahedral elements and inflation layers just like the baseline model. The mesh for the swirl design had 15,095,161 total elements.

Figure 4.45 shows the right half of the meshed swirl engine cut down the middle on the XY plane. The inflation layers for the mesh can be seen in the bottom left corner of Figure 4.45 which is a cross section of a portion of the exhaust manifold. The scale bar is at the bottom of Figure 4.45 to show how long the model is in millimeters.

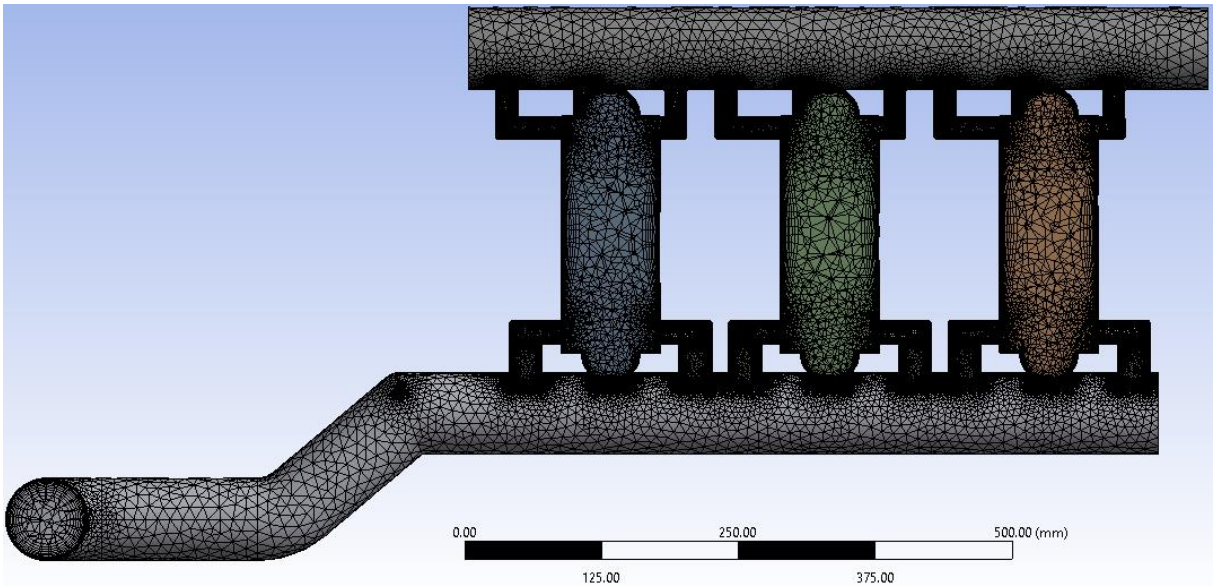

Figure 4.45. Section view of the meshed swirl model for the opposed piston engine

Figure 4.45 shows the length for the intake manifold has larger elements in the top right corner and they gradually shrink as they approach the complex geometry regions of the manifold. Figure 4.45 also shows the elements inside of the cylinders start out small at the top of the cylinders, become large near the center of the cylinder, and then shrink again near the exhaust ports. The meshing software also decreases the size of the elements near the walls to get more accurate results near the walls.

Figure 4.46 is a cross sectional view of one of the intake manifold runners. Figure 4.46 has the scale bar under the cross-sectional view of the runner. The scale bar is ten millimeters which is half the length or width of the port size.

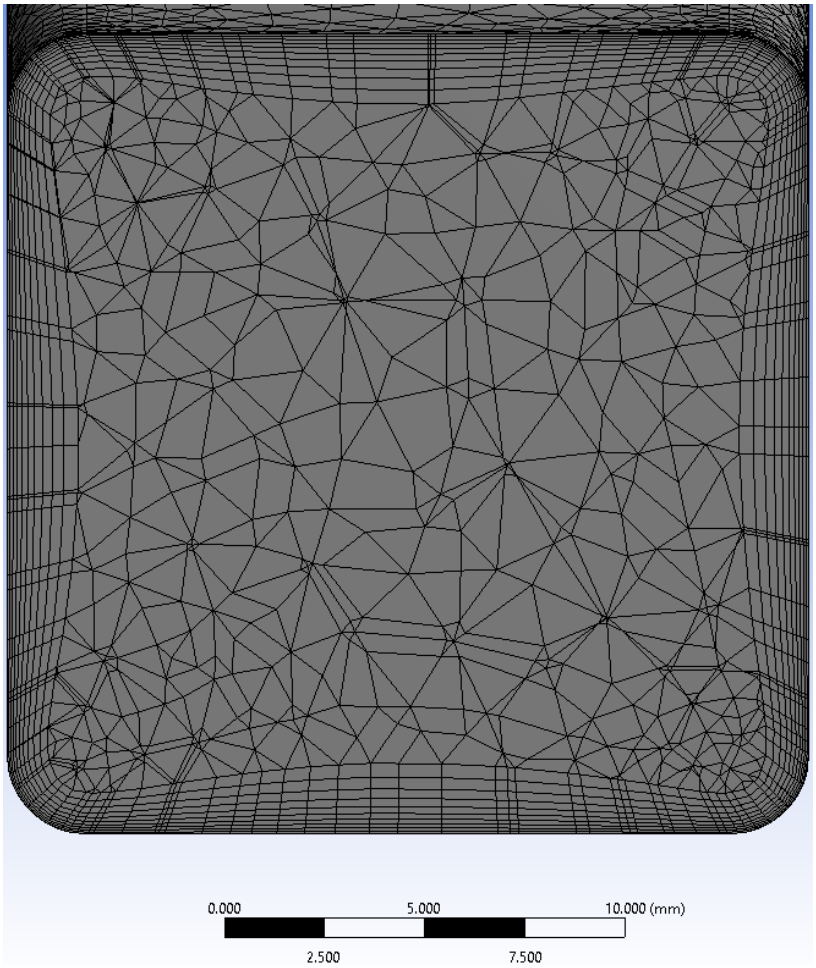

Figure 4.46. Section view of the meshed swirl intake manifold runner for the opposed piston engine

Figure 4.46 shows a close-up of the inflation layers of an intake manifold runner so that the elements are easier to see. Figure 4.46 shows that the layers become thinner closer to the walls. The inflation layers for the mesh of the swirl manifold design had the same settings as for the baseline design.

Figures 4.47 and 4.48 show boundary conditions for the swirl design. Figure 4.47 shows the wall boundaries, highlighted in red. The letter tags seen in Figure 4.47 label each component of the model and correspond to the names in the list in the top left corner of Figure 4.47.

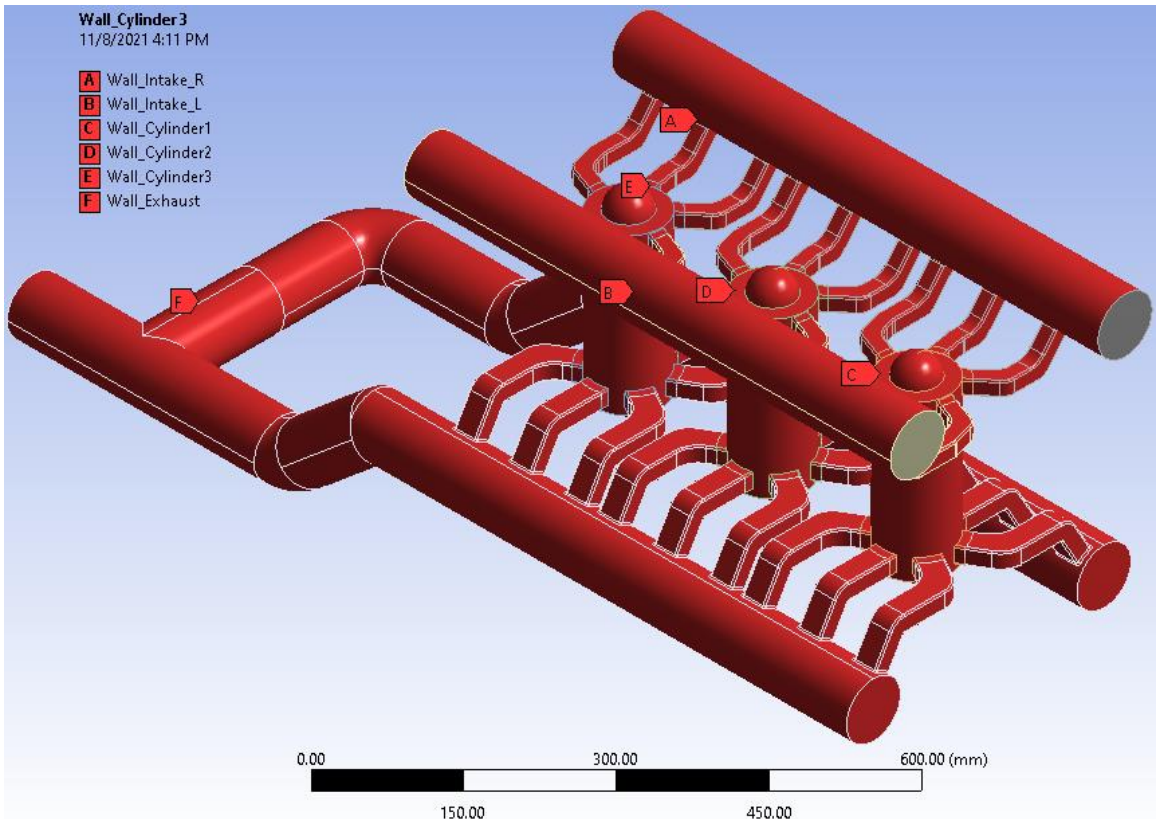

Figure 4.47. Swirl model wall Boundary conditions

The wall boundaries for the swirl design were setup the same as the baseline model. Figure 4.47 shows the different components of the model by name using the letter tags. The unselected areas in Figure 4.47, the non-red areas, are the pressure inlets to the model.

Figure 4.48 shows the pressure inlet and outlet boundary conditions. The left side of Figure 4.48 shows the pressure inlets labeled with the letter tag A. The middle of Figure 4.48 shows the legend for the letter tags. The right side of Figure 4.48 shows the pressure outlet on the backside of the engine with the letter tag B.

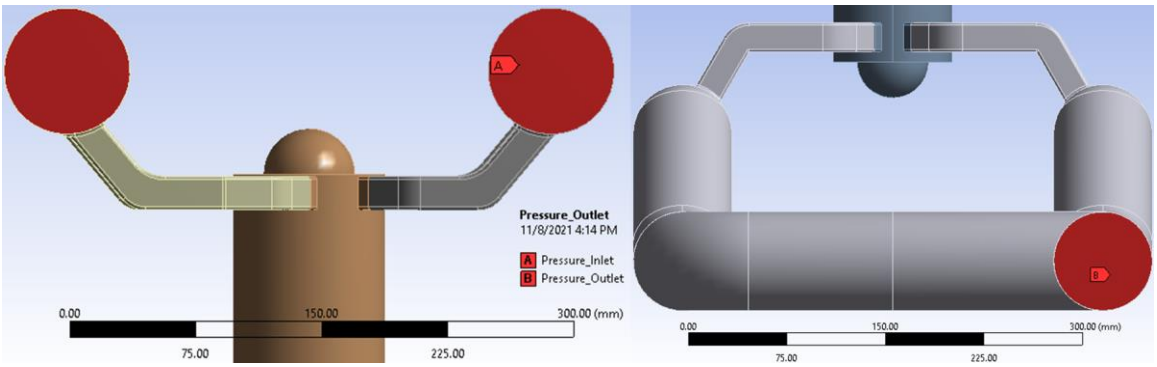

Figure 4.48. Swirl model inlet and outlet boundary conditions

The same pressure as the baseline model was applied to the inlets which was 41.4 kPa (6 psi) gage pressure. The pressure applied to the outlet was atmospheric pressure, zero gage pressure. The temperature of the pressure inlet and outlet was 320 Kelvin and 300 Kelvin.

4.3.3 Balance of Mass Flow

Figure 4.49 shows the mass flow of air through each of the intake and exhaust ports. The intake ports have a positive mass flow rate (top side of the bar chart), and the exhaust ports have a negative mass flow rate (bottom side of the bar chart). Figure 4.49 uses different colored bars for each cylinder as seen in the legend from the right side of Figure 4.49. Across the top of Figure 4.49 are labels sectioning of the different ports, one through six for each cylinder.

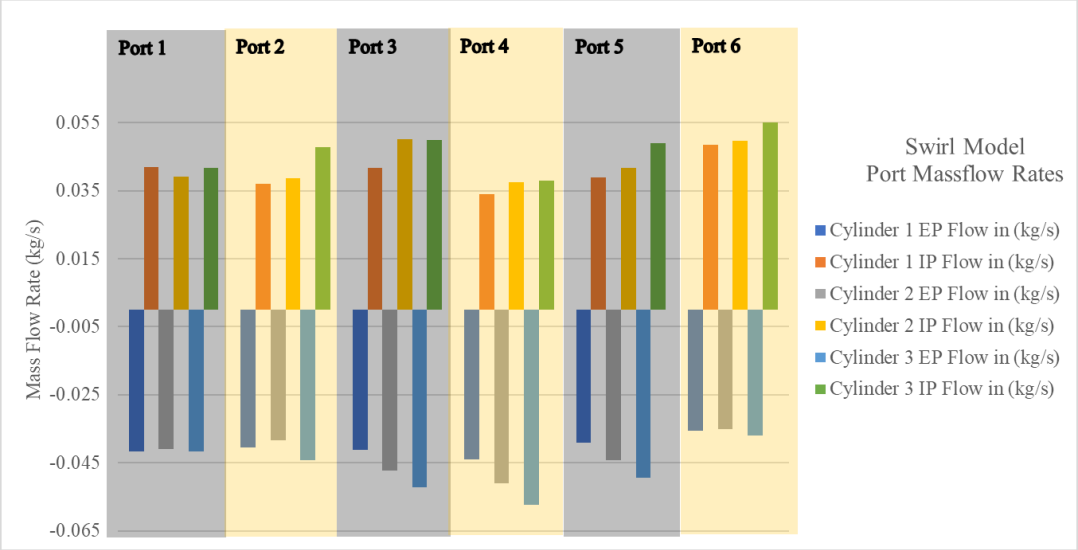

Figure 4.49. Swirl model mass flow through each port of cylinders one, two, and three

Figure 4.49 shows that cylinder three has the highest mass flow rate for the swirl design. However, some of the ports for cylinder three have similar flow rates to the other two cylinders ports. The swirl model unintentionally balanced the mass flow rate through the cylinders better than the tapered manifold model. There were four intake ports and three exhaust ports for each cylinder that had similar mass flow rates through them for the swirl design.

Figure 4.50 shows the velocity magnitude in m/s extracted from three sections of the engine model. The order of the sections is top to bottom intake ports, middle of the cylinder, and exhaust ports. Each section of Figure 4.50 also has three circular contour plots for cylinders three, two, and one, from left to right. The color bar on the right of Figure 4.50 shows the values for velocity magnitude.

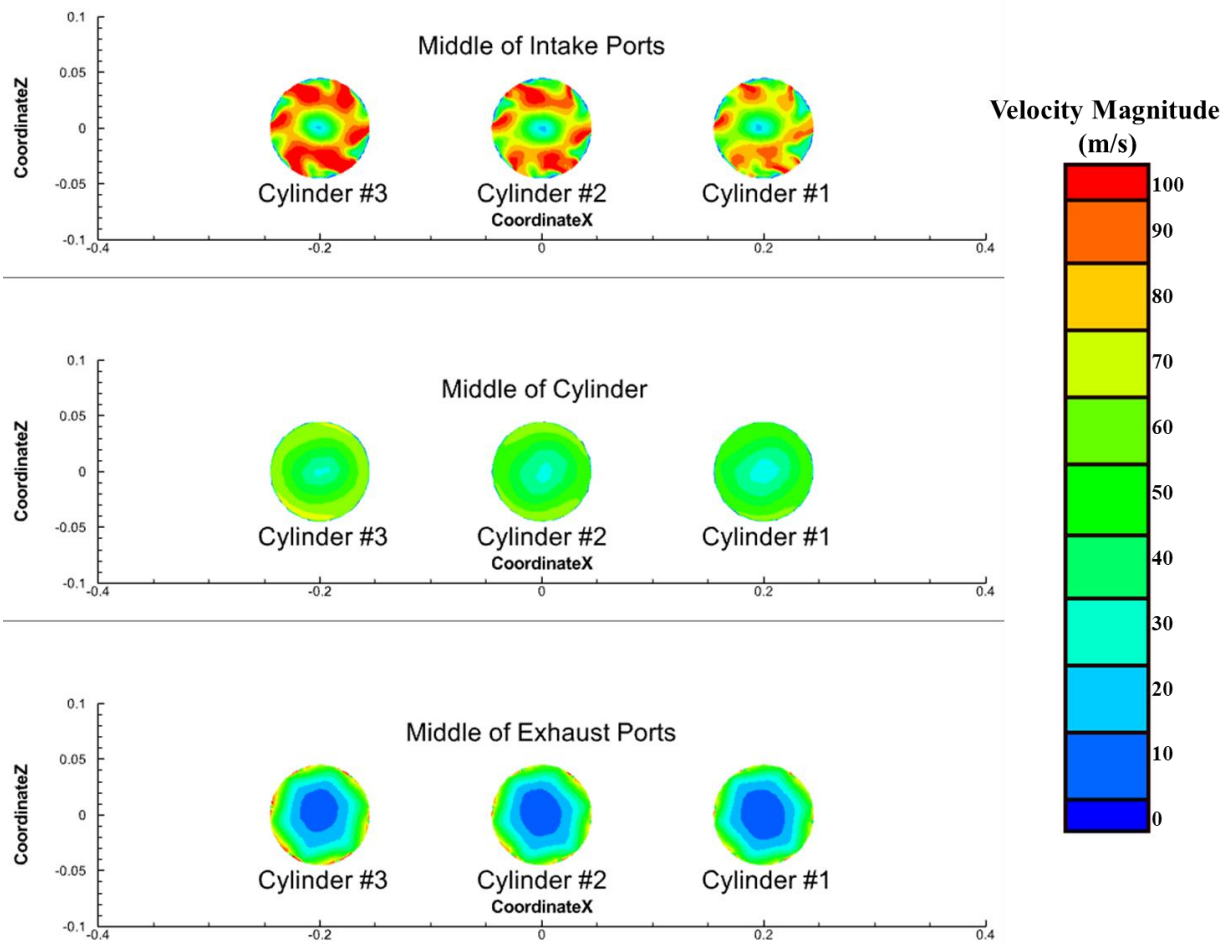

Figure 4.50. Swirl model velocity magnitude (m/s) for different sections of the cylinder

Figure 4.50 shows the magnitude of the flow velocity through the engine. Cylinder three had the highest velocity magnitude and all three cylinders had higher velocity in regions of the cylinder than the baseline design. The velocity contour plots show that the velocity is higher out of the center for each cylinder. From Figure 4.50 a swirling motion can be seen from the velocity of the flow in the cylinder. The velocity in the center of the cylinder of the exhaust ports for each cylinder has higher velocity at the walls and exhaust ports.

Figure 4.51 shows the velocity magnitude for a vertical (XY) plane section of cylinders one, two, and three. The order of the cylinders from left to right is cylinder three, two, and one. On the right side of Figure 4.51 is the color bar for the contour plot which shows the values of the velocity magnitude within the cylinder on the XY plane.

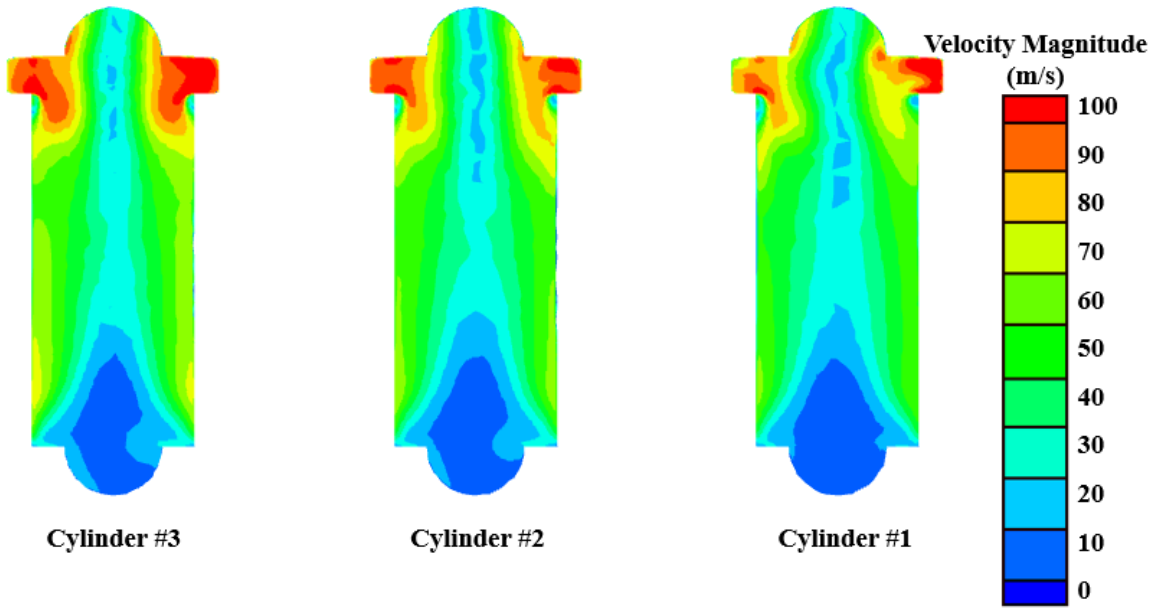

Figure 4.51. Swirl model velocity magnitude (m/s) on the XY plane for cylinders one through three

Figure 4.51 shows a low velocity section through the center of each cylinder. As seen in Figure 4.50 the velocity near the walls was higher than in the center of the cylinders. The results of Figure 4.50 and Figure 4.51 imply that the flow is swirling around in the piston on its way out of the cylinder.

4.3.4 Swirl Circulation

Figure 4.52 shows Y-vorticity contour plots. Figure 4.52 is laid out similarly to Figure 4.50 where it has three sections that are separated by each section of the engine. The labels for each section appear above the contour plot. The three sections are from top to bottom the intake ports, middle of the cylinder, and exhaust ports. Like Figure 4.50, each section of Figure 4.52 has three sections of contour plots for cylinders three, two, and one, respectively.

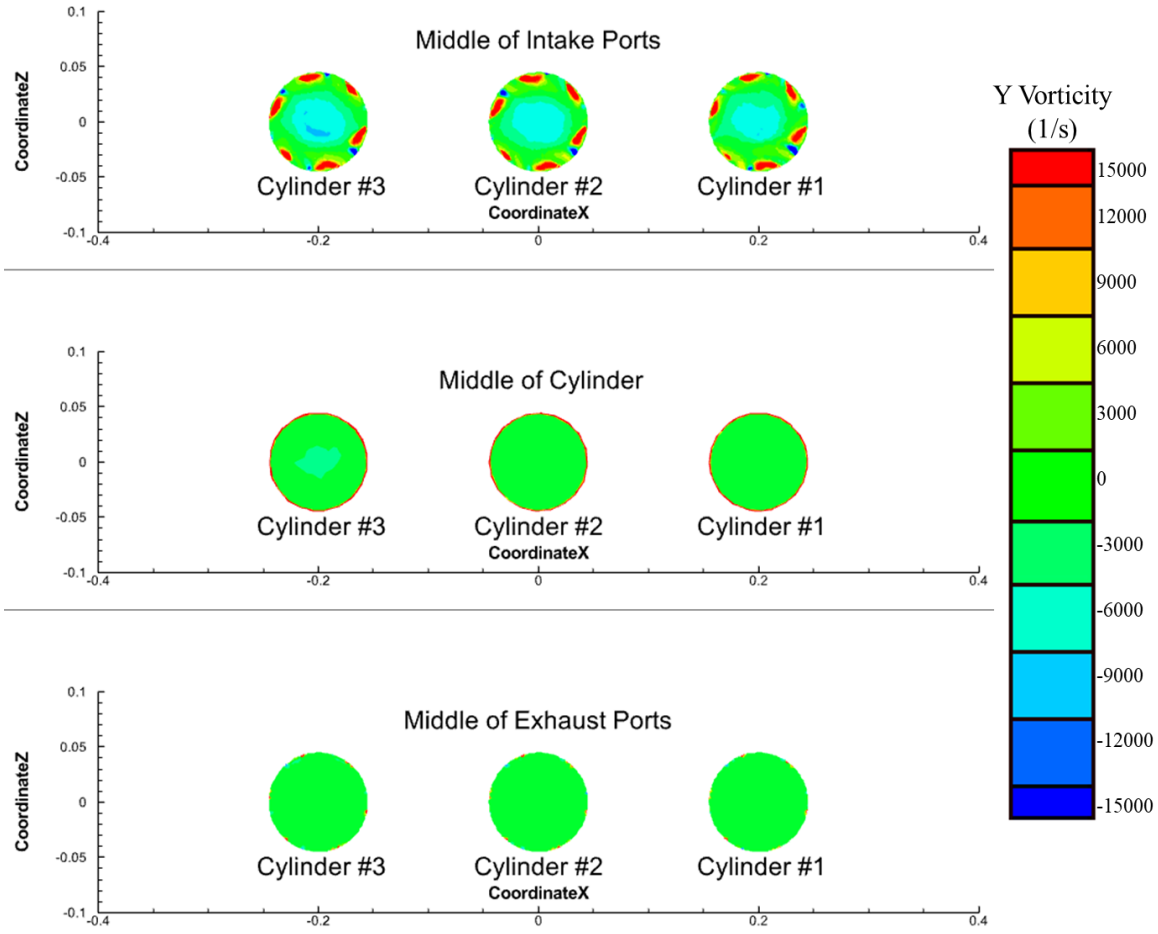

Figure 4.52. Swirl model vorticity for the three different sections for cylinders one through three

Figure 4.52 shows the swirl circulation for the swirl design. Figure 4.52 also shows that there are regions of high Y-vorticity near the outlets of the intake ports in the cylinders. Figure 4.52 has more regions of higher Y-vorticity on the intake port plane than the baseline design. The

Y-vorticity is nearly zero at the middle of the cylinder and at the exhaust ports just like for the baseline design.

Table 4.9 shows the swirl calculated for each cylinder section and is formatted the same as Table 4.6. The new addition to Table 4.9 from Table 4.6 is the added column showing the swirl design swirl values. The highlighted numbers in red for Table 4.9 represent a decrease in swirl magnitude compared to the baseline design. The numbers highlighted in green for Table 4.9 represent an increase of swirl magnitude from the baseline design.

Table 4.9. Comparison of swirl values for the three sections of three engine designs

Section	Cylinder	Swirl (m^2/s) Baseline	Swirl (m^2/s) Tapered	Swirl (m^2/s) Swirl
Middle of the intake ports	1	-0.1	0	-3.0
	2	0.1	0	-2.5
	3	0	-0.2	-3.4
Midway through the cylinder	1	0	0	-11.7
	2	0	0	-12.3
	3	0	0	-14.3
Middle of the exhaust ports	1	0	0.1	-6.0
	2	0	0.1	-6.5
	3	-0.1	-0.1	-7.1

Table 4.9 shows that the magnitude of swirl increased for every plane of every cylinder for the increased swirl design compared to the baseline design. The order of magnitude increase ranged from 1E02 to 1E05 m^2/s when comparing the results to the baseline design. The swirl magnitude increased compared to the tapered manifold model and its order of magnitude increased from 1E03 to 1E06 m^2/s. Table 4.9 shows that the goal for this engine design has been achieved.

4.3.5 Tumble Circulation

Figure 4.53 shows the Z-vorticity contour plot for cylinders three, two, and one from left to right. The cylinders all have a label underneath the contour plot identifying each cylinder. Like

Figure 4.51, Figure 4.53 is based on the XY plane which is a vertical plane through the center of the engine. The right portion of Figure 4.53 shows the color bar values for the contour plot.

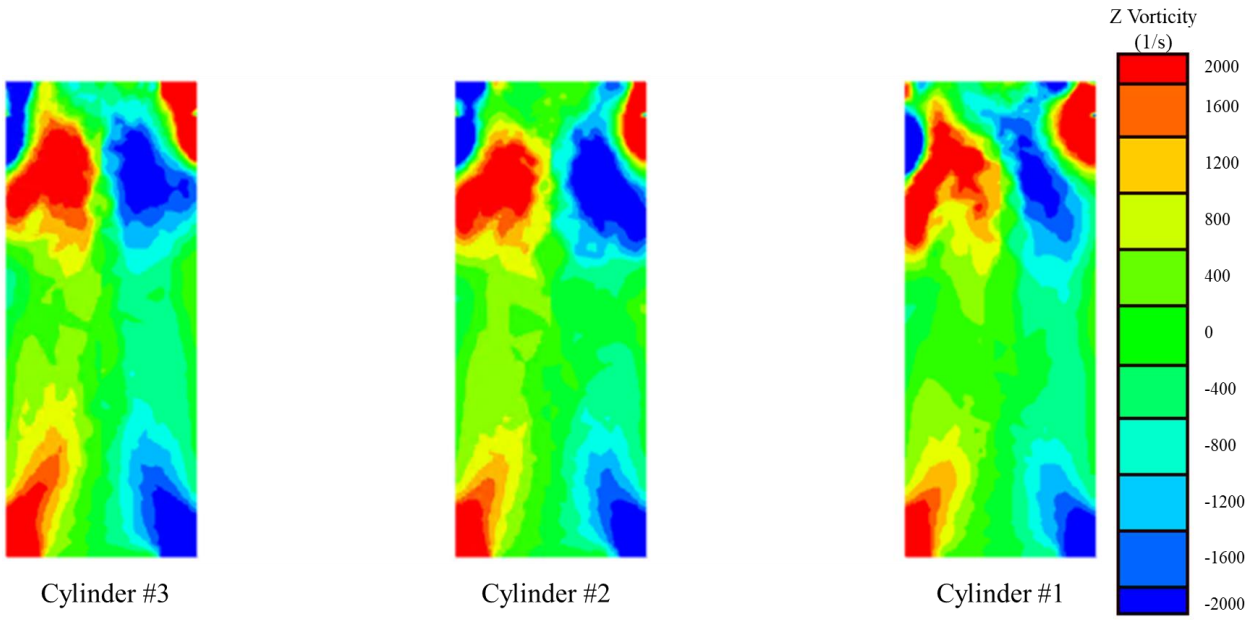

Figure 4.53. Swirl model vorticity on the XY plane for cylinders one through three

Figure 4.53 shows the in-cylinder tumble regions with red being positive tumble and blue being negative tumble. Smaller rectangular regions were used for calculating the tumble values as discussed on page 62. The tapered manifold design produced tumble in the same direction as the baseline model and roughly the same amount. Figure 4.53 shows the full half of the cylinders to show where the regions of tumble are significant. Most of the tumble in the center of the cylinder for the swirl design.

Table 4.10 was set up similarly to Table 4.7. The newest addition to Table 4.10 is a column on the right that shows the tumble of the swirl design in m^2/s. The highlighted numbers in red for Table 4.10 represent a decrease in tumble magnitude compared to the baseline design. The numbers highlighted in green for Table 4.10 represent an increase of tumble magnitude from the baseline design.

Table 4.10. Comparison of tumble values for the three sections of three engine designs

Cylinder	Rectangular Region Location	Tumble (m^2/s) Baseline	Tumble (m^2/s) Tapered	Tumble (m^2/s) Swirl
1	Left	-3.7	-0.7	5.6
	Right	4.6	6.0	-4.3
2	Left	-4.0	-4.1	5.8
	Right	4.4	6.2	-6.3
3	Left	-6.0	-7.3	6.6
	Right	5.3	4.8	-6.0

Table 4.10 shows that the tumble for the swirl design was larger in magnitude than baseline engine design for each region except the right side of cylinder one. The tumble was not expected to increase as the swirl angle of the ports was the only geometry change within the cylinder. The tumble for the swirl design was also larger than the tumble for most of the regions of the tapered manifold design.

4.3.6 Turbulent Kinetic Energy (TKE)

The volume average TKE was calculated for the swirl design and then compared to the other two engine designs. Table 4.11 is formatted the same as Table 4.8. Table 4.11 has one more column on the right than Table 4.8. The column on the right of Table 4.11 shows the volume average TKE in m^2/s^2 for the swirl design. The highlighted numbers in red for Table 4.11 represent a decrease in TKE compared to the baseline design. The numbers highlighted in green for Table 4.11 represent an increase in TKE from the baseline design.

Table 4.11. Comparison of volume average TKE for three engine designs of cylinders one, two, and three

Cylinder	Volume Average TKE Baseline (m^2/s^2)	Volume Average TKE Tapered (m^2/s^2)	Volume Average TKE Swirl (m^2/s^2)
1	225	231	378
2	313	271	444
3	435	359	557

Table 4.11 shows that the swirl design has higher volume average TKE values for all three cylinders when compared to the baseline and tapered manifold designs. The volume average TKE for the cylinders of the swirl design increased from cylinders one to three. Table 4.11 shows that cylinder three had the highest volume average TKE for each engine.

Figure 4.54 is a contour plot that shows the TKE on a vertical plane through the middle of each cylinder. The cylinders are ordered from left to right three, two, and one. The color bar on the right of Figure 4.54 shows the values for each color in m^2/s^2 on the contour plot.

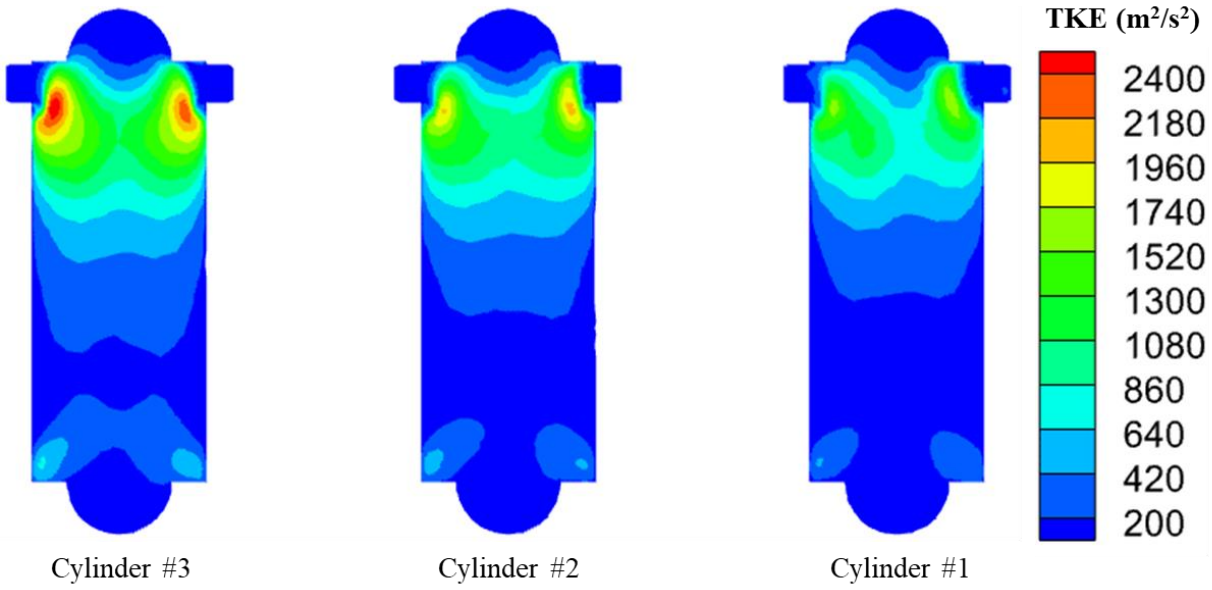

Figure 4.54. Swirl model TKE on the XY plane for the middle of each cylinder

Figure 4.54 shows that cylinder three has the highest TKE values just like for the baseline design. The regions in the cylinder that had the highest values of TKE were near the intake ports of the cylinders. The scale for the TKE more than double what it was for the baseline design because the values of TKE for the swirl much larger.

Figure 4.55 is a contour plot of TKE on the ZX plane for the middle of the intake ports of each cylinder. The cylinders are ordered from left to right three, two, and one. The color bar on the right of Figure 4.55 shows the values for each color in m^2/s^2 on the contour plot.

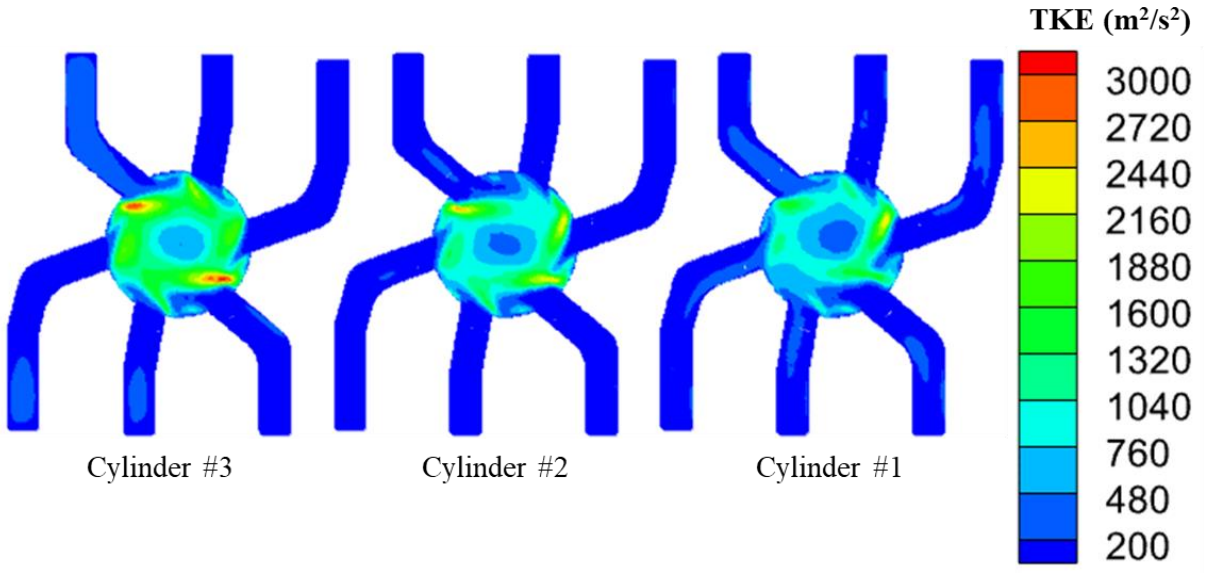

Figure 4.55. Swirl model TKE on the ZX plane of the middle of the intake ports for each cylinder

Figure 4.55 shows a swirling motion within the intake ports with the strongest one being in cylinder three. Just like the baseline model cylinder three has the highest TKE but instead of the highest being in the center of the cylinder it is between the center and the walls of the cylinder. The TKE for the swirl engine intake port plane had higher TKE than the baseline design. The highest TKE value on the color bar of Figure 4.18 was 1400 m^2/s^2. The highest TKE value on the color bar for Figure 4.55 was 3000 m^2/s^2 which is twice as high as the baseline design.

Figure 4.56 is a contour plot of TKE on the ZX plane for the middle of each cylinder. The cylinders are ordered from left to right three, two, and one. The color bar on the right of Figure 4.56 shows the values for each color in m^2/s^2 on the contour plot.

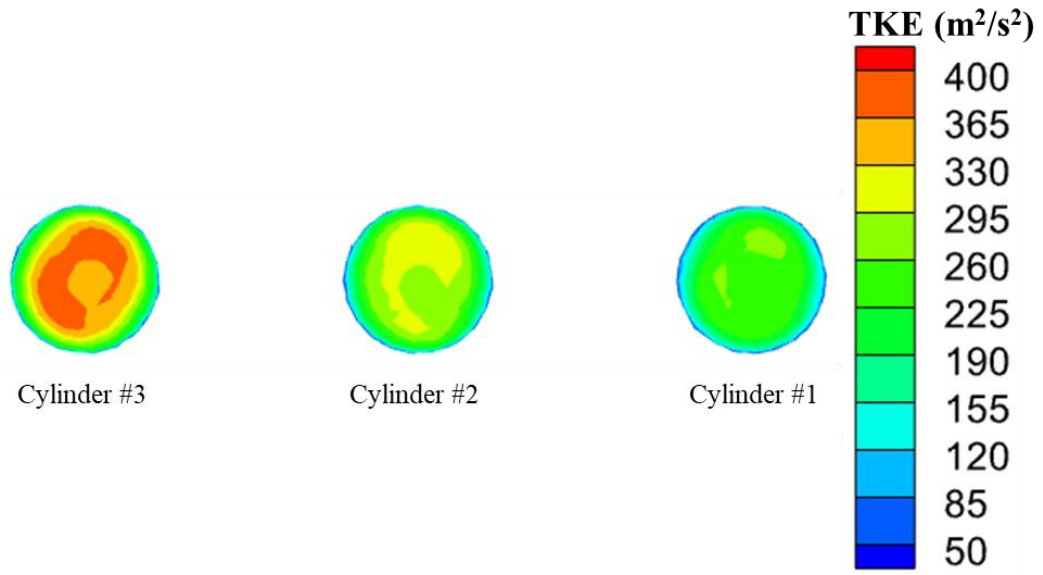

Figure 4.56. Swirl model TKE on the ZX plane of the middle of the cylinders

Figure 4.56 shows the region of higher TKE is in the center of each cylinder. The TKE was lower in the middle of the cylinder for the swirl model in comparison to the baseline design. The maximum value on the color bar for the baseline design was at 500 m^2/s^2 whereas the Maximum for the swirl design is 400 m^2/s^2. Figure 4.56 shows that the swirl design has less TKE for the middle of the cylinder than the baseline design.

Figure 4.57 is a contour plot of TKE in m^2/s^2 on the ZX plane for the middle of the exhaust ports for each cylinder. The cylinders are ordered from left to right three, two, and one. The color bar on the right of Figure 4.57 shows the values for each color in m^2/s^2 on the contour plot.

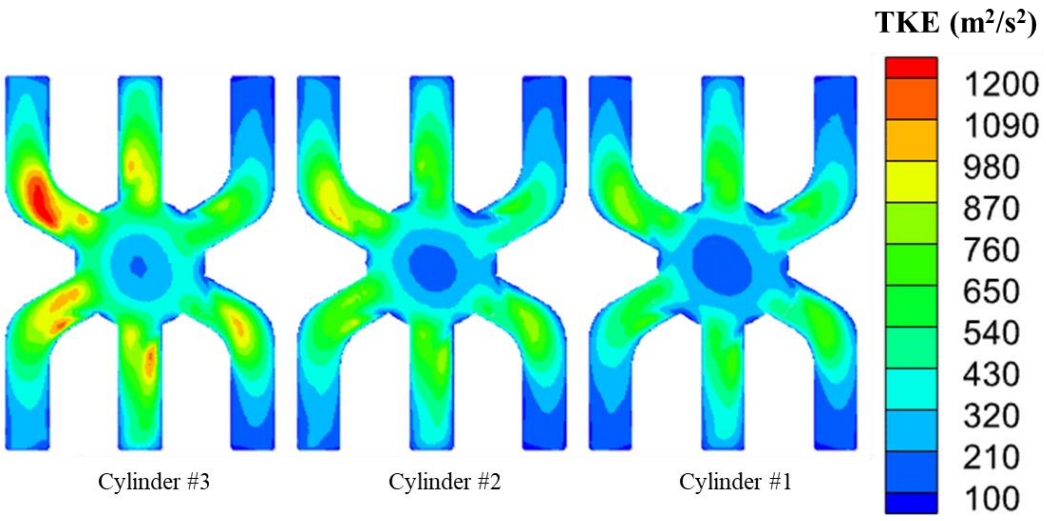

Figure 4.57. Swirl model TKE on the ZX plane of the middle of the exhaust ports for each cylinder

Figure 4.57 shows the highest TKE was near the cylinder walls and the exhaust ports. The maximum value on the color bar for the swirl design and the baseline design was 1200 and 700 m^2/s^2. Cylinder three had the highest TKE just like the baseline and the tapered manifold designs.

Figure 4.58 is a contour plot of TKE on the YZ plane for the middle of cylinder one. The color bar on the right of Figure 4.58 shows the values for each color in m^2/s^2 on the contour plot. The top of Figure 4.58 is the intake side of the cylinder and the exhaust is the bottom of Figure 4.58.

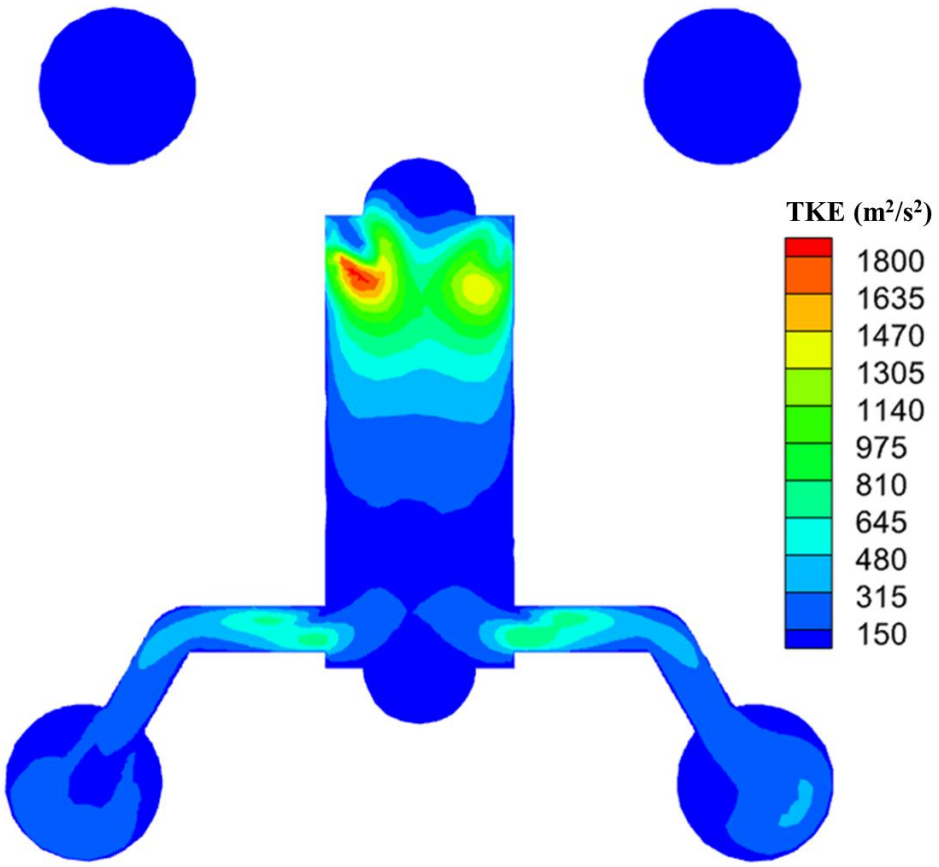

Figure 4.58. Swirl model TKE on the YZ plane of the middle of cylinder one

The two blue circles at the top of Figure 4.58 are part of the intake manifold but the runners are not connected to them because they did not line up with the mid plane of the cylinder. Figure 4.58 shows that the highest TKE for the cylinder is near the intake ports. Figure 4.58 does not show the ports to the cylinder because they rotated by ten degrees when angling the ports so they no longer line up with the midplane of the cylinder.

Figure 4.59 is a contour plot of TKE on the YZ plane for the middle of cylinder two. The color bar on the right of Figure 4.59 shows the values for each color in m^2/s^2 on the contour plot. The top of Figure 4.59 is the intake side of the cylinder and the exhaust is the bottom of Figure 4.59.

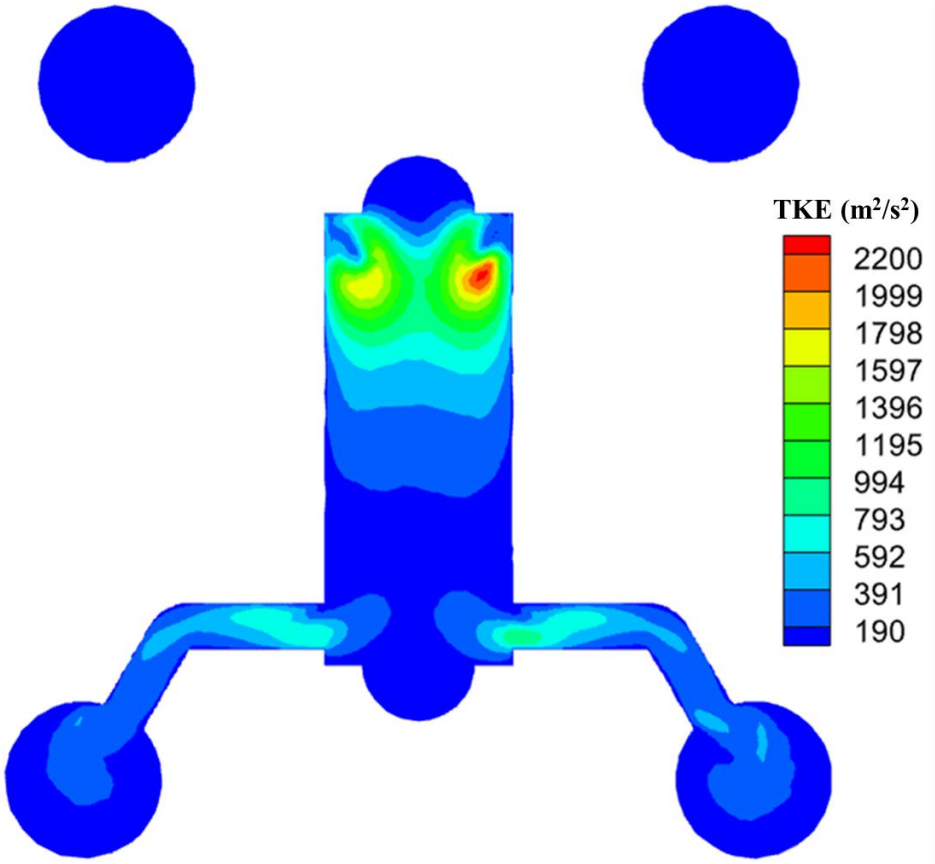

Figure 4.59. Swirl model TKE on the YZ plane of the middle of cylinder two

Figure 4.59 showed the TKE in an increased scale than the baseline design. The baseline design was at 1000 m^2/s^2 for the highest TKE value on the color bar whereas the highest value for the swirl design was 2200 m^2/s^2. Figure 4.59 shows that the highest levels of TKE occur at the top of the cylinder near the intake ports.

Figure 4.60 is a contour plot of TKE on the YZ plane for the middle of cylinder three. The color bar on the right of Figure 4.60 shows the values for each color in m^2/s^2 on the contour plot. The top of Figure 4.60 is the intake side of the cylinder and the exhaust is the bottom of Figure 4.60.

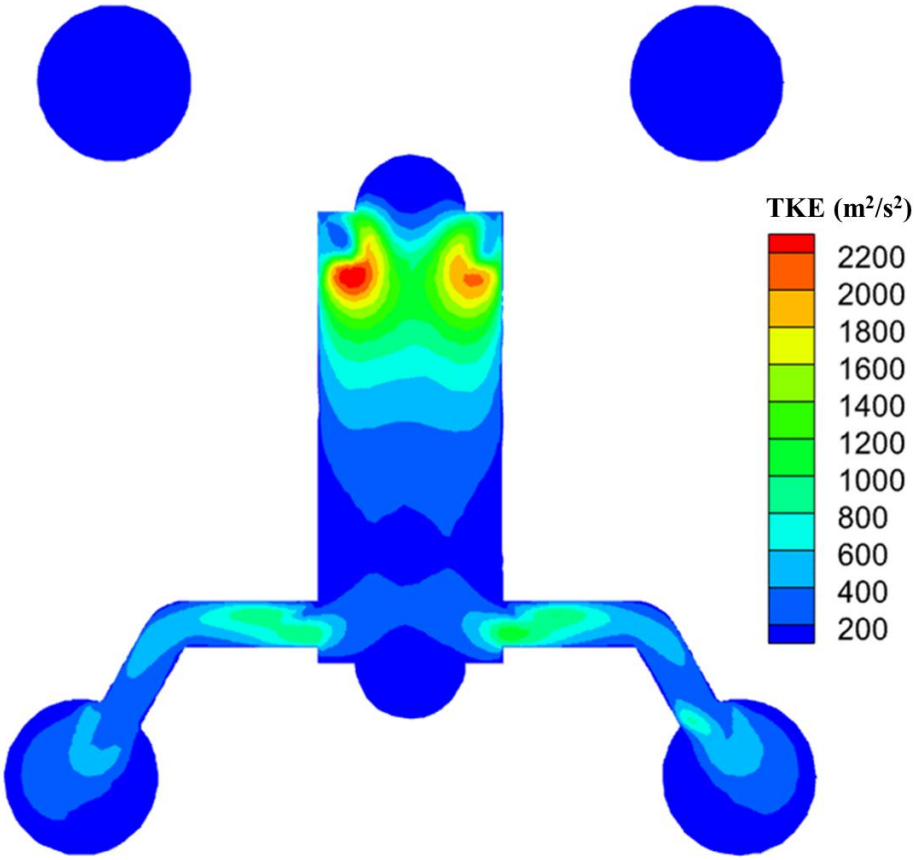

Figure 4.60. Swirl model TKE on the YZ plane of the middle of cylinder three

Figure 4.60 shows the TKE for cylinder three in the same scale as for cylinder two of the swirl design. The highest value for TKE of cylinder three of the baseline design was 1800 m^2/s^2. The highest values of TKE for cylinder three occur near the intake ports as they have for every design so far.

4.3.7 Swirl Design Summary

Angling the ports by ten degrees increased the swirl in the cylinders significantly from the baseline values. One interesting discovery with the swirl design was that the mass flow rates through the ports were more balanced than for the tapered manifold and baseline designs. The tumble values also increased for the swirl model when compared to the baseline and tapered manifold designs for most regions within the cylinders. Lastly, the volume average TKE was higher for the swirl design than the baseline design and the tapered manifold design.

4.4 Tumble Design

The goal for the fourth design of the engine was to increase the tumble in each of the cylinders. Rather than tilting the ports downward towards the exhaust ports, the ports were tilted up towards the piston above intake ports. Reversing the tumble angle will result in more turbulence in the ball of the piston rather than in the middle of the cylinder.

4.4.1 Geometric Model

Figure 4.61 shows the internal geometry of the opposed piston engine that has an intake manifold designed to increase tumble. The blue components in Figure 4.61 show the intake manifold and intake manifold runners. The orange components in Figure 4.61 represent the cylinders and a portion of the intake and exhaust ports. The red component in Figure 4.61 represents exhaust manifold runners, exhaust manifolds, and an exhaust collector.

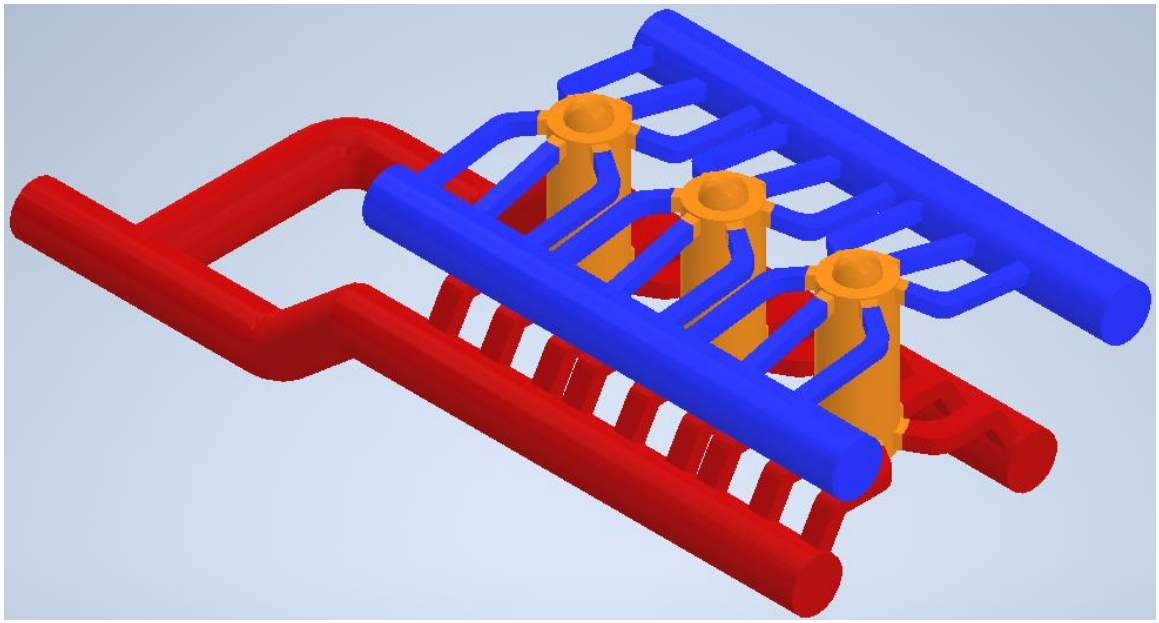

Figure 4.61. CAD model for the tumble design of the opposed piston engine

Figure 4.61 shows the tumble design with ports that are tilted up. This design is expected to produce higher tumble in the cylinders than the other designs. No methods were implemented to balance the mass flow rates of the ports or to increase swirl.

Figure 4.62 is a front view of the intake manifold for the tumble design. The blue sections on the left and the right of Figure 4.62 is the left and right half of the intake manifold. The orange portion of Figure 4.62 is one of the cylinders for the engine.

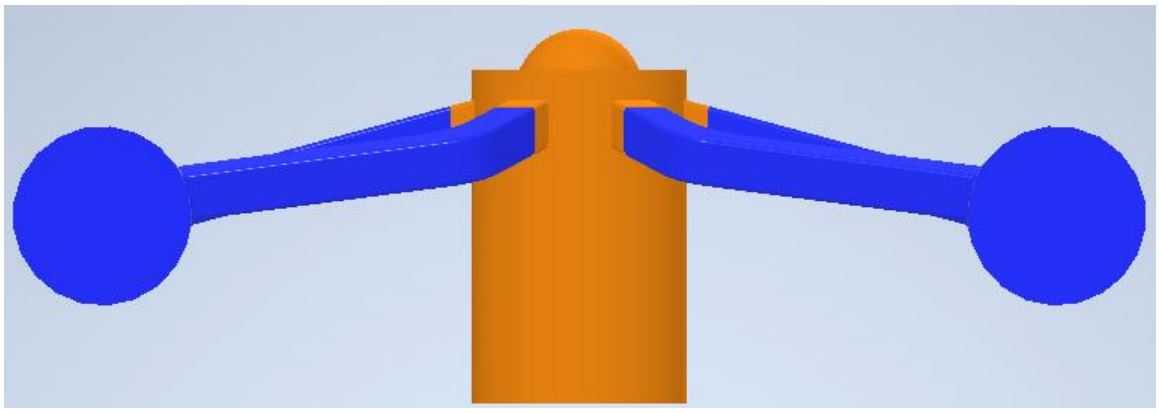

Figure 4.62. Front view of the intake manifold for the tumble opposed piston engine design

Figure 4.62 shows the upward tilt of the intake manifold runners for the tumble design. The ports were tilted up to avoid allowing the flow to go straight from the intake ports to the exhaust ports. The angle that the ports are tilted up by is fifteen degrees.

4.4.2 Mesh and Boundary Conditions

Figure 4.63 is an isometric view of the mesh for the tumble design. The scale is located at the bottom of Figure 4.63. The top of the model in Figure 4.63 is the intake manifold for increased tumble. The runners from the intake and exhaust manifolds have a smaller mesh size than most of the other regions which makes them appear as black sections. The exhaust manifold is the bottom component in Figure 4.63. The cylinders are in between the intake and exhaust manifolds in Figure 4.63.

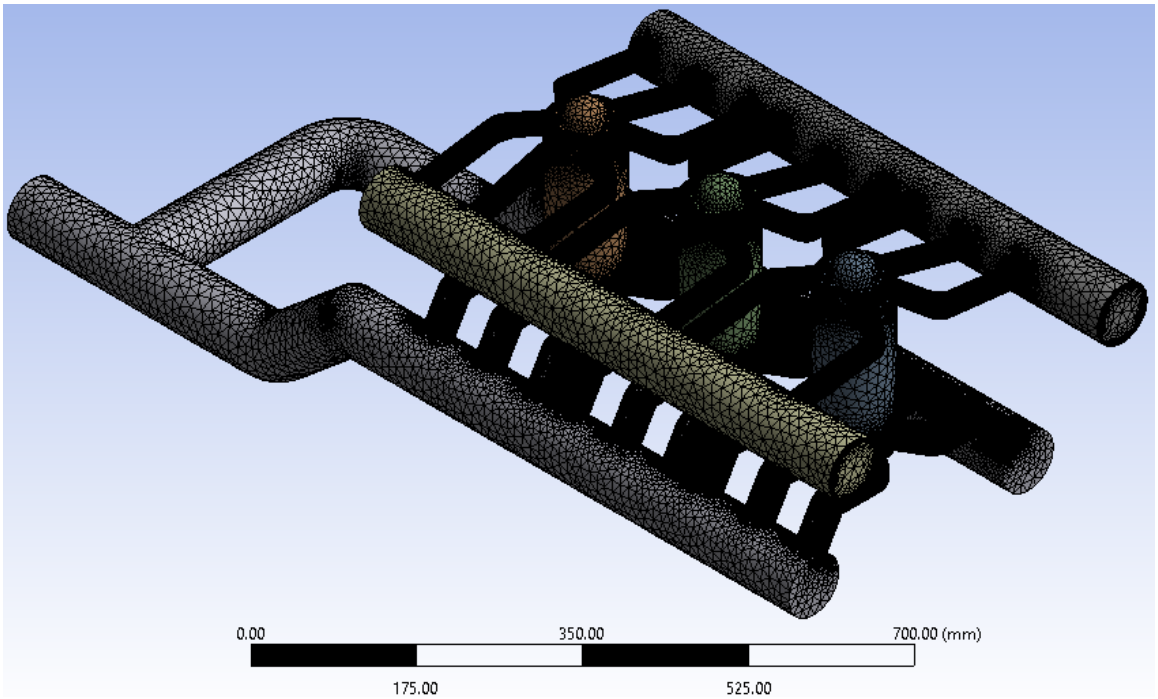

Figure 4.63. Isometric view of the mesh for the tumble design of the opposed piston engine

The element size for the mesh seen in Figure 4.63 was set to the same size and sizing constraints as the baseline model. The mesh for the tumble model used tetrahedral elements and inflation layers just like the baseline model. The mesh for the tumble design had 15,496,223 total elements.

Figure 4.64 shows the right half of the meshed tumble engine cut down the middle on the XY plane. The inflation layers for the mesh can be seen in the bottom left corner of Figure 4.64 which is a cross section of a portion of the exhaust manifold. The scale bar is at the bottom of Figure 4.64 to show how long the model is in millimeters.

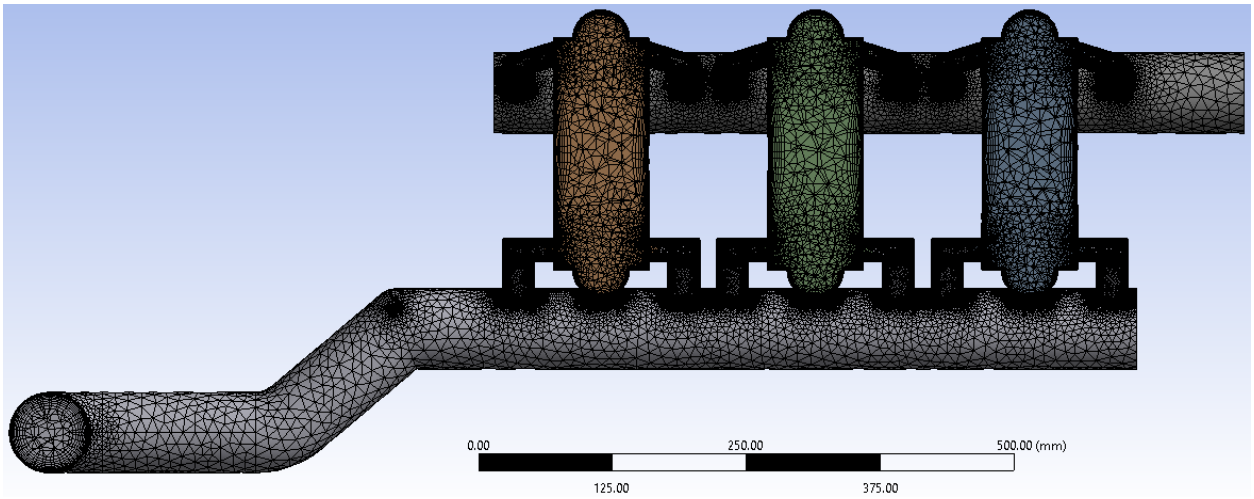

Figure 4.64. Section view of the meshed model for the tumble design of the opposed piston engine

Figure 4.64 shows the elements inside of the cylinders start out small at the top of the cylinders, become large near the center of the cylinder, and then shrink again near the exhaust ports. The meshing software also decreases the size of the elements near the walls to get more accurate results near the walls.

Figure 4.65 is a cross sectional view of one of the intake manifold runners rotated upside down. Figure 4.65 has runner rotated upside down to allow the scale bar located under the cross-sectional view of the runner to be readable. The scale bar is ten millimeters which is half the length or width of the port size.

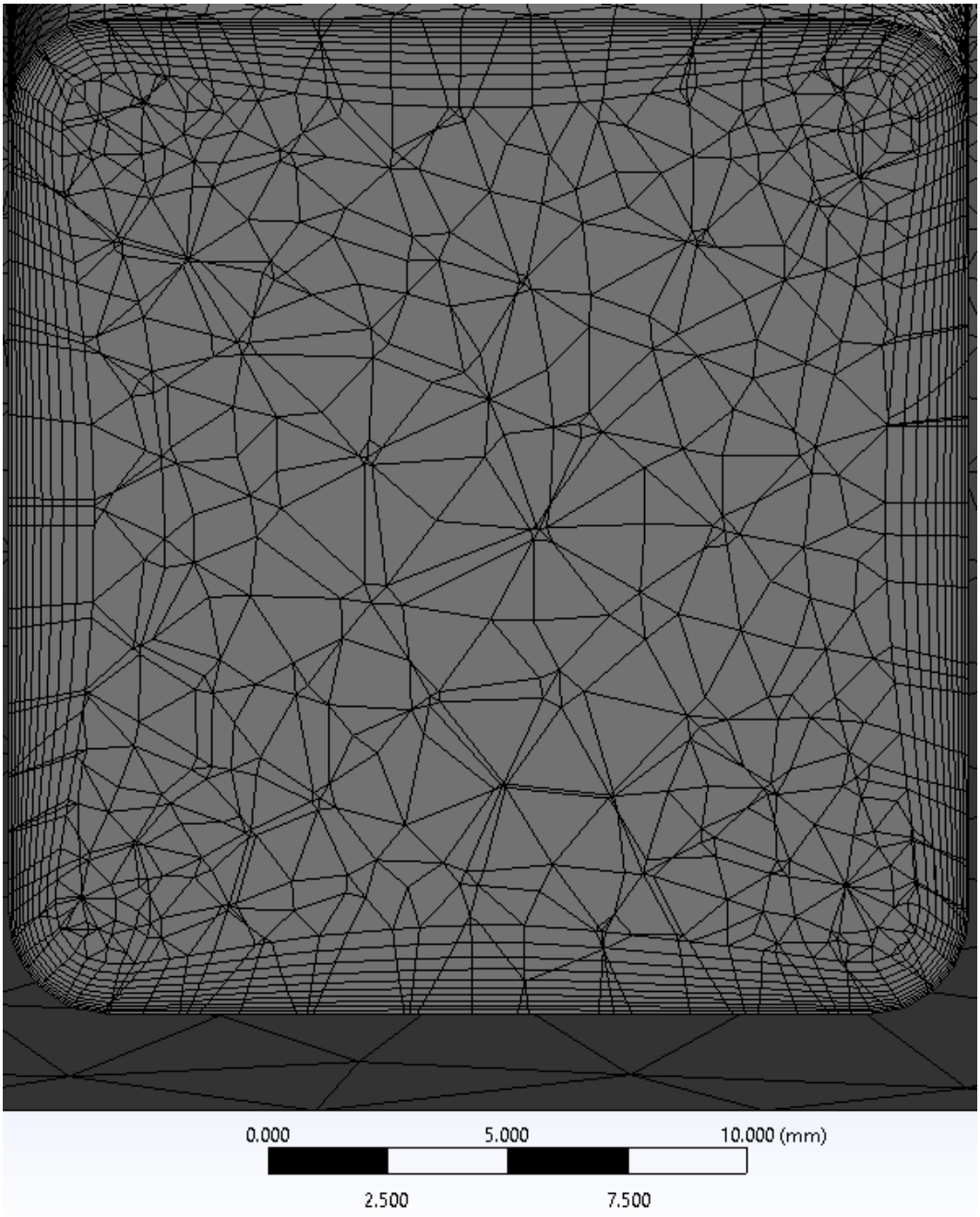

Figure 4.65. Section view of the meshed intake manifold runner for the tumble design

Figure 4.65 shows a close-up of the inflation layers of an intake manifold runner so that the elements are easier to see. Figure 4.65 shows that the layers become thinner closer to the walls. The inflation layers for the mesh of the tapered manifold design had the same settings as for the baseline design. Figure 4.65 shows that the corners of the ports have smaller elements than the center area of the intake ports.

Figures 4.66 and 4.67 show boundary conditions for the tapered manifold design. Figure 4.66 shows the wall boundaries, highlighted in red. The wall boundaries were setup the same as the baseline model. The letter tags seen in Figure 4.66 label each component of the model and correspond to the names in the list in the top left corner of Figure 4.66.

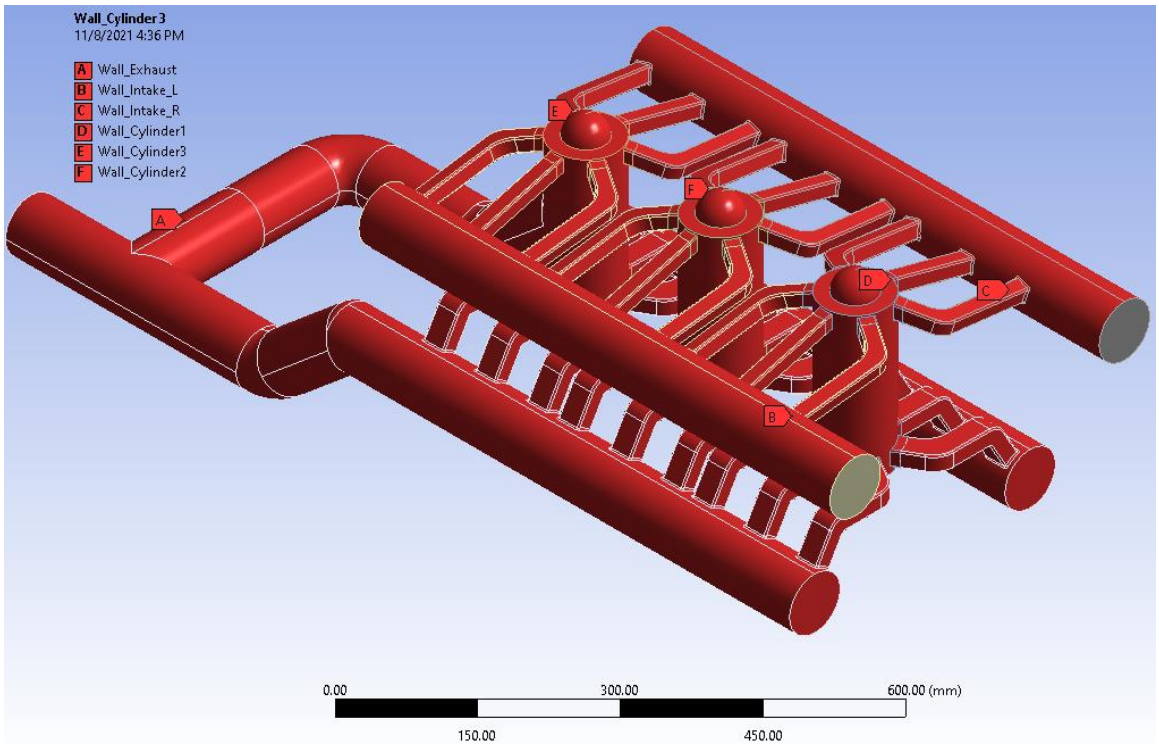

Figure 4.66. Wall Boundary conditions for the tumble design

The wall boundaries for the tumble design were setup the same as the baseline model. Figure 4.66 shows the different components of the model by name using the letter tags. The unselected areas in Figure 4.66, the non-red areas, are the pressure inlets to the model.

Figure 4.67 shows the pressure inlet and outlet boundary conditions. The left side of Figure 4.67 shows the pressure inlets labeled with the letter tag A. The middle of Figure 4.67 shows the legend for the letter tags. The right side of Figure 4.67 shows the pressure outlet on the backside of the engine with the letter tag B.

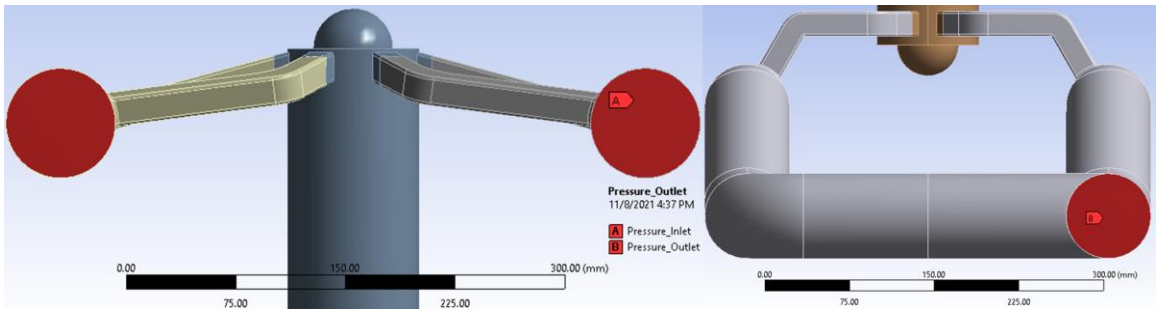

Figure 4.67. Inlet and outlet boundaries for the tumble design

The same pressure as the baseline model was applied to the inlets which was 41.4 kPa (6 psi) gage pressure. The pressure applied to the outlet was atmospheric pressure, zero gage pressure. The temperature of the pressure inlet and outlet was 320 Kelvin and 300 Kelvin.

4.4.3 Balance of Mass Flow

Figure 4.68 shows the mass flow of air through each of the intake and exhaust ports. The intake ports have a positive mass flow rate (top side of the bar chart), and the exhaust ports have a negative mass flow rate (bottom side of the bar chart). Figure 4.68 uses different colored bars for each cylinder as seen in the legend from the right side of Figure 4.68. Across the top of Figure 4.68 are labels sectioning of the different ports, one through six for each cylinder.

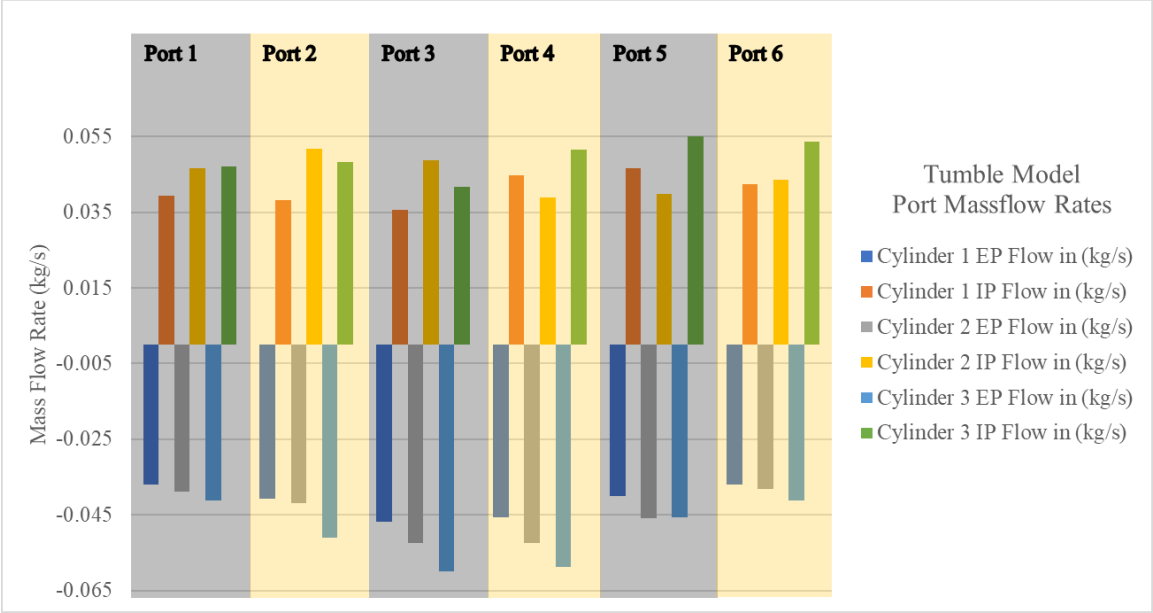

Figure 4.68. Mass flow through each port of cylinders one, two, and three for the tumble design

Figure 4.68 shows that the mass flow rates through the ports of each cylinder are not balanced for the tumble design. The goal for the tumble design was not to increase the balance of the mass flow rates through the ports. Cylinder three still had the highest mass flow rate through the cylinder but intake ports two and three for cylinder two had higher mass flow rates than those ports for cylinder three.

Figure 4.69 shows the velocity magnitude in m/s extracted from three sections of the tumble engine model. The order of the sections is top to bottom intake ports, middle of the cylinder, and exhaust ports. Each section of Figure 4.69 also has three circular contour plots for cylinders three, two, and one, from left to right. The color bar on the right of Figure 4.69 shows the values for velocity magnitude.

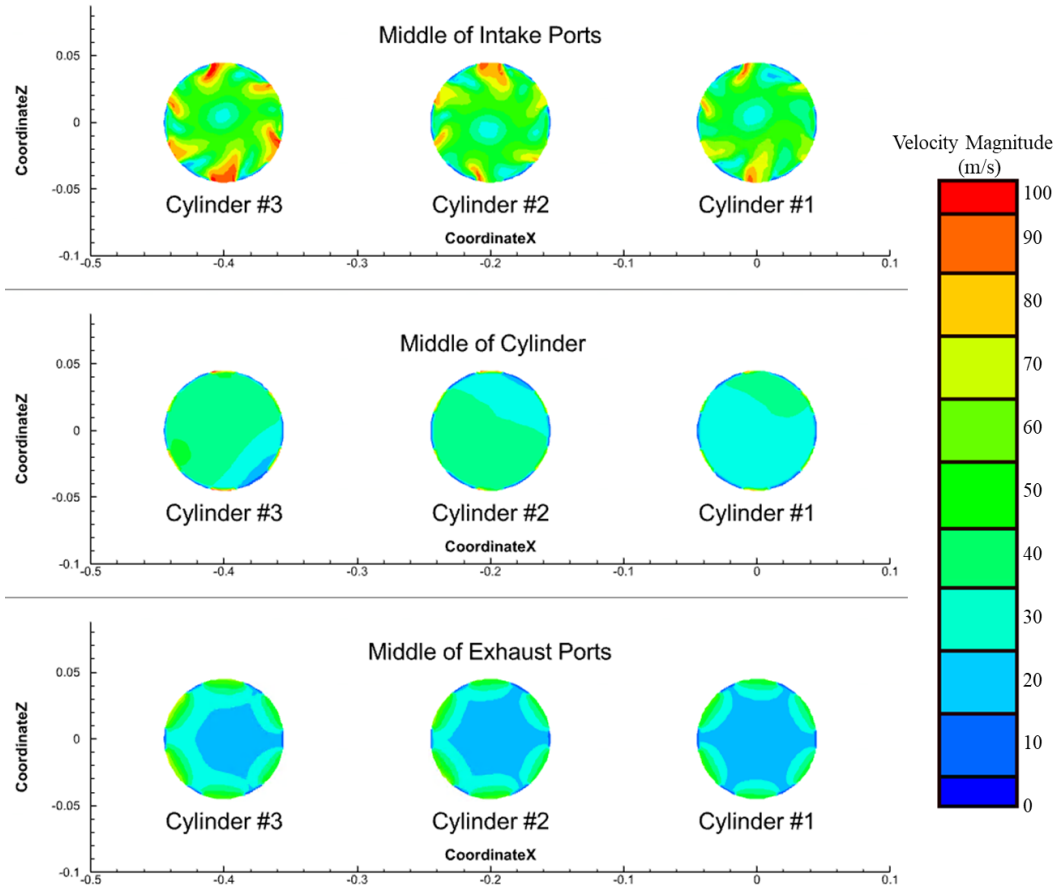

Figure 4.69. Velocity magnitude (m/s) for different sections of the cylinders for the tumble design

Figure 4.69 shows that the intake ports had a higher velocity magnitude near the intake ports and lower velocity in the center of the cylinders. The middle of the cylinders for the tumble model had a higher velocity magnitude than the baseline design. Figure 4.69 shows the magnitude of the flow velocity at the exhaust ports was roughly the same as the baseline design.

Figure 4.70 shows the velocity magnitude for a vertical (XY) plane section of cylinders one, two, and three for the tumble design. The order of the cylinders from left to right is cylinder three, two, and one. On the right side of Figure 4.70 is the color bar for the contour plot which shows the values of the velocity magnitude within the cylinder on the XY plane.

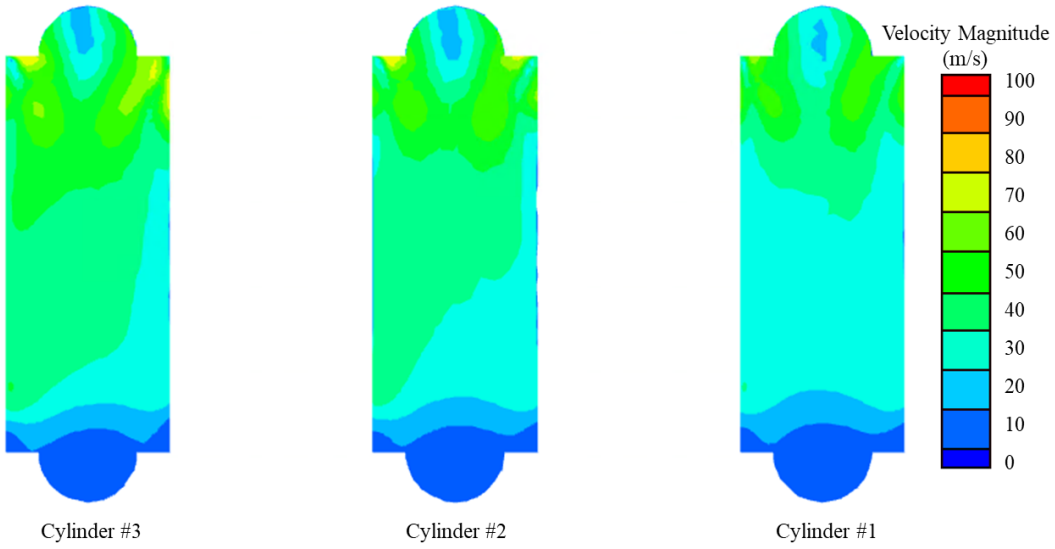

Figure 4.70. Velocity magnitude (m/s) on the XY plane for cylinders one through three of the tumble design

Figure 4.70 shows that the flow has a low velocity area in the ball of the piston above the intake ports. The velocity magnitude through the cylinder is lower than the baseline design. The velocity magnitude shows that the flow was exiting the cylinder through the ports on the left of cylinders three and two. The velocity magnitude was more uniform for the tumble design in comparison to the baseline design.

4.4.4 Swirl Circulation

Figure 4.71 shows Y-vorticity contour plots for the tumble design. Figure 4.71 is laid out similarly to Figure 4.69 where it has three sections that are separated by each section of the engine. The labels for each section appear above the contour plot. The three sections are from top to bottom the intake ports, middle of the cylinder, and exhaust ports. Like Figure 4.69, each section of Figure 4.71 has three sections of contour plots for cylinders three, two, and one, respectively.

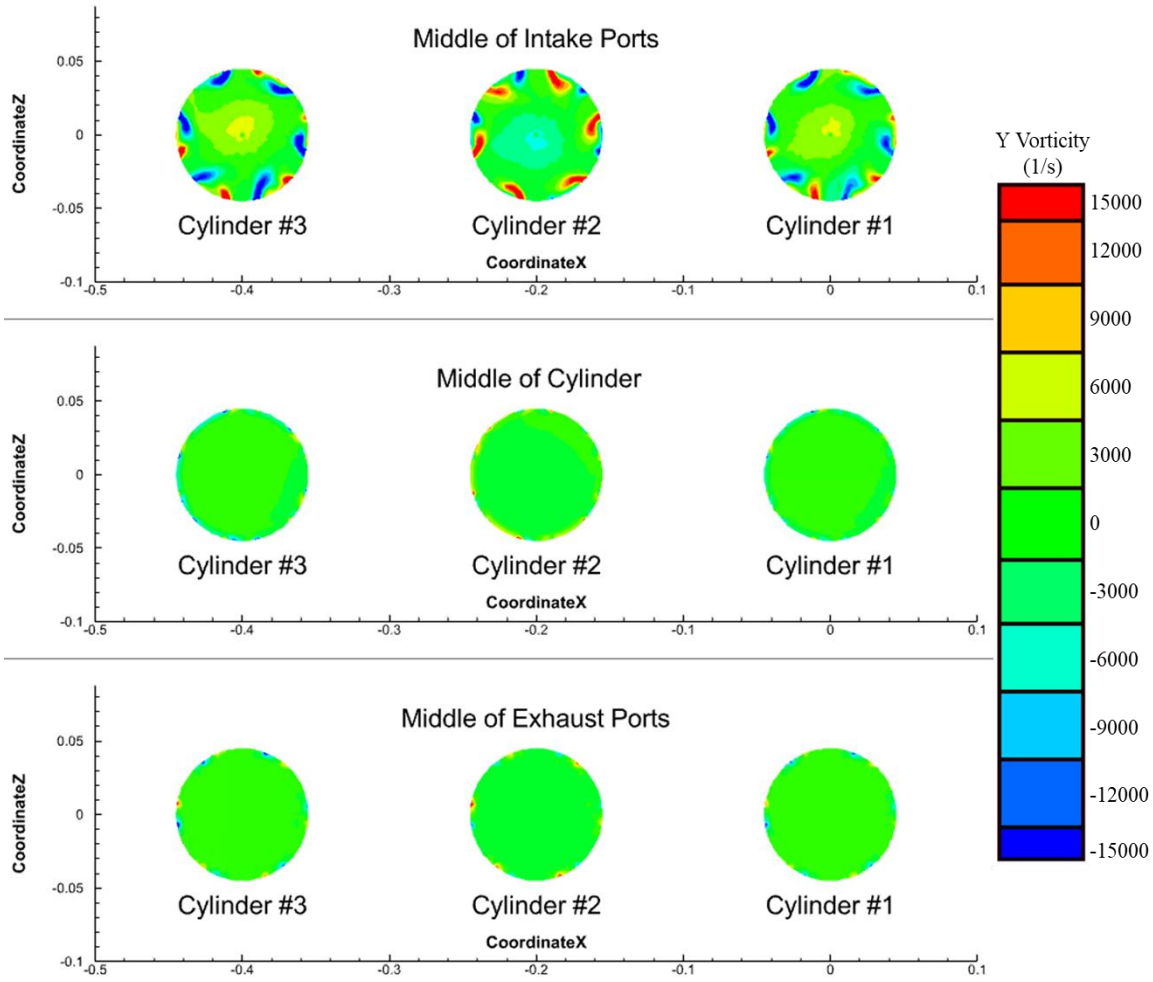

Figure 4.71. Vorticity for the three different sections for cylinders one through three of the tumble design

Figure 4.71 shows an interesting pattern for the swirl where cylinders one and three have higher negative swirl regions near the intake ports and cylinder two has larger positive regions. The swirl for the intake ports had a similar pattern to the baseline design but had higher values in the center of the cylinders. The middle of the cylinder and the exhaust ports did not have noticeable swirl at the scale of the color bar.

Table 4.12 shows the swirl calculated for each cylinder section and is formatted the same as Table 4.9. The new addition to Table 4.12 from Table 4.9 is the added column showing the swirl design swirl values. The highlighted numbers in red for Table 4.12 represent a decrease in swirl magnitude compared to the baseline design. The numbers highlighted in green for Table 4.12 represent an increase of swirl magnitude from the baseline design.

Table 4.12. Swirl values for the three sections of the four engine designs

Section	Cylinder	Swirl (m^2/s) Baseline	Swirl (m^2/s) Tapered	Swirl (m^2/s) Swirl	Swirl (m^2/s) Tumble
Middle of the intake ports	1	-0.1	0	-3.0	0.7
	2	0.1	0	-2.5	-0.7
	3	0	-0.2	-3.4	0.8
Midway through the cylinder	1	0	0	-11.7	0
	2	0	0	-12.3	0
	3	0	0	-14.3	0
Middle of the exhaust ports	1	0	0.1	-6.0	1.1
	2	0	0.1	-6.5	-1.0
	3	-0.1	-0.1	-7.1	0.9

Table 4.12 shows that the swirl is for tumble design is higher for every plane and cylinder than the baseline design. The swirl for the tumble design was highest on the plane for the exhaust ports for all three cylinders. The tumble model swirl values were close to the values of the baseline model with the largest difference of magnitude being around 1E+02 m^2/s.

4.4.5 Tumble Circulation

Figure 4.72 shows the Z-vorticity contour plot for cylinders three, two, and one from left to right of the tumble design. The cylinders all have a label underneath the contour plot identifying each cylinder. The right portion of Figure 4.72 shows the color bar values for the contour plot. Figure 4.72 is based on the XY plane which is a vertical plane through the center of the engine.

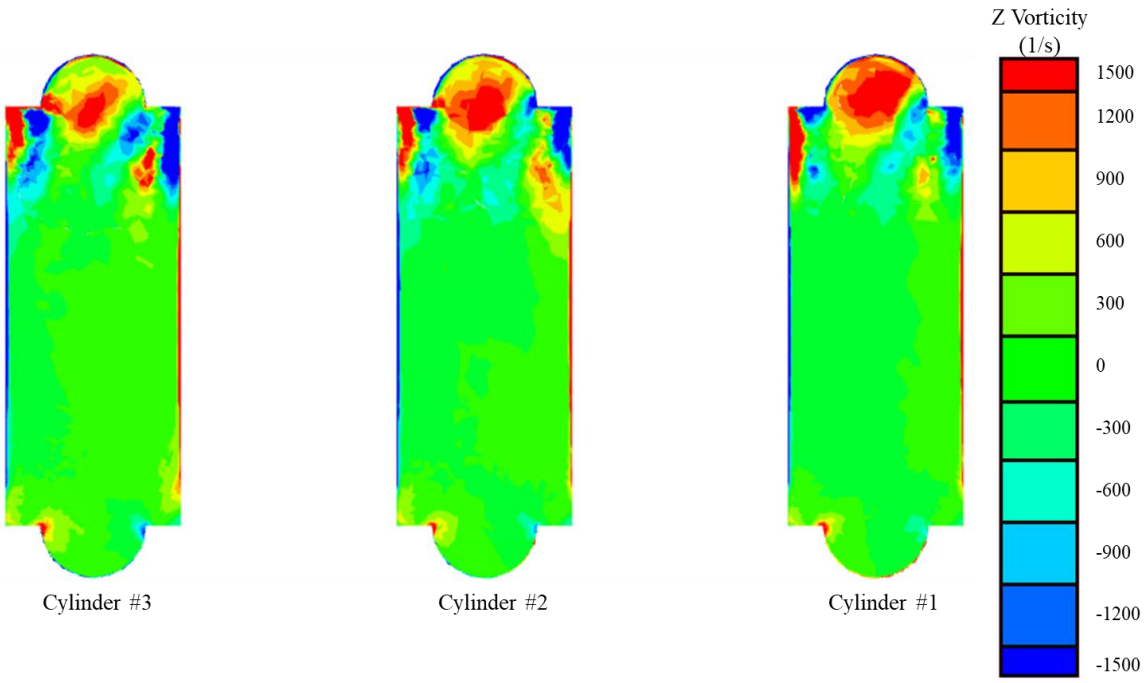

Figure 4.72. Vorticity on the XY plane for cylinders one through three of the tumble design

Figure 4.72 shows that the highest vorticity is in the top of the cylinders. The vorticity in the cylinder below the intake ports is lower than the baseline design. The vorticity in the circular region at the top of the piston had positive values for the tumble design. However, the area where tumble is calculated for the designs is the rectangular regions between the two circular regions at the top and bottom of the cylinders.

Table 4.13 was set up similarly to Table 4.10. The newest addition to the Table is a column on the right that shows the tumble of the tumble design in m^2/s. The highlighted numbers in red for Table 4.13 represent a decrease in tumble magnitude compared to the baseline design. The numbers highlighted in green for Table 4.13 represent an increase of tumble magnitude from the baseline design.

Table 4.13. Comparison of tumble values for the three sections of the four engine designs

Cylinder	Rectangular Region Location	Tumble (m^2/s) Baseline	Tumble (m^2/s) Tapered	Tumble (m^2/s) Swirl	Tumble (m^2/s) Tumble
1	Left	-3.7	-0.7	5.6	-0.1
	Right	4.6	6.0	-4.3	-0.5
2	Left	-4.0	-4.1	5.8	0
	Right	4.4	6.2	-6.3	0
3	Left	-6.0	-7.3	6.6	0
	Right	5.3	4.8	-6.0	0

Table 4.13 shows that the tumble for the tumble design was smaller than the baseline design. As mentioned earlier this design resulted in regions of the higher vorticity being in the circular region which was outside of the rectangular regions of the comparison. Surprisingly the swirl design increased the tumble the most out of each design.

4.4.6 Turbulent Kinetic Energy (TKE)

The volume average TKE was calculated for the swirl design and then compared to the other two engine designs. Table 4.14 is formatted the same as Table 4.11. Table 4.14 has one more column on the right than Table 4.11. The column on the right of Table 4.14 shows the volume average TKE in m^2/s^2 for the swirl design. The highlighted numbers in red for Table 4.14 represent a decrease in TKE compared to the baseline design. The numbers highlighted in green for Table 4.14 represent an increase in TKE from the baseline design.

Table 4.14. Comparison of volume average TKE for four engine designs of cylinders one, two, and three

Cylinder	Volume Average TKE Baseline (m^2/s^2)	Volume Average TKE Tapered (m^2/s^2)	Volume Average TKE Swirl (m^2/s^2)	Volume Average TKE Tumble (m^2/s^2)
1	225	231	378	326
2	313	271	444	391
3	435	359	557	469

Table 4.14 shows that the volume average TKE for the tumble model was higher than the baseline model. The swirl design had the highest volume average TKE, and the tumble design had the second highest. Cylinder three had the highest volume average TKE for each design. Cylinder one had the lowest volume average TKE for each design. The results for cylinders one and three make sense since the mass flow rate into cylinder three is higher than the mass flow rate into cylinder one.

Figure 4.73 is a contour plot that shows the TKE on a vertical plane through the middle of each cylinder for the tumble design. The cylinders are ordered from left to right three, two, and one. The color bar on the right of Figure 4.73 shows the values for each color in m^2/s^2 on the contour plot.

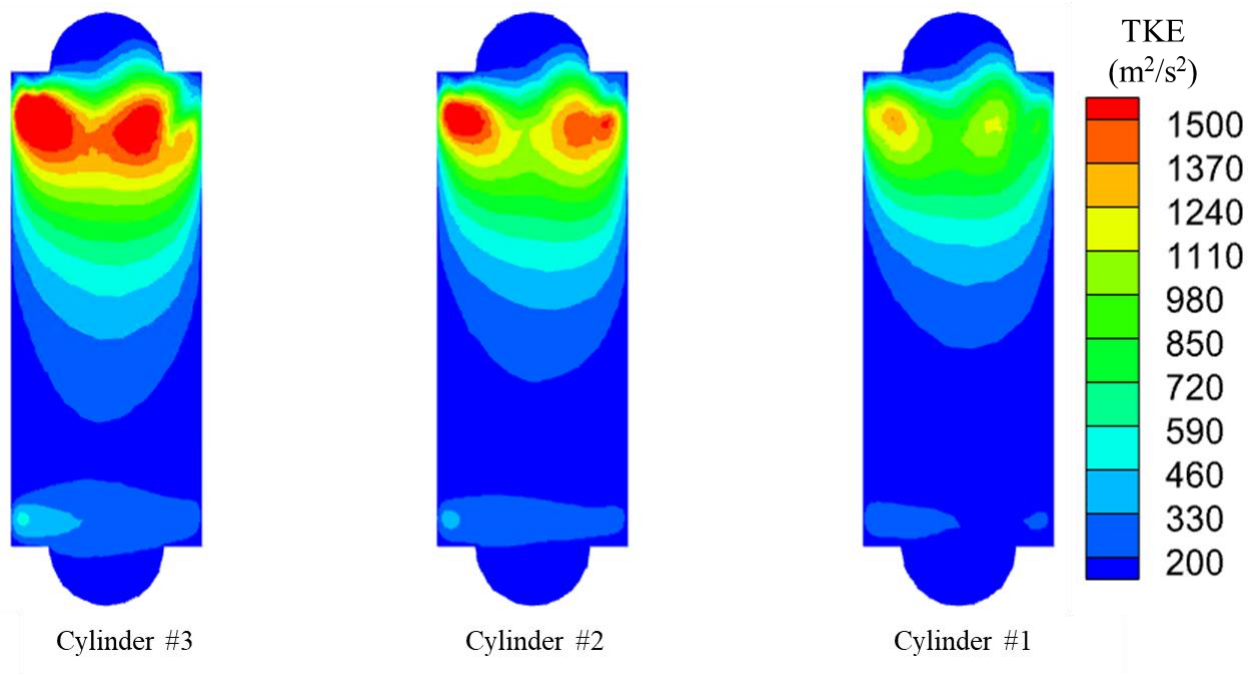

Figure 4.73. TKE on the XY plane for the middle of each cylinder for the tumble design

Figure 4.73 shows that cylinder three has the highest TKE values just like for the baseline design. The regions in the cylinders that had the highest values of TKE were near the intake ports of the cylinders. The fact that the TKE was highest near the intake ports makes sense since that is where the velocity magnitude in the cylinders were the highest.

Figure 4.74 is a contour plot of TKE on the ZX plane for the middle of the intake ports of each cylinder for the tumble design. The cylinders are ordered from left to right three, two, and one. The color bar on the right of Figure 4.74 shows the values for each color in m^2/s^2 on the contour plot.

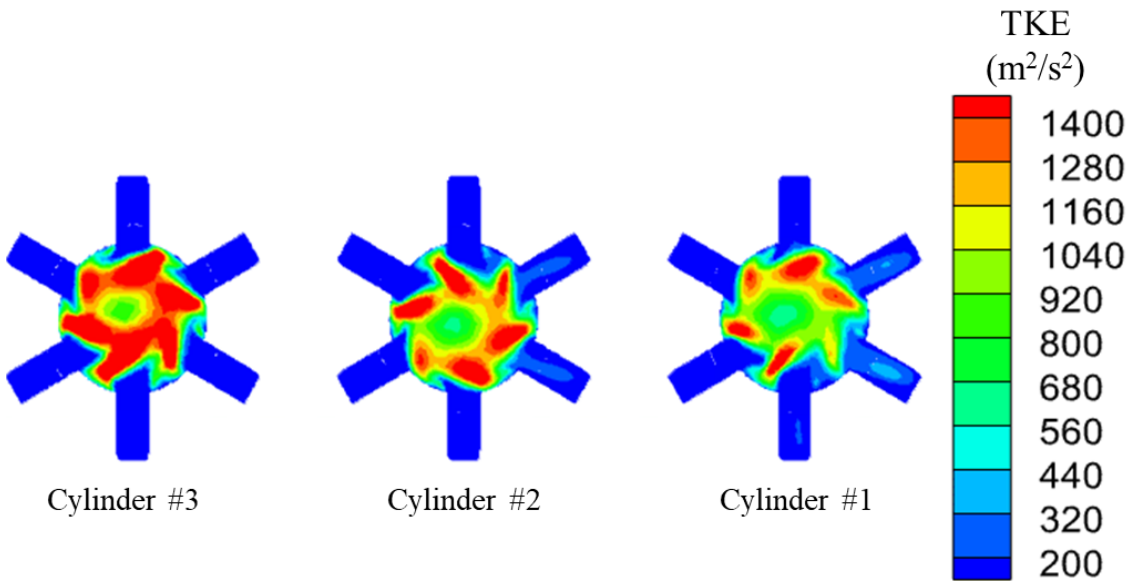

Figure 4.74. TKE on the ZX plane of the middle of the intake ports of the tumble design

Figure 4.74 shows that cylinders one and three had a similar region of TKE but different values. Cylinder one had the lowest TKE and cylinder three had the highest. The region of TKE seen in cylinder two was flipped in the opposite direction of the region seen in cylinder three.

Figure 4.75 is a contour plot of TKE on the ZX plane for the middle of each cylinder for the tumble design. The cylinders are ordered from left to right three, two, and one. The color bar on the right of Figure 4.75 shows the values for each color in m^2/s^2 on the contour plot.

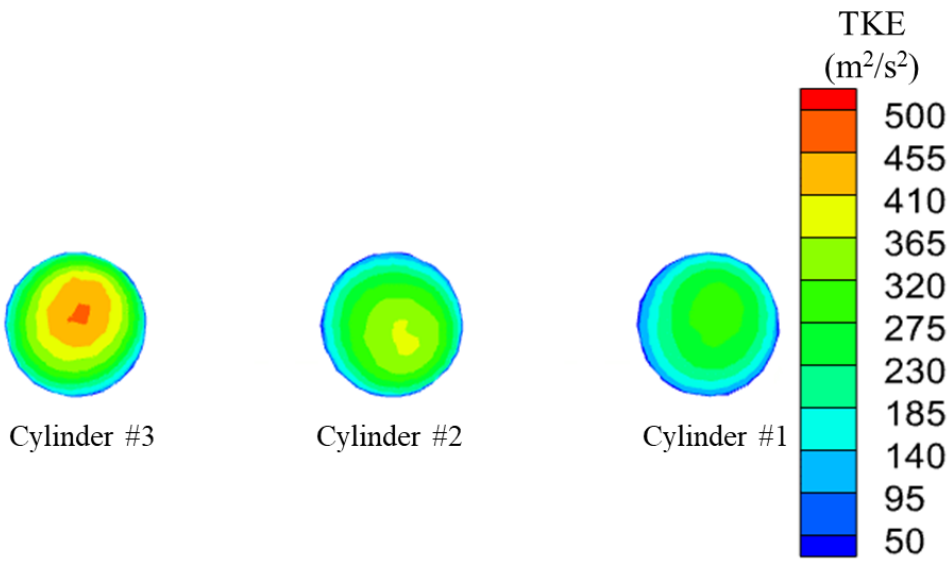

Figure 4.75. TKE on the ZX plane of the middle of the cylinders for the tumble design

Figure 4.75 shows that cylinder three hade the most TKE in the middle of the cylinders for the tumble design. The tumble design had less TKE in the middle of the cylinders than the baseline design. The intake ports were tilted up so the flow energy in the middle of the cylinders was lower.

Figure 4.76 is a contour plot of TKE on the ZX plane for the middle of the exhaust ports for each cylinder of the tumble design. The cylinders are ordered from left to right three, two, and one as seen from the labels across the bottom of Figure 4.76. The color bar on the right of Figure 4.76 shows the values for each color in m^2/s^2 on the contour plot.

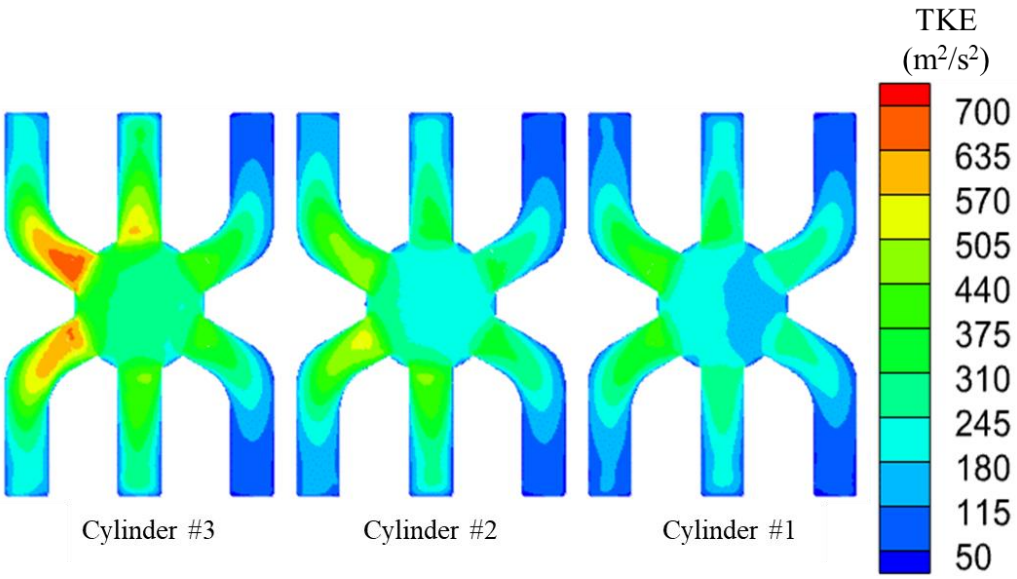

Figure 4.76. TKE on the ZX plane of the middle of the exhaust ports for each cylinder

Figure 4.76 shows that the TKE for the exhaust plane had the lowest TKE values for the cylinders of the tumble design. The TKE on the exhaust port plane was lower for the tumble design than it was for the baseline design. Cylinder three had the highest TKE for the tumble design on the exhaust plane.

Figure 4.77 is a contour plot of TKE on the YZ plane for the middle of cylinder one for the baseline design. The color bar on the right of Figure 4.77 shows the values for each color in m^2/s^2 on the contour plot. The top of Figure 4.77 is the intake side of the cylinder and the exhaust is the bottom of Figure 4.77.

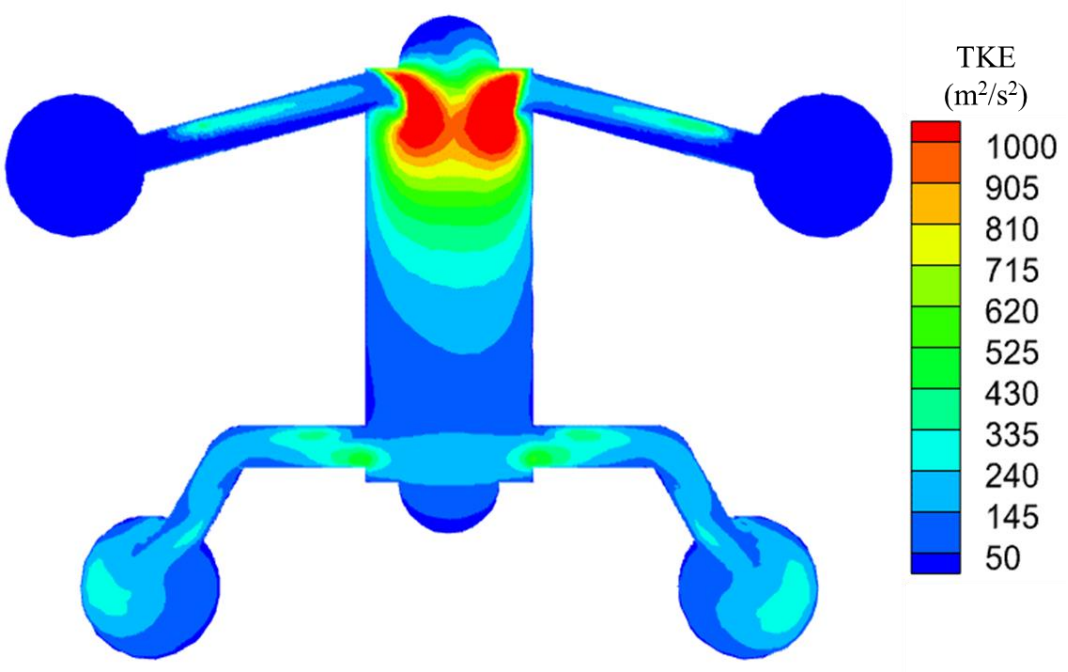

Figure 4.77. TKE on the YZ plane of the middle of cylinder one for the tumble design

Figure 4.77 shows that the regions that experience the highest TKE in the YZ plane are near the intake and exhaust ports. The TKE near the intake ports is higher than the TKE near the exhaust ports. The TKE for the tumble engine on the YZ plane of cylinder one for the tumble design was higher than the TKE on the YZ plane of cylinder one of the baseline design.

Figure 4.78 is a contour plot of TKE on the YZ plane for the middle of cylinder two for the tumble design. The color bar on the right of Figure 4.78 shows the values for each color in m^2/s^2 on the contour plot. The top of Figure 4.78 is the intake side of the cylinder and the exhaust is the bottom of Figure 4.78.

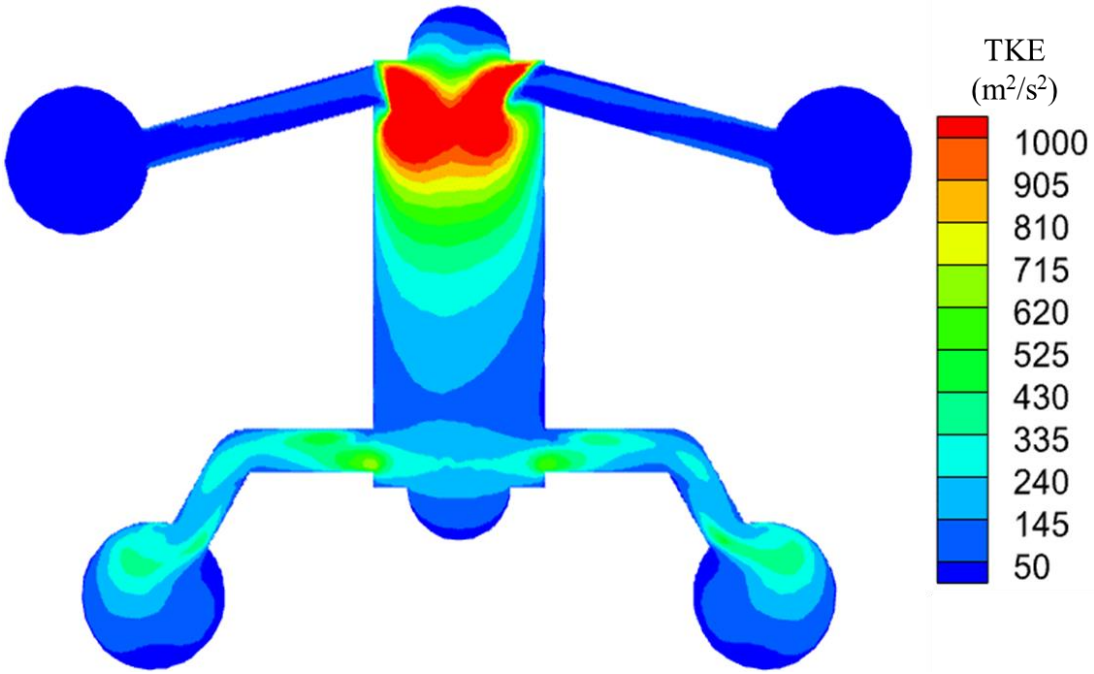

Figure 4.78. TKE on the YZ plane of the middle of cylinder two for the tumble design

Figure 4.78 shows the that just like for cylinder, the regions of the highest TKE are near the intake and exhaust ports of the cylinder for the tumble design. Cylinder two has a similar shaped region of high TKE as cylinder one near the intake manifold but it has shifted to the left slightly. The TKE on the YZ plane of cylinder two is higher than the TKE on the YZ plane for cylinder one.

Figure 4.79 is a contour plot of TKE on the YZ plane for the middle of cylinder three of the tumble design. The color bar on the right of Figure 4.79 shows the values for each color in m^2/s^2 on the contour plot. The top of Figure 4.79 is the intake side of the cylinder and the exhaust is the bottom of Figure 4.79.

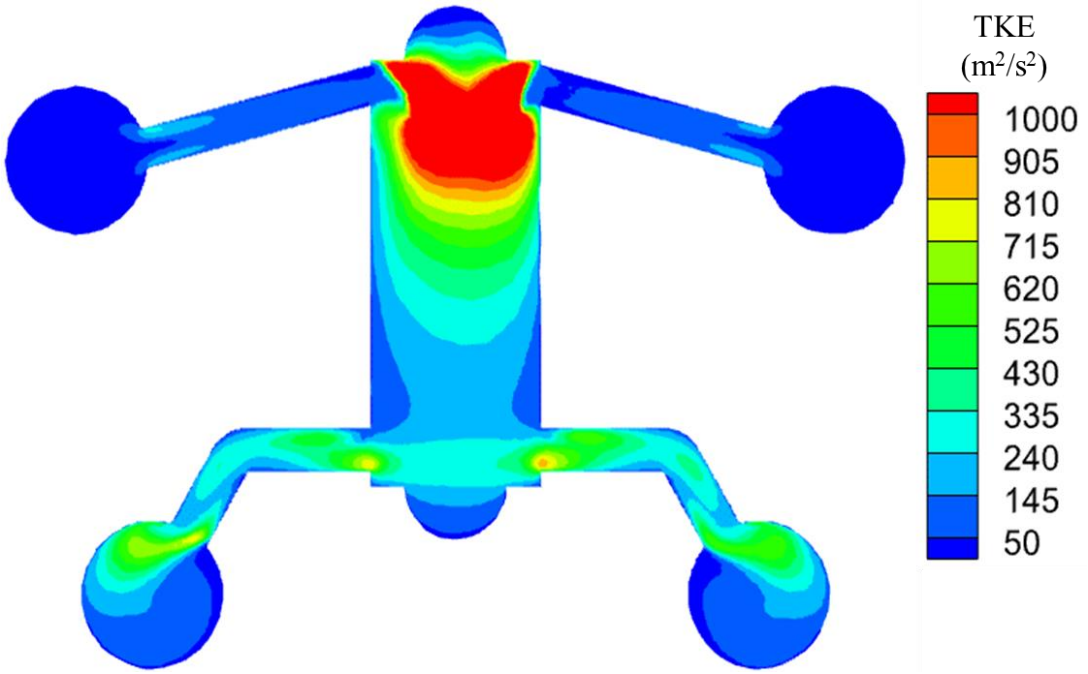

Figure 4.79. TKE on the YZ plane of the middle of cylinder three for the tumble design

Figure 4.79 shows that the highest region of TKE on the YZ plane for cylinder three was near the intake ports in a similar shape to the one seen for cylinder one. The TKE for the YZ planes of the tumble design was highest for cylinder three. Cylinder three had a region of higher TKE that connected the high TKE from the intake ports to the exhaust port TKE region. Cylinders one and two had a section of lower TKE in between the intake ports and the exhaust ports.

4.4.7 Tumble Design Summary

The tumble design was meant to increase the tumble in the cylinder when compared to the baseline model. The tumble design had increased swirl and TKE but had lower tumble than the baseline design. One reason for the lower tumble was because the regions of high vorticity for the tumble design were in the ball of the pistons which was outside of the region where tumble was calculated. The reason that the vorticity was highest in the balls of the pistons was because of the fifteen-degree upward tilt angle of the intake ports. Lastly the mass flow rates for the tumble design were not balanced for each of the ports.

4.5 Balanced Mass Flow Discussion

The mass flow rate through the ports was unbalanced for each engine design. However, one engine design was closer to achieving a balanced mass flow rate than the others. Observing the mass flow rates into each cylinder rather than each intake port allows the data to show which model was closest to being balanced.

Table 4.15 has a column on the left that shows the engine number where engine one is the baseline design, two is the tapered manifold design, three is the swirl design and four is the tumble design. The second column shows the mass flow rate into the cylinder in kilograms per second for cylinder one of each engine. The third column shows the mass flow rate into the cylinder in kilograms per second for cylinder two of each engine. The fourth column shows the mass flow rate into the cylinder in kilograms per second for cylinder three of each engine.

Table 4.15. Mass flow rates into the cylinders for each engine design

	Cylinder 1 (kg/s)	Cylinder 2 (kg/s)	Cylinder 3 (kg/s)
Engine 1 Baseline	0.2400	0.2780	0.3081
Engine 2 Tapered	0.2368	0.2600	0.3124
Engine 3 Swirl	0.2421	0.2571	0.2818
Engine 4 Tumble	0.2470	0.2695	0.2974

The comparison of the cylinder mass flow rates is a matter of looking at the cylinder with the highest mass flow rate, cylinder three for each design, and comparing to the cylinder with the lowest mass flow rate, cylinder one. Table 4.15 showed that out of the four engine designs the engine designed to increase swirl had the closest mass flow rate balance for each cylinder. The engine designed to balance the mass flow rate was engine two which produced the most unbalanced results. Therefore, angling the intake manifold runners will make more of an impact for the balance of mass flow than tapering the manifold will.

CHAPTER 5. SUMMARY, CONCLUSIONS, and RECOMMENDATIONS

5.1 Summary

The research investigated the role of intake manifold and port geometry on flow and turbulence through an opposed-piston, two-stroke engine. Four engine designs were considered. The baseline engine design featured an intake manifold having constant cross-section and straight intake ports. A tapered manifold design featured an intake manifold having decreasing cross section. A swirl port design featured an intake manifold having constant cross-section and intake ports having 10 degrees of swirl angle. Finally, a reverse tumble port design featured an intake manifold having constant cross-section and intake ports having zero swirl angle but a reverse tilt angle of 15 degrees. The effect of geometry on flow and turbulence was quantified using four flow parameters: mass flow rate through each port, swirl circulation, tumble circulation, and turbulent kinetic energy (TKE).

5.2 Conclusions

The engine designed for increased swirl had a more balanced mass flow rate than the other engine designs. The engine designed to balance the mass flow rate was the one with tapered manifolds and it did not balance the mass flow rate. The results from the comparison of the swirl and tapered designs show that the angling of the ports is more beneficial for balancing the mass flow rates than tapering the intake manifold.

The next flow parameter to discuss the results for is swirl. The engine designed for increased swirl had higher values of swirl than the baseline engine. The swirl engine design was designed to increase the swirl from the values of the baseline model which did happen. The swirl engine design had the highest swirl out of all the engine designs.

The next flow parameter to discuss the results for is tumble. The engine designed to increase tumble was meant to increase the tumble within the cylinder through tilting the ports upwards towards the intake piston. However, the engine with the most tumble was the swirl engine design. The tumble engine had the lowest tumble out of each engine which is because the vorticity was in the ball of piston and out of the area used to calculate the tumble over.

The last flow parameter looked at in this work was the in-cylinder volume average TKE. The volume average TKE calculation was performed in Fluent using the volume integral function and specifying the cylinders which also included a portion of the intake and exhaust runners. The amount of the runner included was a twenty-millimeter section from the cylinder wall to the rest of the intake manifold for each model. The engine with the highest volume average TKE was the engine designed to increase swirl within the cylinders.

5.3 Answers to Research Questions

5.3.1 First Research Question:

How does the geometry of the manifolds effect the balance of the mass flow through each port?

5.3.2 Answer to First Research Question:

The engine design with angled ports to increase the swirl had mass flow rates into the cylinder that were closest to being balanced. Therefore, the engine designed for swirl had the most uniform flow.

5.3.3 Second Research Question:

How does the intake manifold and port geometries effect the turbulence within the cylinder?

5.3.4 Answer to Second Research Question:

The three metrics used to quantify turbulence were swirl, tumble, and volume average TKE within each of the cylinders. Quantifying the three metrics required designing two engines, one to increase the swirl, and one to increase the tumble. The engine for increasing the swirl utilized a cylinder with the intake ports being tilted by ten-degrees to encourage a swirling motion within the cylinder. Angling the intake ports resulted in a large increase of swirl in comparison to the baseline model. The engine for improved tumble was setup to have an upward tilt of fifteen-degrees to reduce short-circuiting in the engine.

The intake ports being angled for swirl had the biggest increase for swirl and volume average TKE for each cylinder. The tumble design resulted in much lower tumble because the vorticity caused by the angle of the ports was in the ball of the cylinder above the region where the tumble was calculated for each engine design. Therefore, angling the ports significantly increases the swirl and TKE for each cylinder while tilting the ports upwards results in much lower tumble in most of the cylinder.

5.4 Recommendations

The first recommendation for future work is to extend the present analysis using dynamic-mesh CFD simulations. Including the motion of the piston will capture the dynamic pressure changes, leading to more reliable results.

A second recommendation for future work is to consider swirl and tilt angle at the exhaust ports. Modifications to intake port angle had a large effect on in-cylinder turbulence. The effect of exhaust port angle should be considered.

A final recommendation for future work is to consider tapering or other geometric modification to the ports and runners in an attempt to achieve a more balanced mass flow distribution to the three cylinders.

LIST OF REFERENCES

Abani, N., Nagar, N., Zermeno, R., Chiang, M., & Thomas, I. (2017). Developing a 55% BTE Commercial Heavy-Duty Opposed-Piston Engine without a Waste Heat Recovery System. *SAE Technical Paper Series*. doi:10.4271/2017-01-0638

Ansys. (2020). ANSYS Meshing User's Guide. Retrieved from http://www.ansyhelp.ansys.com. Retrieved 11/30/2021 from: http://www.ansyhelp.ansys.com

Ausserer, J. K., Polanka, M. D., Baranski, J. A., Grinstead, K. D., & Litke, P. J. (2017). Measurement of Loss Pathways in Small, Two-Stroke Internal-Combustion Engines. *SAE International Journal of Engines, 10*(2), https://doi.org/10.4271/2017-01-9276

Changming, H., & Sichuan, X. (2016). Transient Gas Exchange Simulation and Uniflow Scavenging Analysis for a Unique Opposed Piston Diesel Engine. *SAE Technical Paper Series*. https://doi.org/10.4271/2016-01-1087

Frei, W. (2013, November 4). *Meshing your geometry: When to use the various element types*. COMSOL. Retrieved on December 1, 2021, from https://www.comsol.com/blogs/meshing-your-geometry-various-element-types/.

Huo, M., Huang, Y., & Hofbauer, P. (2015). Piston Design Impact on the Scavenging and Combustion in an Opposed-Piston, Opposed-Cylinder (OPOC) Two-Stroke Engine. *SAE Technical Paper Series*. doi:10.4271/2015-01-1269

Jilakara, S., Vaithianathan, J. V., Natarajan, S., Ramakrishnan, V. R., Subash, G., Abraham, M., … Das, L. M. (2015). An Experimental Study of Turbocharged Hydrogen Fuelled Internal Combustion Engine. *SAE International Journal of Engines*, *8*(1), https://doi.org/10.4271/2015-26-0051

Krishna, A., Mallikarjuna, J., Davinder, K., & Babu, Y. (2013). In-Cylinder Flow Analysis in a Two-Stroke Engine - A Comparison of Different Turbulence Models Using CFD. *SAE International Journal of Engines*, doi:10.4271/2013-01-1085

Luderer, G., Vrontisi, Z., Bertram, C., Edelenbosch, O. Y., Pietzcker, R. C., Rogelj, J., … Kriegler, E. (2018). Residual fossil CO2 emissions in 1.5–2 °c pathways. *Nature Climate Change*, *8*(7), 626–633. https://doi.org/10.1038/s41558-018-0198-6

Ma, F.-kang, Zhao, C.-lu, Zhao, Z.-feng, & Zhang, S.-lu. (2015). Scavenge flow analysis of opposed-piston two-stroke engine based on dynamic characteristics. *Advances in Mechanical Engineering*, *7*(4), 168781401558156. Retrieved on 4/23/2021 from: https://doi.org/10.1177/1687814015581569.

Mattarelli, E., Rinaldini, C., Savioli, T., Cantore, G., Warey, A., Potter, M., . . . Balestrino, S. (2017). Scavenge Ports Ooptimization of a 2-Stroke Opposed Piston Diesel Engine. *SAE Technical Paper Series*. doi:10.4271/2017-24-0167

McGlade, C., & Ekins, P. (2015). The geographical distribution of fossil fuels unused when limiting global warming to 2[degrees]C. *Nature, 517*(7533), 187+. https://link.gale.com/apps/doc/A396768550/AONE?u=purdue_main&sid=AONE&xid=69ba5e99. doi:101038/nature14016

Mitianiec, W. (2020). Improvement of Working Parameters in an Opposed Piston CI Two-Stroke Engine by Modelling Research. SAE Technical Paper Series. https://doi.org/10.4271/2020-01-2062.

Montazerin, N., Akbari, G., & Mahmoodi, M. (2015). General introduction of forward-curved squirrel-cage fan. *Developments in Turbomachinery Flow*, 1–23. https://doi.org/10.1016/b978-1-78242-192-4.00001-4

National Academy of Engineers. (n.d.). Grand Challenges - Develop Carbon Sequestration Methods. Retrieved on 1/24/2021 from: http://www.engineeringchallenges.org/9077.aspx.

Nemati, A., Ong, J. C., Jensen, M. V., Pang, K. M., Mayer, S., & Walther, J. H. (2020). Numerical Study of the Scavenging Process in a Large Two-Stroke Marine Engine Using URANS and LES Turbulence Models. *SAE Technical Paper Series*. https://doi.org/10.4271/2020-01-2012

Pirault, J., & Flint, M. (2010). *Opposed piston engines: Evolution, use, and future applications*. Warrendale, PA, SAE International.

Shirvani, S., Shirvani, S., & Shamekhi, A. H. (2020). Effects of Injection Parameters and Injection Strategy on Emissions and Performance of a Two-Stroke Opposed-Piston Diesel Engine. *SAE Technical Paper Series*. doi:10.4271/2020-01-5064

Srivastava, S. (2015). *Modeling and simulations of evaporating spray, turbulent flow, and combustion in internal combustion engines* [Doctoral dissertation, Michigan State University]. Dissertations & Theses @ CIC Institutions; ProQuest Dissertations & Theses Global. https://search.proquest.com/docview/1719521939?accountid=13360

Turner, J. W. G., Head, R. A., Chang, J., Engineer, N., Wijetunge, R., Blundell, D. W., & Burke, P. (2019). 2-Stroke Engine Options for Automotive Use: A Fundamental Comparison of Different Potential Scavenging Arrangements for Medium-Duty Truck Applications. *SAE Technical Paper Series*. https://doi.org/10.4271/2019-01-0071

Zha, K., Busch, S., Warey, A., Peterson, R. C., & Kurtz, E. (2018). A Study of Piston Geometry Effects on Late-Stage Combustion in a Light-Duty Optical Diesel Engine Using Combustion Image Velocimetry. *SAE International Journal of Engines, 11*(6), https://doi.org/10.4271/2018-01-0230

Zhang, Y. Zhao, H. (2012). Measurement of short-circuiting and its effect on the controlled autoignition or homogeneous charge compression ignition combustion in a two-stroke poppet valve engine *SAGE Journals*. Retrieved on 12/8/20 from: https://journals.sagepub.com/doi/10.1177/0954407011434252.

Zhou, L., Li, H., Chen, Z., Zhao, Z., & Zhang, F. (2020). Numerical Simulation and Optimization for Combustion of an Opposed Piston Two-Stroke Engine for Unmanned Aerial Vehicle (UAV). *SAE Technical Paper Series*. doi:10.4271/2020-01-0782

APPENDIX A – MESH SETTINGS FOR THE BASELINE MODEL

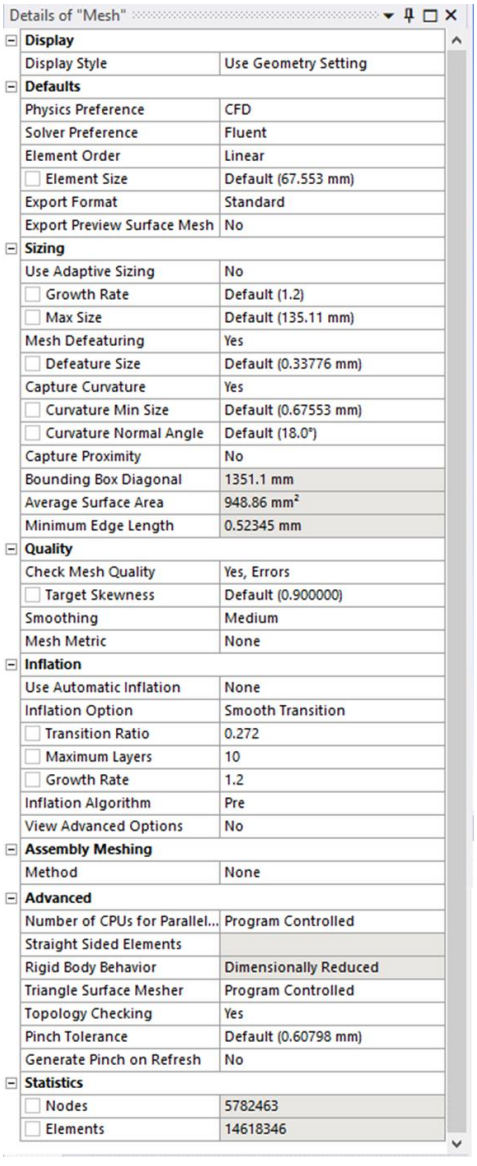

Details of "Mesh"	
Display	
Display Style	Use Geometry Setting
Defaults	
Physics Preference	CFD
Solver Preference	Fluent
Element Order	Linear
Element Size	Default (67.553 mm)
Export Format	Standard
Export Preview Surface Mesh	No
Sizing	
Use Adaptive Sizing	No
Growth Rate	Default (1.2)
Max Size	Default (135.11 mm)
Mesh Defeaturing	Yes
Defeature Size	Default (0.33776 mm)
Capture Curvature	Yes
Curvature Min Size	Default (0.67553 mm)
Curvature Normal Angle	Default (18.0°)
Capture Proximity	No
Bounding Box Diagonal	1351.1 mm
Average Surface Area	948.86 mm²
Minimum Edge Length	0.52345 mm
Quality	
Check Mesh Quality	Yes, Errors
Target Skewness	Default (0.900000)
Smoothing	Medium
Mesh Metric	None
Inflation	
Use Automatic Inflation	None
Inflation Option	Smooth Transition
Transition Ratio	0.272
Maximum Layers	10
Growth Rate	1.2
Inflation Algorithm	Pre
View Advanced Options	No
Assembly Meshing	
Method	None
Advanced	
Number of CPUs for Parallel...	Program Controlled
Straight Sided Elements	
Rigid Body Behavior	Dimensionally Reduced
Triangle Surface Mesher	Program Controlled
Topology Checking	Yes
Pinch Tolerance	Default (0.60798 mm)
Generate Pinch on Refresh	No
Statistics	
Nodes	5782463
Elements	14618346

Figure A.1. Fine mesh settings used within Fluent

APPENDIX B – MESH SETTINGS FOR COARSE AND MEIUM MESHES

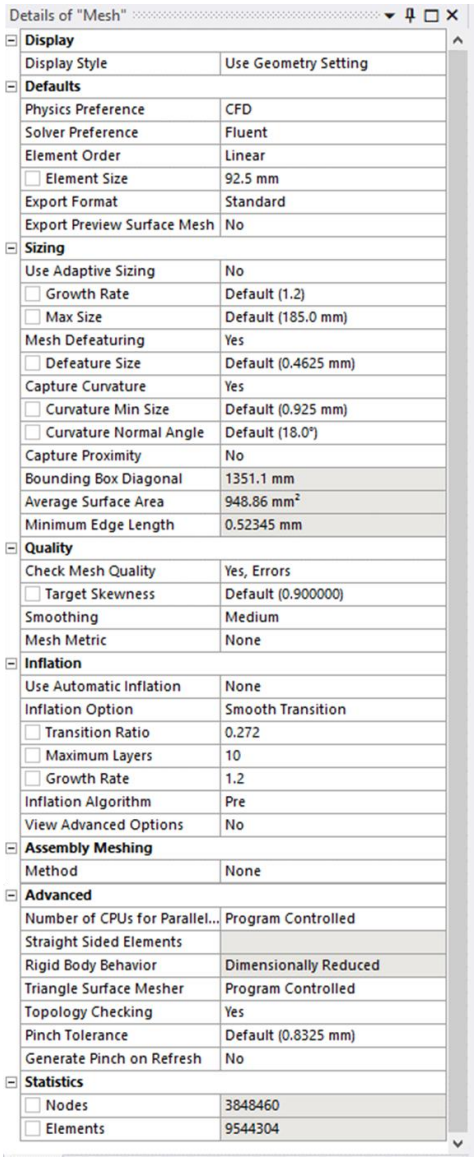

Details of "Mesh"	
Display	
Display Style	Use Geometry Setting
Defaults	
Physics Preference	CFD
Solver Preference	Fluent
Element Order	Linear
Element Size	92.5 mm
Export Format	Standard
Export Preview Surface Mesh	No
Sizing	
Use Adaptive Sizing	No
Growth Rate	Default (1.2)
Max Size	Default (185.0 mm)
Mesh Defeaturing	Yes
Defeature Size	Default (0.4625 mm)
Capture Curvature	Yes
Curvature Min Size	Default (0.925 mm)
Curvature Normal Angle	Default (18.0°)
Capture Proximity	No
Bounding Box Diagonal	1351.1 mm
Average Surface Area	948.86 mm²
Minimum Edge Length	0.52345 mm
Quality	
Check Mesh Quality	Yes, Errors
Target Skewness	Default (0.900000)
Smoothing	Medium
Mesh Metric	None
Inflation	
Use Automatic Inflation	None
Inflation Option	Smooth Transition
Transition Ratio	0.272
Maximum Layers	10
Growth Rate	1.2
Inflation Algorithm	Pre
View Advanced Options	No
Assembly Meshing	
Method	None
Advanced	
Number of CPUs for Parallel...	Program Controlled
Straight Sided Elements	
Rigid Body Behavior	Dimensionally Reduced
Triangle Surface Mesher	Program Controlled
Topology Checking	Yes
Pinch Tolerance	Default (0.8325 mm)
Generate Pinch on Refresh	No
Statistics	
Nodes	3848460
Elements	9544304

Figure B.1. Coarse mesh settings used within Fluent

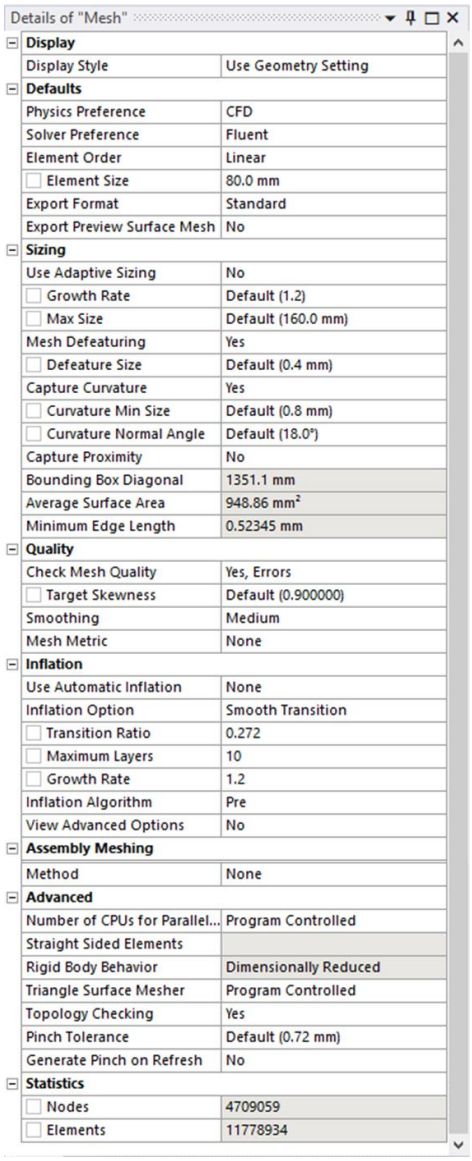

Details of "Mesh"

Display	
Display Style	Use Geometry Setting
Defaults	
Physics Preference	CFD
Solver Preference	Fluent
Element Order	Linear
Element Size	80.0 mm
Export Format	Standard
Export Preview Surface Mesh	No
Sizing	
Use Adaptive Sizing	No
Growth Rate	Default (1.2)
Max Size	Default (160.0 mm)
Mesh Defeaturing	Yes
Defeature Size	Default (0.4 mm)
Capture Curvature	Yes
Curvature Min Size	Default (0.8 mm)
Curvature Normal Angle	Default (18.0°)
Capture Proximity	No
Bounding Box Diagonal	1351.1 mm
Average Surface Area	948.86 mm²
Minimum Edge Length	0.52345 mm
Quality	
Check Mesh Quality	Yes, Errors
Target Skewness	Default (0.900000)
Smoothing	Medium
Mesh Metric	None
Inflation	
Use Automatic Inflation	None
Inflation Option	Smooth Transition
Transition Ratio	0.272
Maximum Layers	10
Growth Rate	1.2
Inflation Algorithm	Pre
View Advanced Options	No
Assembly Meshing	
Method	None
Advanced	
Number of CPUs for Parallel...	Program Controlled
Straight Sided Elements	
Rigid Body Behavior	Dimensionally Reduced
Triangle Surface Mesher	Program Controlled
Topology Checking	Yes
Pinch Tolerance	Default (0.72 mm)
Generate Pinch on Refresh	No
Statistics	
Nodes	4709059
Elements	11778934

Figure B.2. Medium mesh settings used within Fluent